

Absolute Added Correlative Coding: A Novel Higher-Order Modulation Format for High-Speed Optical Communication Systems

NGUYEN DONG NHAT

Thesis submitted to The University of Nottingham,

Department of Electrical and Electronic Engineering,

Faculty of Engineering, for the degree of

Doctor of Philosophy, April 2018

Abstract

A multilevel modulation format, namely absolute added correlative coding (AACC) is proposed to overcome the effect of fibre dispersion. A novel modulation and demodulation systems are proposed along with bit-error rate (BER) estimation technique. Transmission properties and system applications are also discussed. The research topics are categorised according to the type of the proposed multilevel signalling. It is worth mentioning that AACC can also be implemented with both NRZ and RZ pulse coding based upon the applications in order to optimise their performance.

In the first section, the focus lies on the performance of the BER, noise contributions and spectral efficiency. For the first time the signal space model of AACC, is derived and reported. The proposed modulation format is also compared to other well-known techniques such as NRZ at the same bit rate of 10-Gb/s. The results give good agreement with experiments. Secondly, the performance of AACC is numerically examined and compared against other prevailing on–off-keying and multilevel modulation formats at 40-Gb/s e.g. NRZ, 50% RZ, 67% carrier-suppressed return-to-zero (CS-RZ), duobinary and 4-PAM in terms of receiver sensitivity, spectral efficiency and dispersion tolerance. Calculated receiver sensitivity at a BER of 10^{-9} and chromatic dispersion tolerance of the proposed system are -28.3 dBm and -336 ps/nm, respectively. The performance of AACC is delineated to be improved by 7.8 dB in terms of receiver sensitivity compared to 4-PAM in back-to-back scenario. The comparison results also show a clear advantage of AACC in achieving longer fibre transmission distance due to the higher dispersion tolerance in optical access networks. The research work is extended to propose return-to-zero AACC (RZ-AACC) signal with three different duty cycles of 33, 50 and 67% utilising a lithium niobate ($LiNbO_3$) Mach–Zehnder modulator with a sinusoidal drive waveform. The spectral width and receiver sensitivity of 4-intensity level RZ-AACC with 33, 50 and 67% are discussed and compared against conventional AACC and RZ 4-PAM format. Short-range transmission of 3 bits per symbol is also proposed using AACC with eight levels at bit rates of 30- and 60-Gb/s back-to-back, and up to 75-Gb/s over 2-km and 3-km standard single-mode fibre using a single-drive multiple quantum-well Mach–

Zehnder modulator. The transmission performance was compared against the conventional 8-PAM.

In the third topic, the transmission performance of AACC using NRZ and RZ pulse shapes with a binary direct detection receiver in 40-Gb/s optical access and metro networks is comparatively investigated. It is shown that for AACC transmission, the NRZ impulse shaping is superior in comparison to RZ in spectral efficiency, dispersion tolerance, residual dispersion and self-phase modulation tolerance. However, RZ-AACC experiences about 1–2 dB advantage in receiver sensitivity over NRZ-AACC for back-to-back configuration as well as after 300-km single-mode fibre delivery. Next, the experimental consideration of AACC modulation format is investigated. In fact, the electrical components needed to construct and generate AACC signal are presented. DSP-based AACC generation is also developed and transferred into the arbitrary waveform generator. Its eye diagram after electrical back-to-back transmission is also shown thanks to the digital communication analyser. The experimental results have qualitatively matched our numerical results as a proof of concept. This work is carried out at Photonics Systems Research Lab in Korea Advanced Institute of Science and Technology (KAIST), Korea.

Finally, two approaches that commonly used nowadays to improve the transmission distance namely optical equaliser and electrical equaliser are studied. The numerical results show that optical equalisation technique can improve the performance significantly. In fact, for the first time combining duobinary signal with optical equaliser at 25-Gb/s can reach 40-km with the receiver sensitivity of -13 dBm while at 50-Gb/s it has a receiver sensitivity of -10 dBm over 11-km in optical simplified access networks. Note that without optical equaliser, the corresponding maximum distances of 30-km and 5-km are witnessed. For electrical equaliser, this technique is investigated by mean of experiments, a proposal of a transmission setup that introducing a great amount of distortions into the received NRZ at 10-Gb/s. With offline electrical equalisation, the waveform distortions are completely diminished observing by the clear received eye diagram which corresponds to a remarkable improvement in BER. This work is also acquired at KAIST.

Acknowledgements

A simple “thanks” for the people that have contributed directly or indirectly to this thesis is certainly not enough. Nevertheless, the few words below give me the chance to remember and thank them with all my heart, not only because of their help, but most importantly, for all the priceless moments that we have shared.

First and foremost, I would like to express my great appreciation and sincere gratitude to my supervisor, Prof. Amin Malek Mohammadi who brought me to *the world of optical communications* in 2013. I am eternally indebted to him for his constant encouragement and advice throughout my Ph.D research. In addition, I would like to thank my internal examiner, Dr. Nafizah Khan for her time and willingness to examine my work. I would also like to thank my senior, Dr. Mohamed Elsherif for his help with the numerical simulations and for many fruitful discussions during his time at UNMC.

I am deeply thankful to my mentors, Prof. Lim Nguyen from University of Nebraska-Lincoln and Prof. Hoa Le Minh from Northumbria University for their wise knowledge and invaluable guidance to improve this research work.

A special thanks to Prof. Hoon Kim from KAIST, Korea for accepting me as a visiting student researcher during spring 2017 to study experimentally the cost-effective optical access networks. I also would like to thank all the lab members in KAIST, for the useful technical discussions and considerate assistance on DSP algorithms.

On a personal note, I would like to express my deep gratitude to my parents for many sacrifices they have made for me over the years. Thanks also to my brothers and sisters and to the rest of my family for their continuous support and encouragement. Many thanks to my friends M. Long, H. Nghĩa, Đ. Yên, X. Phát, Q. Việt, K. Tường, M. Trân, V. Khoa, T. Thúy, Moataz, Mahmoud, Yaasiin, LeeWai and many more, especially all the ‘Futsal lads’ that have made my time outside of work much easier.

Finally, I am dedicating this thesis to my fiancée Nhân Ái (*benevolence* in English) for all her caring and understanding. I would like to thank her for sharing this adventure with me and for the unconditional love and patience. I look forward to our lifelong journey. Cảm ơn em vì tất cả.

Contents

Abstract i
Acknowledgements iii
Contents iv
List of Abbreviations viii
List of Figures xii
List of Tables xvi
Chapter 1 – Introduction 1
1.1 Background 2
1.2 Problem Statement 4
1.3 Research Motivation 4
1.4 Objectives 6
1.5 Principal Contributions of this Research 7
1.6 Scope of Study 9
1.7 Thesis Organisation 12
Chapter 2 – Fundamentals of Optical Fibre Communications 14
2.1 Introduction 15
2.2 Optical Modulation Technologies 15
2.2.1 Directly Modulated Lasers (DMLs) 16
2.2.2 External Modulators 16
2.3 Performance Evaluation Metrics 18
2.3.1 Bit-Error Rate (BER) and Q-factor 19
2.3.2 Receiver Sensitivity 22
2.3.3 Chromatic Dispersion 23
2.3.4 Self-Phase Modulation 25
2.3.5 Spectral Efficiency 26
2.3.6 Eye Diagram 27
2.4 Advanced Modulation Formats 28
2.4.1 Non-Return-to-Zero (NRZ) 28

2.4.2 Duobinary 30
2.4.3 4-ary Pulse Amplitude Modulation (4-PAM) 32
2.5 Chromatic Dispersion Compensation Techniques 35
2.5.1 Dispersion Compensation Fibre (DCF) 35
2.5.2 Optical Equalisers 36
2.5.3 Electrical Equalisers 38
2.6 Concluding Remarks 40
Chapter 3 – AACC System Model and Performance Metrics 42
3.1 Introduction 43
3.2 AACC Transceiver Model 44
3.2.1 Transmitter Model 44
3.2.2 Receiver Model 48
3.2.3 Signal Space Model 48
3.2.4 Power Performance Metrics 50
3.3 Analytical Performance Evaluation 53
3.3.1 Sensitivity and BER Calculation 54
3.3.2 Total Noise Variance 56
3.3.3 Impact of RIN on AACC 59
3.4 Concluding Remarks 61
Chapter 4 – Numerical Performance Analysis of AACC-based Signalling 63
4.1 Introduction 64
4.1.1 Numerical Simulation Software 64
4.2 AACC 66
4.2.1 Simulation Setup 66
4.2.2 Results and Discussion 72
4.3 RZ-AACC 84
4.3.1 Simulation Setup 84
4.3.2 Results and Discussion 86
4.4 8-AACC 90
4.4.1 Simulation Setup 90

4.4.2 Results and Discussion 92
4.5 Concluding Remarks 94
Chapter 5 – Comparison of NRZ versus RZ Pulse Shapes over AACC in Linear and Nonlinear Transmission Medium 96
5.1 Introduction 97
5.2 System Model and Performance Settings 98
5.2.1 Comparison of the Transmission Performance in Erbium-Doped Fibre Amplifier (EDFA)-free and Dispersion Compensation Fibre (DCF)-free Configuration 100
5.2.2 Comparison of Self-Phase Modulation (SPM) Tolerance as a Function of the Residual Dispersion 101
5.2.3 Comparison of the Transmission Performance in Optical Metro Networks 104
5.3 Concluding Remarks 105
Chapter 6 – AACC Experimental Verification 106
6.1 Introduction 107
6.2 Options to Construct the AACC Transmitter 107
6.3 DSP-based AACC Generation 110
6.4 Concluding Remarks 113
Chapter 7 – Alternative Dispersion Compensation Techniques 114
7.1 Introduction 115
7.2 Optical Equalisers 115
7.2.1 Simulation Setup 116
7.2.2 Performance at 25-Gb/s without OEQs 118
7.2.3 Performance at 25-Gb/s with OEQs 120
7.2.4 Performance at 50-Gb/s 123
7.3 Electrical Equalisers 125
7.4 Concluding Remarks 129
Chapter 8 – Conclusions and Future Works 131
8.1 Thesis Conclusion 132
8.2 Future Works 134

Appendix 136
References 144
List of Publications and Awards 162

List of Abbreviations

AACC	Absolute Added Correlative Coding
APD	Avalanche Photodiode
APDCDM	Absolute Polar Duty Cycle Division Multiplexing
ASE	Amplified Spontaneous Emission
ASK	Amplitude Shift Keying
AWG	Arbitrary Waveform Generator
AWGN	Additive White Gaussian Noise
B2B	Back-to-Back
BER	Bit-Error Rate
CD	Chromatic Dispersion
CML	Chirp Managed Laser
CMOS	Complementary Metal-Oxide-Semiconductor
CO	Central Office
CS-RZ	Carrier-Suppressed Return-to Zero
CW	Continuous Wave
DB	Duobinary
DCA	Digital Communication Analyser
DCF	Dispersion Compensation Fibre
DFE	Decision Feedback Equaliser
DML	Directly Modulated Laser
DSF	Dispersion Shifted Fibre
DSO	Digital Storage Oscilloscope

DSP	Digital Signal Processing
DPSK	Differential Phase Shift Keying
DQPSK	Differential Quadrature Phase-Shift-Keying
DWDM	Dense Wavelength Division Multiplexing
EDFA	Erbrium-Doped Fibre Amplifier
EEQ	Electrical Equaliser
FBG	Fibre Bragg Gratings
FEC	Forward-Error Correction
FFE	Feed Forward Equaliser
FWHM	Full-Width at Half-Maximum
GVD	Group Velocity Dispersion
IC	Integrated Circuit
IDF	Inverse Dispersion Fibre
IEEE	Institute of Electrical and Electronics Engineers
IM/DD	Intensity Modulation and Direct Detection
InP	Indium Phosphide
I/Q	In-phase/Quadrature
ISI	InterSymbol Interference
ITU	International Telecommunication Union
LD	Laser Diode
$LiNbO_3$	Lithium Niobate
LMS	Least-Mean Square
LP	Launch Power
LPF	Low-Pass Filter
LS	Level Shifter
MZM	Mach-Zehnder Modulator

MMT	Mapping Multiplexing Technique
MMF	Multi-Mode Fibre
MMR	Micro-Ring Resonator
NRZ	Non-Return-to-Zero
OOK	On-Off-Keying
OBF	Optical Bandpass Filter
OEQ	Optical Equaliser
PAM	Pulse Amplitude Modulation
PDF	Probability Density Function
PMD	Polarisation-Mode Dispersion
PIC	Photonic Integrated Circuit
PPG	Pulse Pattern Generator
PRBS	Pseudo Random Bit Sequence
PSBT	Phase-Shaped Binary Transmission
RIN	Relative Intensity Noise
RMS	Root Mean Square
RZ	Return-to-Zero
RZ-AACC	Return-to-Zero Absolute Added Correlative Coding
RoF	Radio over Fibre
RSOA	Reflective Semiconductor Optical Amplifier
Rx	Receiver
SDM	Space Division Multiplexing
SMA	SubMiniature version A
SMF	Single-Mode Fibre
SPM	Self-Phase Modulation
SOA	Semiconductor Optical Amplifier

SER	Symbol Error Ratio
TDM	Time Division Multiplexing
TO	Transistor-Outline
Tx	Transmitter
VCSEL	Vertical-Cavity Surface-Emitting-Laser
VOA	Variable Optical Attenuator
WDM	Wavelength Division Multiplexing

List of Figures

Figure 1.1: A wide range of optical fibre communications applications to our society..... 3
Figure 1.2: Schematic of concepts to be handled in this research. 6
Figure 1.3: Overall system study and performance evaluation aspects discussed throughout this thesis. 11
Figure 2.1: Dual-drive Mach-Zehnder modulator.....17
Figure 2.2: A received NRZ signal with its histogram. 21
Figure 2.3: Illustration of CD causes pulses to spread into adjacent bit slots. The broadening of pulses due to CD leads to optical eye closure. 23
Figure 2.4: Example of typical NRZ eye diagrams to determine the signal quality. (a) A closure of the eye reveals the system imperfections or impairments. (b) An open eye corresponds to minimal distortion of the signal..... 27
Figure 2.5: Structure of a MZM-based NRZ generation. 29
Figure 2.6: Measured NRZ eye diagram. 30
Figure 2.7: Principle of Duobinary modulation using MZM. 31
Figure 2.8: Measured Duobinary eye diagram. 31
Figure 2.9: Optical 4-PAM generation based on MZM. 33
Figure 2.10: Measured 4-PAM eye diagram. 33
Figure 2.11: The block diagram representing the placement of the OEQ to cancel the accumulated dispersion. 37
Figure 2.12: Arrangement of the electrical equalisers in optical transmission systems..... 39
Figure 3.1: AACC concept (a) AACC transmitter model and (b) AACC symbols..... 44
Figure 3.2: (a) AACC receiver and (b) Anatomy of a decision module algorithm..... 48
Figure 3.3: (a) Basis function and (b) signal space constellation geometry of AACC..... 50
Figure 3.4: Theoretical BERs versus received optical power for OOK and AACC transmission formats at 10-Gb/s. 57
Figure 3.5: Contributions from shot noise, thermal noise, and RIN at a receiver bandwidth of 20-GHz for AACC. 58

Figure 3.6: Contributions from shot noise, thermal noise, and RIN versus bit rate for AACC. 58
Figure 3.7: Total noise variance σtotal2 in [A2] versus the received optical power for OOK and AACC. 59
Figure 3.8: BER curves for various levels of RIN, shown for OOK at 40-Gb/s..... 60
Figure 3.9: Influence of RIN on expected BER, shown for AACC at 40-Gb/s..... 61
Figure 4.1: Schematic of the AACC transmitter for numerical evaluation. ..66
Figure 4.2: Characteristics of absorption ($\Delta\alpha 0$) and phase difference ($\Delta\beta$) in the simulated optimised dual-drive MZM [58]. 68
Figure 4.3: Simulation setup. 68
Figure 4.4: Sample of 4-level intensity eye diagram and its conditional probability density functions with Gaussian noise. 70
Figure 4.5: Receiver sensitivity as a function of (a) optical filter bandwidth and (b) electrical filter bandwidth. 72
Figure 4.6: BER curves for the three received eyes of AACC (top, middle and bottom) in B2B scenario. Inset is the corresponding eye diagram. 73
Figure 4.7: B2B receiver sensitivity of AACC, 4-PAM, duobinary and NRZ..... 75
Figure 4.8: Spectral width of AACC in comparison to (a) NRZ (b) 50% RZ, (c) 67% CSRZ, (d) null-to-null spectral width 4-PAM and (e) full spectrum 4-PAM, all at the same aggregate bitrate of 40-Gb/s. 77
Figure 4.9: Measured BER versus chromatic dispersion. DB: Duobinary. 78
Figure 4.10: Optically preamplified receiver sensitivity measured as a function of SMF transmission distance for AACC and 4-PAM systems at $10-9$ BER 81
Figure 4.11: BER versus received optical power over different lengths of SMF for AACC (black curves, solid markers) and 4-PAM (blue curves, hollow markers) at an aggregate bit rate of 40-Gb/s in EDFA-free DCF-free configuration..... 82
Figure 4.12: BER versus received power for AACC (solid symbols) and 4-PAM (hollow symbols) for B2B, 1-km and 2-km at 100-Gb/s data rate in EDFA-free DCF-free transmission scheme. 83
Figure 4.13: Schematic diagram for RZ-AACC Tx. Insets: (i) Simulated eye diagram of optical AACC signal and (ii) optical RZ-AACC signal at 40-Gb/s..... 85

Figure 4.14: Transfer charateristics of the MZM2, indicating the excursion of drive waveform ***V2t*** for generating RZ-AACC with different duty cycles (black circles: MZM quadrature point). 85
Figure 4.15: Optical spectra of 33%, 50% and 67% RZ-AACC for 40-Gb/s bit rate..... 87
Figure 4.16: Comparison of optical spectra of 50% RZ-AACC to RZ 4-PAM and standard binary 50% RZ signals at 40-Gb/s. 88
Figure 4.17: BER curves for 50% RZ-AACC, 33% RZ-AACC, CS-RZ-AACC, AACC, RZ and RZ 4-PAM formats in B2B configuration at 40-Gb/s. 88
Figure 4.18: The electrical 8-AACC signal. (a) 8-AACC encoding and (b) 8-AACC waveform..... 90
Figure 4.19: 8-AACC and 8-PAM transmission setup. Insets: (i) B2B eye diagram of 8-AACC and (ii) Optical spectra. 91
Figure 4.20: Receiver sensitivity at 30-Gb/s, 60-Gb/s and 75-Gb/s in B2B configuration for 8-AACC (solid markers) and 8-PAM (hollow markers)..... 92
Figure 4.21: Receiver sensitivity at 75-Gb/s over 2-km and 3-km of SMF. ..93
Figure 4.22: Eye diagrams of 8-AACC and 8-PAM at 75-Gb/s after transmisison over 2-km and 3-km of SMF. 94
Figure 5.1: Schematic configuration of NRZ-AACC and RZ-AACC transmitter and direct detection used in the simulation. 98
Figure 5.2: Optical spectral width of NRZ-AACC and RZ-AACC measured at 20-Gbaud/s. The spectrum analysers are placed right after the modulators..... 98
Figure 5.3: Calculated BER performance in optical access networks using (a) NRZ-AACC and (b) RZ-AACC data. 100
Figure 5.4: Setup for scrutinising SPM effects and residual dispersion of optical NRZ- and RZ-AACC transmission systems. 101
Figure 5.5: BER versus simulated positive residual dispersion using (a) NRZ-AACC and (b) RZ-AACC data. 102
Figure 5.6: Calculated BER characteristics as a function of the transmission distance in optical metro networks using (a) NRZ-AACC and (b) RZ-AACC..... 104
Figure 6.1: (a) AACC experimental schematic and (b) AACC components..... 108
Figure 6.2: Low-pass filters. 109
Figure 6.3: Tektronix arbitrary waveform generator (AWG7122B)..... 110
Figure 6.4: Offline DSP stack employed at the transmitter. 111

Figure 6.5: AACC eye diagram displayed on the digital communication analyser.....112
Figure 6.6: Optical spectra.....112
Figure 7.1: Simulation setup at 25-Gb/s. Insets (i) and (ii) are the electrical spectra of NRZ and duobinary respectively. 116
Figure 7.2: SMF links with (a) 1st order OEQ pre-equalisation and (b) 2nd order pre-equalisation. 117
Figure 7.3: NRZ and duobinary performance without OEQ for various SMF link distances at 25-Gb/s. 119
Figure 7.4: NRZ eye diagrams w/o OEQ over various link distance. 120
Figure 7.5: Duobinary eye diagrams w/o OEQ over various link distances. DB: duobinary.....120
Figure 7.6: NRZ and duobinary performance at 25-Gb/s for (a) 1st order OEQ pre-equalisation and (b) 2nd order OEQ pre-equalisation. 121
Figure 7.7: Received NRZ and duobinary eye diagrams at 25-Gb/s (a) 1st order pre-OEQ and (b) 2nd order pre-OEQ. 122
Figure 7.8: Optical spectra of duobinary signal with and without 1st order and 2nd order pre-OEQs at 25-Gb/s. 123
Figure 7.9: NRZ and duobinary performance without OEQ for various link distances at 50-Gb/s. 124
Figure 7.10: NRZ and duobinary performance (a) 1st order OEQ pre-equalisation and (b) 2nd order OEQ pre-equalisation.....124
Figure 7.11: Working space to carry out the experiments at KAIST, Korea..... 126
Figure 7.12: (a) System schematic and (b) Demonstration of EEQ in equalising the waveform distortion. Inset is the electrical eye diagram at the Tx. 126
Figure 7.13: (a) 10-G VCSEL and (b) 2.5-G PIN. 127
Figure 7.14: Received 3D eye diagrams (a) w/o EEQ and (b) w/ EEQ. 128
Figure 7.15: Corresponding signal levels (a) before and (b) after equalisation.....128
Figure 8.1: Progression of advanced modulation formats integrated with equalisers..... 134

List of Tables

Table 2.1: Comparison of NRZ, Duobinary and 4-PAM formats [101]. 34
Table 2.2: Summary of transmission systems using optical equalisation techniques and DD receivers within the last 5 years.....37
Table 3.1: Transmitted and received bit stream for AACC modulation. 46
Table 3.2: Gray and natural coding for AACC.....55
Table 4.1: Data recovery rules at the receiver. 70
Table 4.2: Fibre parameters used in the schematic [10]. 80
Table 4.3: Comprehensive comparison between MZM-based advanced optical modulation formats reported recently at 40-Gb/s (BER = $10-9$) [29], [44], [72].....89

Chapter 1– Introduction

1.1 Background

Since their introduction thirty years ago, photonics technologies have largely contributed to the massive development of communication networks and it can be easily predicted they serve as grounds for most of the network revolutions ahead [1]–[4]. As a matter of fact, it has been forecasted that the photonics market size is about to reach USD 724.22 billion by 2021, at a Compounded Annual Growth Rate (CAGR) of 8.4 % between 2016 and 2021 [5]. Obviously, optical communications reveal themselves as the most important sector since they are the largest end-use industry in photonics technologies. These statistics and information can be well comprehended by cogitating the rapid growth in Internet traffic i.e. flow of data across the Internet. They have been driven by the enormous demand for Internet services such as video streaming, social media, cloud computing, interactive e-learning and online gaming as illustrated in Fig 1.1 [6]–[9]. Due to these high bandwidth applications, the need for high capacity transmission links is required and over the last decade optical fibre communication systems have emerged as the dominant technology capable of satisfying these demands [1], [10], [11]. As a response to these never-ending traffic demands, the IEEE organisation has started a P802.3bm fibre optic task force for 40-G and 100-G Ethernet standardisation, as well as 400-GbE to address such needs [12].

Current fibre-optic transmission systems mostly employ binary modulation formats with inherently low spectral efficiency due to their low system complexity and cost-effectiveness at the transmitters and receivers [13]–[15]. Multilevel modulation formats, which have been extensively deployed in various communication links are leading to increase the spectral efficiency of optical transport networks. They are capable to increase the transmission capacity by transmitting more information not only in the amplitude but also phase, polarisation or a combination of all [16], [17]. Especially multilevel modulation has also been scrutinised as one of the approaches to scale the date rate of optical interfaces without increasing the number of wavelengths. Combining optical coherent receivers with advanced modulation formats have attracted considerable attention from not only the increase in spectral efficiency but also the compensation of fibre impairments caused by chromatic and

polarisation mode dispersions [17]–[19]. However, this approach is costly due to the use of high-speed optoelectronics, e.g. local oscillators, multiple balanced detectors, digital-to-analog converters as well as sophisticated digital signal processing, the systems would be ideally suited for long-haul (multi-span) transmission.

In contrast with coherent systems, advanced modulation formats such as a typical binary signalling – NRZ is widely exploited and well-matched for intensity modulation and direct detection (IM/DD) applications such as optical short-range, access and metro networks. However its usage is questionable since it is not tolerant to fibre dispersion which is the main limitation in high-speed IM/DD systems. Additionally, direct detection receivers are subjected to nonlinear signal distortion due to the square-law photo-detection, limiting the transmission distance.

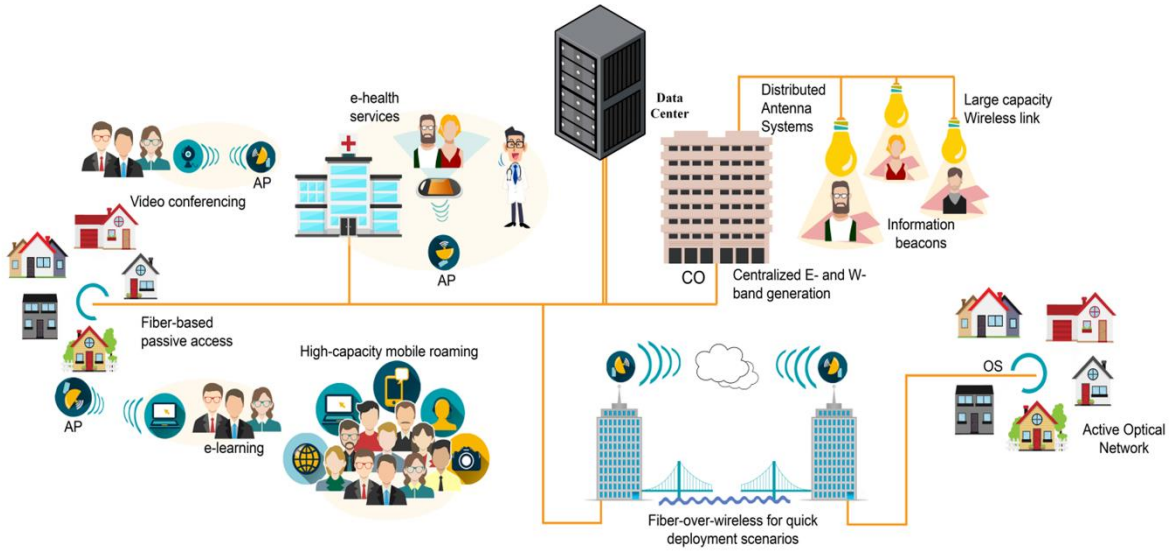


Figure 1.1: A wide range of optical fibre communications applications to our society.

1.2 Problem Statement

Increasing the data rate leads to a higher spectral efficiency in optical communication systems, especially in wavelength-division multiplexing (WDM) networks resulting in a more efficient use of optical bandwidth. However, as the bit rate increases, the systems becomes more and more sensitive to the fundamental limitations of optical transmission such as noise, nonlinear effects and more seriously chromatic dispersion. For example, at a single channel bit rate of 40-Gb/s the signal is 16 times more sensitive to dispersion than at 10-Gb/s, and it costs a great amount of received optical power degradation in dB [10].

In other words, the intersymbol interference (ISI) caused by such a substantial amount of dispersion is certainly a limiting factor for transmitted data (*how fast*) or maximum link reach (*how far*). These shortcomings could be found in a typical direct-detected system employing non-return-to-zero (NRZ) and 4-ary pulse amplitude modulation (4-PAM). In order to overcome the system reach limitation in NRZ and 4-PAM transmission, researchers nowadays try to apply the fully integrated equaliser in optical domain (optical equalisers) to mitigate the waveform distortions engendered by the fibre dispersion or an electronic dispersion compensation also known as electrical equalisers implemented at the receiver side, to dynamically compensate the accumulated chromatic dispersion. However such equalisation techniques become cumbersome in optical communications systems requiring low system latency and complexity.

1.3 Research Motivation

Countering the dispersion-induced ISI requires an increase in signal launch power which prompts the nonlinear signal distortion in the fibre, as described later in this thesis. In addition, one could say that the best solution to reduce the dispersion limitations and then speed up the optical communication networks is to replace all the already installed standard single-mode fibre (SMF)

with the dispersion shifted fibre (DSF) since its operating wavelength is close to zero dispersion. However this is not a practical and viable option from the companies' point of view since it necessitates an extremely high cost of new fibre installation (fibre length can be up to thousands of kilometres). As such more targeted research on dispersion tolerances and compensation devices is obligatory and is the topic of discussion in this thesis. For example a possible solution comes from the dispersion compensation devices in optical domain such as dispersion compensation fibre (DCF), inverse dispersion fibre (IDF) and fibre Bragg gratings (FBG); nevertheless these techniques are usually high insertion loss which may severely degrade the system power budget. Hence optical amplifiers for loss compensation are necessary, making the practical system very expensive which is not desired in IM/DD applications. Moreover intervening these optical devices into the optical link for compensating the dispersion is quite bothersome.

Therefore in the search for a steady high-speed optical IM/DD systems, use of new advanced modulation formats with better spectral efficiency may be an answer. These modulation formats themselves should be resilient to the detrimental medium impairments e.g. chromatic dispersion. Since they are stand-alone and implemented in electrical domain, thus they can be flexibly applied into any systems just by placing the electronic chip at the transmitter in practice.

The scope of this work encompasses four main different subject areas. Their concept and effects are closely related to each other. It can be considered that the investigation on this research and development as a puzzle, illustrated in Fig 1.2 where intensity modulation formats, fibre chromatic dispersion tolerance, equalisation techniques and cost efficiency are essential pieces.

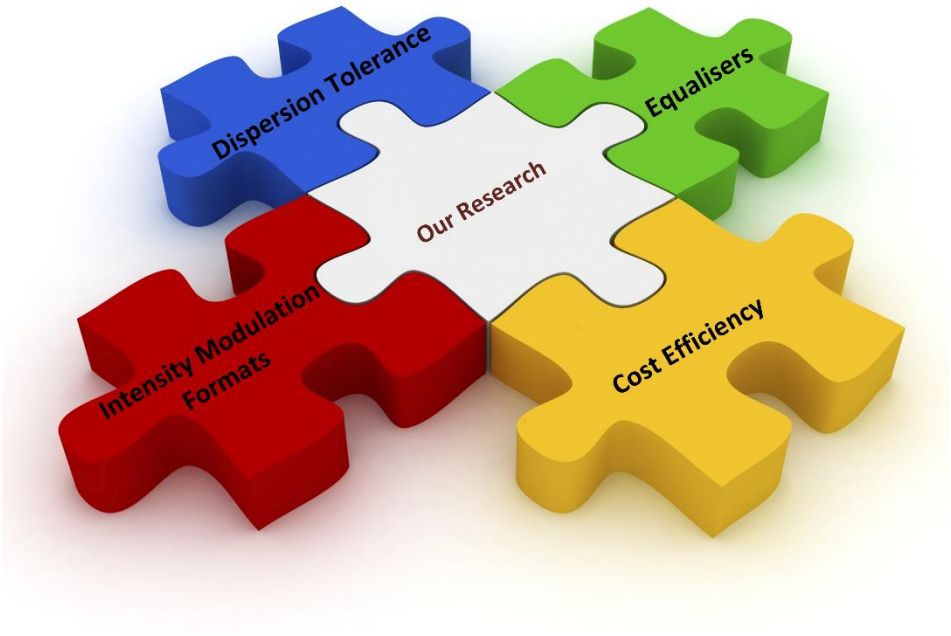


Figure 1.2: Schematic of concepts to be handled in this research.

1.4 Objectives

The goal of this research above all is the design and evaluation of a novel multilevel IM/DD modulation format named *Absolute Added Correlative Coding (AACC)* that can be practically employed in future optical transmission applications related to but not limited to optical data centres interconnects, high-speed short-range systems and metro-access networks. The AACC system is not only cost-efficient since its structure is based on commercial electronic components but also highly tolerant to fibre dispersion. The improved dispersion tolerance is realised due to the existence of the differential encoders in AACC structure that distort the transmitted pulse (pre-distortion technique) which make itself robust to dispersion.

The main objectives of this research are:

1. To design novel cost-efficient multilevel intensity modulation formats. The proposed scheme is robust to the performance degradation factors e.g. chromatic dispersion.

2. To formulate a mathematical model for the structure and properties of AACC transmission format.

3. To develop the principles and bit-error rate estimation methods for each type of AACC-based signalling.

4. To investigate the use of equalisers for combating the harmful dispersion effect on NRZ signal.

1.5 Principal Contributions of this Research

This thesis has been carried out mostly at *The University of Nottingham Malaysia Campus* and partly at *Korea Advanced Institute of Science and Technology* in the Photonics Systems Research Laboratory.

The work has been primarily developed within the scope of extending the transmission distance in optical intensity modulation and direct detection systems. The most important results accomplished from this thesis are:

1) Detailed investigation of novel transceiver design of AACC system and its signal space model with the average electrical and optical power derivations.

2) Comprehensive demonstration of AACC compared to various renowned modulation formats such as NRZ, RZ, duobinary and 4-PAM signals at 40-Gb/s in optical access networks.

3) Proposal of new AACC format with RZ pulse shaping with different duty cycles featuring improved receiver sensitivity for high-speed optical transport.

4) Proposal of new high-order modulation format which is eight-level AACC at bit rates of 30- and 60- and 75-Gb/s with the aim of improving the spectral efficiency and dispersion tolerance in optical interconnects.

5) In-depth comparison study of AACC with NRZ and RZ pulse shapes in 40-Gb/s optical metro-access networks considering linear and nonlinear effects.

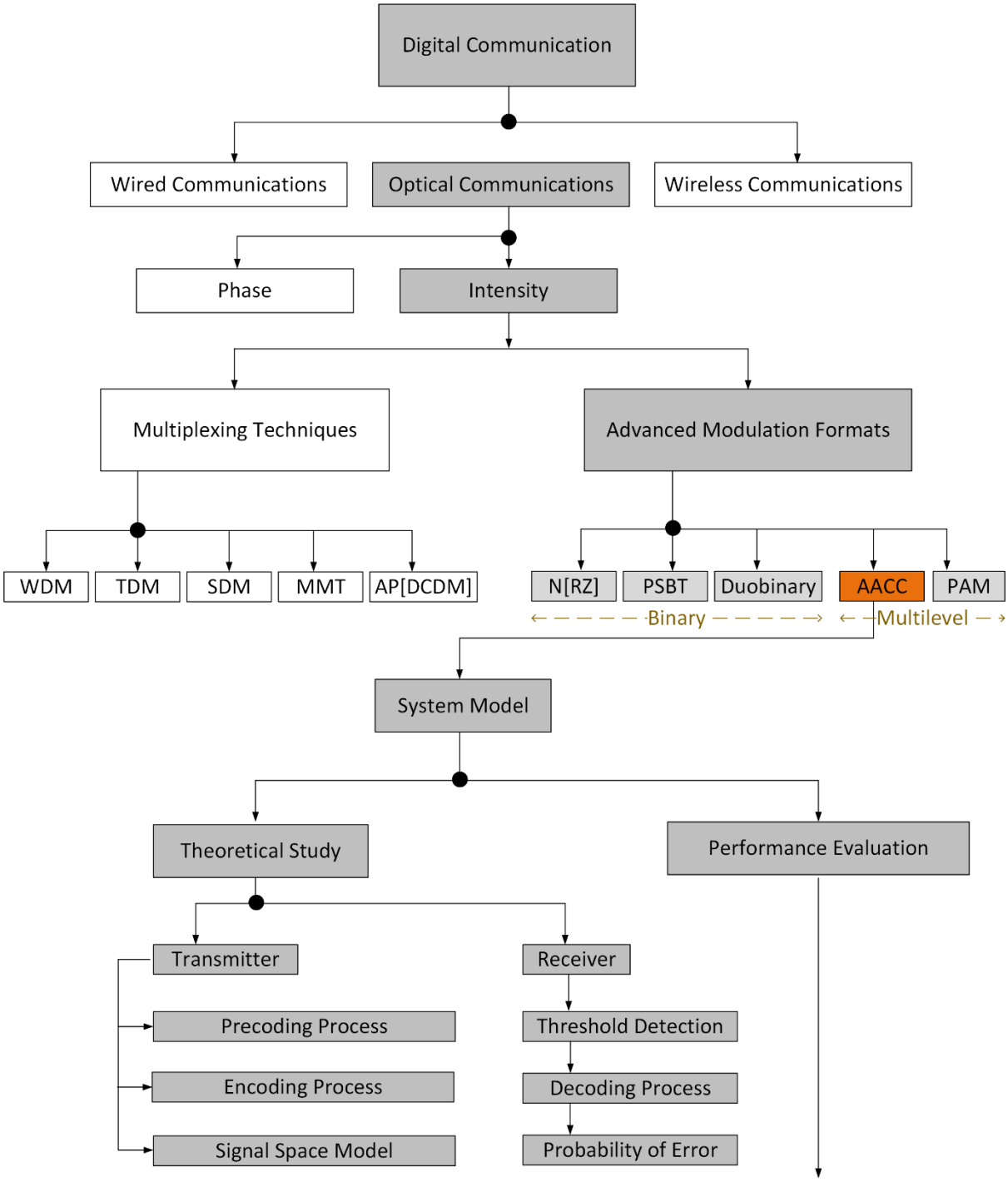
6) Investigation on a few of practical AACC transmitters based on the commercial components for proof-of-concept. Proposal of a digital signal processing-based module to produce the electrical AACC signal.

7) First demonstration of duobinary signal with 1^{st} and 2^{nd} order optical equalisers at the transmitter output to significantly enhance the system reach in simplified optical access networks.

8) Experimentally scrutinising the effectiveness of electronic dispersion compensation in equalising the waveform distortions after transmission for 10-Gb/s NRZ signal.

1.6 Scope of Study

Fig. 1.3 shows the hierarchical schematic as a scope of study to monitor analytically, numerically and experimentally the AACC signalling in every aspects (grey boxes). This is to comprehend the sheer scale of its unique characteristics and compared with other familiar modulation formats. In addition, the figure also indicates the study on equalisations for NRZ signal as well as the performance evaluation features.


Digital Communication
Wired Communications
Optical Communications
Wireless Communications
Phase
Intensity
Multiplexing Techniques
Advanced Modulation Formats
WDM
TDM
SDM
MMT
AP[DCDM]
N[RZ]
PSBT
Duobinary
AACC
PAM
Binary
Multilevel
System Model
Theoretical Study
Performance Evaluation
Transmitter
Receiver
Precoding Process
Threshold Detection
Encoding Process
Decoding Process
Signal Space Model
Probability of Error

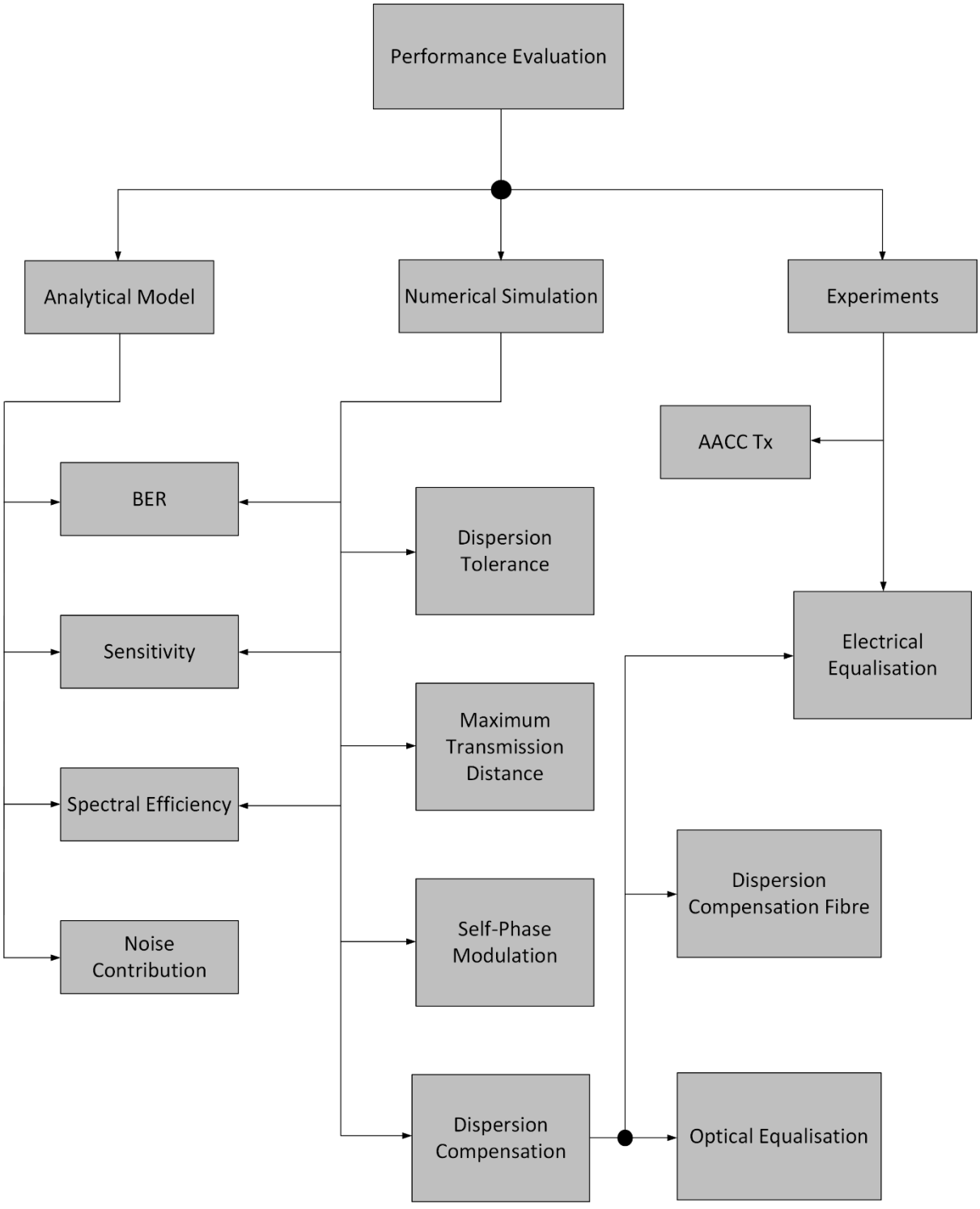


Figure 1.3: Overall system study and performance evaluation aspects discussed throughout this thesis.

1.7 Thesis Organisation

The different topics were organised in such a way that make this document concise and clear in order to provide the best understanding possible. In the following, the chapters briefly describe:

- Chapter 2: Fundamentals of Optical Fibre Communications – This chapter contains a general overview about directly modulated lasers and external modulators, whose function is to imprint information into the optical carrier. Essential parameters for quantifying the system performance are then described. The third section discusses the primary advanced modulation formats about their generation as well as properties. Finally, various techniques for compensating the chromatic dispersion-induced waveform distortions are also taken into account.

- Chapter 3: AACC System Model and Performance Metrics – In this chapter, for the first time the transceiver structure, working principle and data recovery of the AACC transmission system over additive white Gaussian noise channel are described. This chapter also delineates the signal space model of AACC, where the average electrical and optical power expressions are derived. Analytical performance of AACC in terms of BER versus received optical power, noise variance and its impact is also presented.

- Chapter 4: Numerical Performance Analysis of AACC-based Signalling – After presenting the analytical outcomes, plentiful results on AACC-related signalling with different applications based on numerical simulation software are addressed in this chapter. The performance of AACC-based schemes are compared with a number of well-known modulation formats with respect to spectral efficiency, dispersion tolerance and receiver sensitivity. Bit-error rate computation method is also demonstrated in this chapter.

- Chapter 5: Comparison of NRZ versus RZ Pulse Shapes over AACC in Linear and Nonlinear Transmission Medium – This chapter meticulously characterises the AACC signal with two different line codes (NRZ and RZ) in both optical access and metro networks. The linear effects such as chromatic dispersion and residual dispersion and nonlinear effect e.g. self-phase modulation effect of NRZ- and RZ-AACC transmission systems at 40-Gb/s are investigated.

- Chapter 6: AACC Experimental Verification – Work in this chapter is carried out in the experimental laboratory in Korea. Several techniques to construct the electrical AACC transmitter to prove its viability for future implementation are stated. The needed components for construction are also clearly displayed. Next section presents a fruitful development of a digital signal processing-based module in order to produce an electrical AACC generation and also validate the simulation analysis.

- Chapter 7: Alternative Dispersion Compensation Techniques – This chapter numerically and experimentally presents state-of-the-art equalisers implemented in both optical and electrical domain to mitigate the NRZ signal distortions triggered by fibre dispersion. Its performance enhancement is visually comprehended by the received eye diagram.

- Chapter 8: Conclusions and Future Works – As the name indicates itself, the main important findings and conclusions about this research study is presented in this chapter. Furthermore, it ends with future research activities and perspectives.

Chapter 2– Fundamentals of Optical Fibre Communications

2.1 Introduction

This chapter gives a brief introduction to the basic concepts of optical modulation technologies that presenting how to convert the information in electrical signal to optical one to be carried by light. This chapter also discusses the performance evaluation parameters used to compare the different modulation formats presented in this thesis. The parameters covered in this chapter are the BER/Q-factor, receiver sensitivity, chromatic dispersion tolerance, self-phase modulation effect, spectral efficiency and eye diagram.

Another important section of this chapter introduces several standard digital optical modulation formats that have gained a considerable attention in IM/DD systems research such as non-return-to-zero, duobinary and 4-ary pulse-amplitude modulation. The generation, detection schemes and properties for each modulation format are explained in details showing the corresponding eye diagrams. These modulation formats are useful to fully understand the proposed multilevel modulation formats later mentioned in chapters three, four, five and six.

Last section of this chapter discusses three methods that are commonly used in the current literature to compensate for fibre dispersion. The effect of fibre dispersion is very harmful since it causes pulse spreading and ISI that result in a limited transmission distance in IM/DD systems.

2.2 Optical Modulation Technologies

In optical communication systems, light is used to transmit data signals. Hence, an optoelectronic device to emit the light and a modulator or a combination of both to imprint the telecommunication data onto the light are needed. The process of converting the electrical signal to optical is also called E-O conversion. This section describes the two most common technologies that used to carry out this process. The first option is called direct modulation while the

second one is called external modulation. Their details are described in the following subsections.

2.2.1 Directly Modulated Lasers (DMLs)

Direct modulation of lasers using DMLs is the easiest way to impose data on an optical carrier. DMLs have the advantage of low cost, a small form factor and low power consumption in comparison to externally modulated lasers [20]–[22]. Therefore DMLs are broadly utilised in optical metro networks at low bit rate (<10-Gb/s). In principle, the intensity of light emitted from a laser is linearly proportional to the bias current when operated above threshold. By modulating the current, the electrical modulation signal can be transferred to the light output from the laser. Direct modulation technique for that reason provides a cost-effective optical transmitter.

However the main limitation of DMLs when operated in high data-rate transmission systems is its residual phase modulation always accompanying the desired intensity modulation; this inherent effect is known as highly component-specific chirp which broadens the optical spectrum restricting WDM channel spacing. In case this chirp interactes with chromatic dispersion (CD), it would cause exaggerated signal distortions and limit the bitrate length product [23]–[25]. Therefore in order to maintain the low-cost optical transmitter as well as high performance, chirp managed laser (CML) has been proposed [26], [27].

2.2.2 External Modulators

The optical modulators convert the transmitted data from the electrical domain to the optical domain by modulating the physical properties of an optical field. As stated above, amplitude and phase are the physical quantities relevant for fibre-optic transmission. There are different external modulator types based on different physical principles such as electro-absorption modulators (EAM) and Mach-Zehnder modulator, differing in complexity and achievable performance.

In the following the so-called Mach-Zehnder modulator (MZM) type is discussed comprehensively, because it allows for chirp-free modulation and better control over both the amplitude and phase of the optical signal than other modulator types or direct modulation [28], [29]. In addition, all modulation formats discussed in this thesis are generated using this modulator.

2.2.2.1 Mach-Zehnder Modulator (MZM)

A MZM made in $LiNbO_3$ material or III – V compound semiconductors has been dominant as a superior optical transmitter for the past 30 years [30]–[32]. With the recent advancement of silicon photonics (SiP), it is favourable that silicon-based modulator confidently outperform the conventional modulator and be widely exploited in the near future [33]–[35]. However their working principle and structure basically remain unchanged. It is interesting to know that at the largest conference in optical fibre communications this year (OFC – 2017), a well-known group of researchers from McGill University has presented a highest reported data rate of 84-Gbaud 4-PAM signal for short-reach optical interconnects using three types of SiP modulator structure [4].

A schematic of a dual-drive MZM is shown in Fig. 2.1. The light from a LD, $E_{in}(t)$ is divided by a 3 dB coupler into two equal parts that propagate in the lower and upper arms of the MZM. Two electrical drive voltages controlled independently are applied to the modulator.

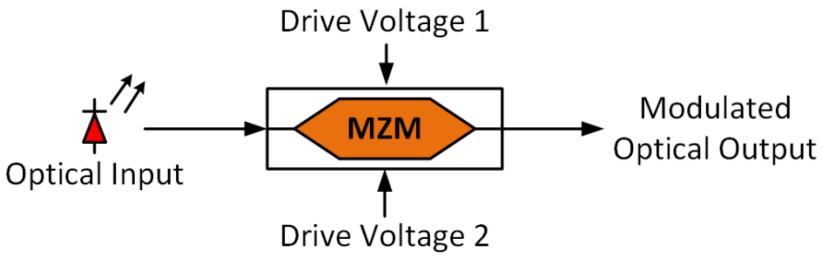


Figure 2.1: Dual-drive Mach-Zehnder modulator.

The relationship between optical input and output is defined as [31], [36], [37]

$$E_{out}(t) = \frac{E_{in}(t)}{2}\left[exp\left(j\frac{\pi}{V_\pi}\left(v_{rf,1}(t) + V_{b1}\right)\right) + exp\left(j\frac{\pi}{V_\pi}\left(v_{rf,2}(t) + V_{b2}\right)\right)\right] \quad (2.1)$$

where V_π is the parameter to indicate the drive voltage required to change the output light intensity from its maximum to a minimum level. $v_{rf,1}$ and $v_{rf,2}$ are the electrical drive voltages applied to two arms respectively. V_{b1} and V_{b2} are the corresponding direct current (DC) bias voltages. When the modulator is operated in a differential mode in which V_{b1} is the reverse of V_{b2} for any bias voltage value, Eq. 2.1 then reduces to [38]

$$E_{out}(t) = E_{in}(t)cos\left[\frac{\pi}{2V_\pi}\left(v_{rf,1}(t) - v_{rf,2}(t) + 2V_{b1}\right)\right] exp\left[j\frac{\pi}{2V_\pi}\left(v_{rf,1}(t) + v_{rf,2}(t)\right)\right] \quad (2.2)$$

The dual-drive MZM allows for both optical amplitude and optical phase modulation depending on the relationship between drive voltages. If the voltages are chosen equal, i.e $V_{b1} = V_{b2}$, the MZM is then operated in *push-push mode*. Setting the voltages equal but with opposite site, i.e $V_{b1} = -V_{b2}$, the MZM is activated in *push-pull mode* allowing for chirp-free amplitude modulation. Due to this flexibility and the possibility for integration, the MZM is widely exploited for the generation of various intensity and phase modulation formats [38]–[40].

2.3 Performance Evaluation Metrics

In digital optical transmission systems, many techniques to measure the performance of a system were developed. These can be used to compare system design trade-offs or the effect of transmission impairments on the overall system. In this section, several important metrics used systematically are introduced

and described in order to compare the difference between modulation formats such as bit-error rate, Q-factor, receiver sensitivity, chromatic dispersion tolerance, self-phase modulation, spectral efficiency and eye diagram. A brief explanation for each parameter is given in the following.

2.3.1 Bit-Error Rate (BER) and Q-factor

The fluctuating optical signal caused by all kinds of impairments in fibre link is received by receiver, which converts optical signal to electrical signal. The electrical signal is fed into an error detector, which contains a decision circuit to sample the signal and compares to the transmitted data patterns. The BER evaluation is a straighforward and relatively simple method for performance estimation based on the technique called direct error counting by comparing the input and output digital streams. When the number of errors is known, the BER can be defined as

$$BER = \frac{Number\ of\ errors}{Number\ of\ transmitted\ bits} \tag{2.3}$$

Thus, a BER of 8×10^{-6} corresponds to an average 8 errors per million bits.

Another technique for BER calculation can be based on the probability of incorrect identification of a bit by the decision circuit of the receiver [10], [41], [42]. The error probability is given by

$$BER = p(1)\,\mathrm{P}(0/1) + \mathrm{p}(0)\,\mathrm{P}(1/0) \tag{2.4}$$

where $p(1)$ and $p(0)$ are the probabilities of receiving bits '1' and '0' respectively. $\mathrm{P}(0/1)$ is the probability of deciding '0' when '1' is received, and $\mathrm{P}(1/0)$ is the probability of deciding '1' when '0' is received. Since 1s and 0s are equally likely to occur ($p(1) = p(0) = 0.5$), then the BER becomes

$$BER = \frac{1}{2}[\mathrm{P}(0/1) + \mathrm{P}(1/0)] \tag{2.5}$$

Assuming a Gaussian noise distribution for both 'zeroes' and 'ones', the conditional probabilities $\mathrm{P}(0/1)$ and $\mathrm{P}(1/0)$ are given by

$$\mathrm{P}(0/1) = \frac{1}{\sigma_1\sqrt{2\pi}} \int_{-\infty}^{I_D} \exp\left(-\frac{(I-\mu_1)^2}{2\sigma_1^{\,2}}\right) dI = \frac{1}{2} erfc\left(\frac{\mu_1 - I_D}{\sigma_1\sqrt{2}}\right), \tag{2.6}$$

$$\mathrm{P}(1/0) = \frac{1}{\sigma_0\sqrt{2\pi}} \int_{I_D}^{\infty} \exp\left(-\frac{(I-\mu_0)^2}{2\sigma_0^{\,2}}\right) dI = \frac{1}{2} erfc\left(\frac{I_D - \mu_0}{\sigma_0\sqrt{2}}\right), \tag{2.7}$$

where $\sigma_{1,0}$ and $\mu_{1,0}$ are the corresponding standard deviations and means for 1s and 0s respectively of the eye diagram as displayed in Fig. 2.2, and $erfc$ stands for the complementary error function and can be approximately defined as

$$erfc(x) = \frac{2}{\sqrt{\pi}} \int_{x}^{\infty} \exp\left(-y^2\right) dy \tag{2.8}$$

By substituting Eqs. (2.6) and (2.7) in Eq. (2.5), the BER is given by

$$BER = \frac{1}{4}\left[erfc\left(\frac{\mu_1 - I_D}{\sigma_1\sqrt{2}}\right) + erfc\left(\frac{I_D - \mu_0}{\sigma_0\sqrt{2}}\right)\right] \tag{2.9}$$

Eq. (2.7) shows the dependence of BER on the decision threshold I_D. The optimum BER occurs when I_D is chosen such that

$$\frac{(I_D-\mu_0)^2}{2\sigma_0^2}=\frac{(\mu_1-I_D)^2}{2\sigma_1}+\ln\left(\frac{\sigma_1}{\sigma_0}\right) \tag{2.10}$$

The last term in this equation is negligible in most cases of practical interest. I_D can then be obtained as

$$I_D=\frac{\sigma_0\mu_1+\sigma_1\mu_0}{\sigma_0+\sigma_1} \tag{2.11}$$

Assuming that $\sigma_0=\sigma_1$ which yields $I_D=(\mu_0+\mu_1)/2$ corresponding to setting the decision threshold in the middle of the eye diagram as shown in Fig. 2.2. The intersection point of both BER curves indicates the optimum threshold I_D and the minimum BER depends only on the Q-factor as

$$BER=\frac{1}{2}erfc\left(\frac{Q}{\sqrt{2}}\right)\approx\frac{\exp\left(-Q^2/2\right)}{Q\sqrt{2\pi}} \tag{2.12}$$

With $Q\equiv(I_D-\mu_0)/\sigma_0=(\mu_1-I_D)\sigma_1=|\mu_1-\mu_0|/\sigma_1+\sigma_0$. The BER improves as Q-factor increases.

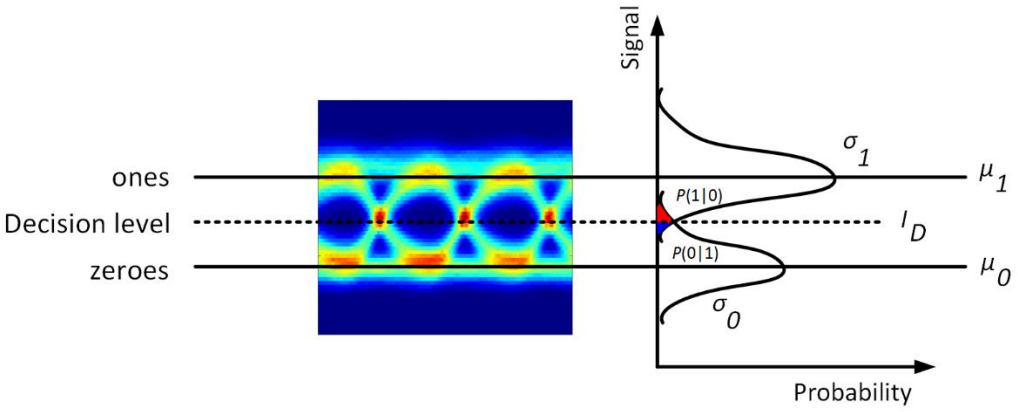


Figure 2.2: A received NRZ signal with its histogram.

In general, BER of 10^{-9} is considered to be error-free and indicates the measurement of a minimum of 10 errors for a total of 10^{10} sampled bits. The Q-factor can be quoted in decibels using the conversion $10\times\log(Q^2)$, and a BER of 10^{-9} corresponds to a Q-factor of 6 or 15.56 dB. This relationship between BER and Q-factor is useful in the comparison of numerical simulations and experimentally measured results. It is clear that in order to measure a BER of 10^{-9} numerically would require a minimum simulation of 10^{10} bits, which is significantly time-consuming. As such, the numerical simulations described in this thesis, quantify system performance based on the Q-factor, and use a pattern length of 2^{10} bits to reduce the computing time. This was shown to be sufficient for accurate modelling of 40-Gbit/s transmission [43]–[45].

2.3.2 Receiver Sensitivity

An important parameter to indicate the receiver performance in an optical transmission system is called the receiver sensitivity. It is usually stated as the minimum average received optical power for which the BER of the optical receiver is 10^{-9}. A receiver is considered to be more sensitive if it achieves the same performance with less required power. The receiver sensitivity can be degraded due to the fibre dispersion as well as various noise sources that lead to power penalties and depend on both the bit rate and the fibre length. The power penalty is defined as the difference of receiver sensitivity at 10^{-9} BER between back-to-back (B2B) and transmission circumstance as described by the following expression:

$$\begin{aligned}\text{Power penalty [dB]} &= \text{Receiver sensitivity (B2B)} \\ &- \text{Receiver sensitivity (transmission)}\end{aligned} \tag{2.13}$$

2.3.3 Chromatic Dispersion

The CD in single-mode transmission fibre represents one of the most important performance limitations in today's transmission systems, resulting in a reduced maximum transmission distance and a poor quality of transmitted signals. The impact of chromatic dispersion becomes even larger with systems upgrade to higher channel bit rates (>10-Gb/s).

The basic physics of CD is the frequency dependence of the refractive index of the fibre $n(\omega)$. Since $v_g(\omega) = c/\, n(\omega)$, with c is the velocity of light at frequency ω is dependent on its refractive index in the transmission media. This phenomenon is also known as *group velocity dispersion* (GVD), since the dispersion is the result of the group velocity being a function of the wavelength. It causes different wavelengths (frequencies) to travel at different velocities leading to the spectral components of different pulses overlap due to such pulse broadening and thus to ISI effect as illustrated in Fig. 2.3.

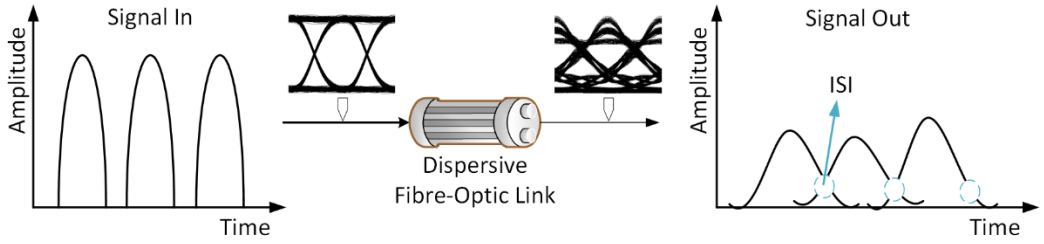


Figure 2.3: Illustration of CD causes pulses to spread into adjacent bit slots. The broadening of pulses due to CD leads to optical eye closure.

To better understand the fibre dispersion, assuming $\Delta\omega$ is the spectral width of a pulse going through a fibre of length L. The different spectral components arriving at different times at the fibre output result in pulse broadening given by [10]

$$\Delta T = L\beta_2\Delta\omega \tag{2.14}$$

The factor $\beta_2 = d^2\beta/d\omega^2$ is the GVD parameter, which provides a measure of how much a pulse broadens in time, as the pulse travels along an optical fibre and β is the mode propagation constant. The spectral width can also be represented by the range of wavelength $\Delta\lambda$ emitted by the optical source. In this case, the equation given above can be rewritten as

$$\Delta T = DL\Delta\lambda \tag{2.15}$$

where the factor $D = \frac{-2\pi c}{\lambda^2}\beta_2$ is called the *dispersion parameter* and is expressed in units of ps/(km.nm).

Fibre types with positive dispersion ($D > 0$) are sometimes referred to as anomalous dispersion, and fibre with negative dispersion ($D < 0$) is understood to exhibit normal dispersion [10], [46], [47]. The latter is used to enable cancellation of accumulated dispersion as discussed later. Systems operating in 1.3 μm band would have very small dispersion effects or also known as zero dispersion wavelength but fibre loss (attenuation) limited. As a result, there is a gigantic interest in today's optical communication systems that operate in 1.55 μm wavelength window due to the low loss (~0.2 dB/km) in this region and the well-developed erbium-doped fibre amplifier (EDFA) technology [10], [48]. However in this band, communications is chromatic dispersion limited.

Given that in this research, numerical simulations and experimental measurements, single channel transmission with a central wavelength of 1.55 μm is considered. In this band the corresponding dispersion parameter of the standard SMF is in the range between 15.5 and 17.8 ps/(km.nm) which remains a major limitation. Therefore compensating the accumulated dispersion is the most attractive topic in current research and development nowadays [49]–[52]. A system is said to be more tolerant to CD, if less extra power is required at the receiver in order to keep the same performance compared to B2B scenario for certain amount of fibre length travelled.

2.3.4 Self-Phase Modulation

It is reasonable to treat the optical fibre as a linear medium, as long as the fibre is being utilised at an adequate power level (a few mW). Nevertheless when launching a sufficiently high transmitted power into the optical fibre in high bit-rates systems e.g. >10-Gb/s, nonlinearity turn out to be a vital issue which can adversely limit on the system performance. For WDM networks, the nonlinear effects become more serious even at moderate powers and bit rate due to the intra- and inter-channel nonlinearities arising among neighbouring wavelengths [10], [53]–[55]. Since the scope of this study is on single wavelength transmission systems, these unfavourable aforementioned aspects can be neglected.

Self-phase modulation (SPM) is one of the nonlinear limitations instigated by the optical Kerr effects and occur in a single channel transmission due to the self-induced nonlinear phase modulation phenomenon. The physical origin of this effect stems from the high level input power temporarily changes the refractive index of the optical fibre. Nonlinear refraction as a result is accounted for by modifying the refractive index [10]

$$n' = n + n_2 \frac{P}{A_{eff}} \tag{2.16}$$

where n is the linear refractive index, n_2 is the nonlinear-index coefficient of silica fibre is 2.6×10^{-20} m^2/W, A_{eff} is the effective core area.

The refractive index n is dependent and directly proportional to the signal power, P. As a result of the intensity-dependent refractive index, the propagation constant also becomes intensity dependent

$$\beta' = \beta + \gamma P \tag{2.17}$$

where $\gamma = 2\pi n_2/(A_{eff}\lambda_0)$ is the nonlinearity coefficient depending on the effective core area and the signal wavelength λ_0.

For standard SMF, a typical value of γ is 1.31 $W^{-1}km^{-1}$. The nonlinear phase shift produced by γ term is given by

$$\emptyset_{SPM} = \gamma P_{in} L_{eff} \tag{2.18}$$

where $L_{eff} = \frac{(1-e^{-\alpha L})}{\alpha}$ is the fibre effective length, P_{in} is the input signal power and α is the fibre loss [10].

The nonlinear phase shift $\emptyset_{SPM}$ varies with time across a pulse dependent on input power P_{in} and causes optical phase changes with time. SPM can be a serious limiting factor for lightwave systems since it often combines with dispersion would lead to additional pulse broadening and exacerbate the performance [45], [55]–[58].

2.3.5 Spectral Efficiency

Increasing the spectral efficiency is essential in fibre optics since higher spectral efficiency is of help to reduce number of wavelengths; especially single channel high-speed systems offer a small footprint and lower power consumption [59], [60]. The spectral efficiency is given as

$$Spectral\ Efficiency = \frac{C_c}{\Delta f} \tag{2.19}$$

where Δf is the channel spacing and C_c is the capacity per channel (bit/s). Spectral efficiency is therefore expressed in units of b/s/Hz.

So, in the search for high spectral efficiency, the use of multilevel modulation formats may be an effective solution since two or more bits are

carried by each transmitted pulse or symbol. Lower signal spectral width is thus attained at high bit rates in comparison to binary schemes.

2.3.6 Eye Diagram

Eye diagram is a very successful methodology of quickly and intuitively assessing the performance of an optical receiver for both numerical simulations and experimental measurements. It is also very useful to compare the transmission performance of various modulation formats or after different lengths of fibre.

The closing of the eye is a quick measure of degradation in receiver performance and is associated with a corresponding increase in the BER as exhibited in Fig. 2.4 (a). On the contrary, clear eye opening indicates the improvement in signal quality and lower BER (Fig. 2.4 (b)). Based on the eye patterns, other system performance parameters such as pulse raise/fall time, duty cycle, extinction ratio, jitter, eye height/width and crossing percentage could also be achieved.

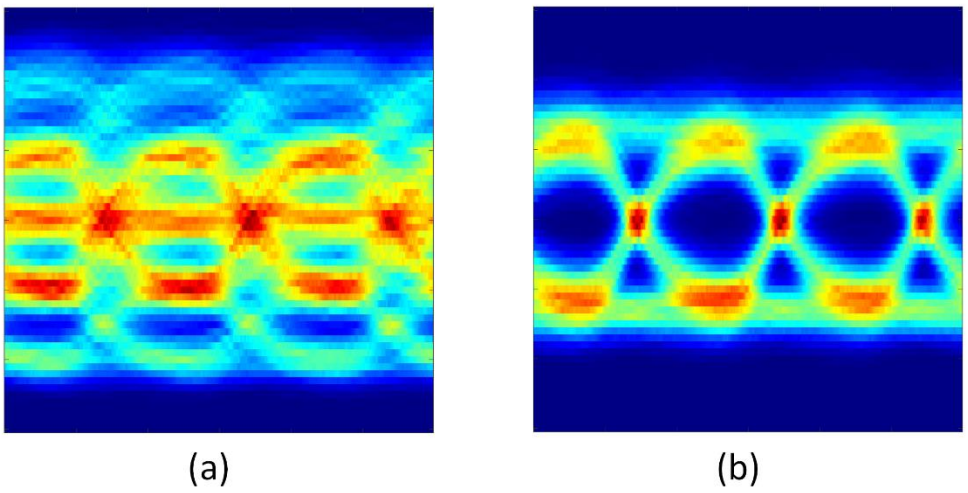


Figure 2.4: Example of typical NRZ eye diagrams to determine the signal quality. (a) A closure of the eye reveals the system imperfections or impairments. (b) An open eye corresponds to minimal distortion of the signal.

2.4 Advanced Modulation Formats

An optical modulation format is a way of applying an electrical data stream to an optical carrier signal. A great deal of research has been carried out in the subject of optical advanced modulation formats, especially on higher-order signalling over the past decade by transmitting more information in the amplitude, polarisation or a combination of all to boost the transmission capacity [16], [17], [52], [61]–[68]. Currently scientists from both academia and industry have been intensively studying on new candidates of modulation formats or advanced data encoding schemes not only cover the aforementioned characteristics but also feature a high resilience to different optical impairments such as fibre chromatic dispersion [16], [18], [25], [44], [52], [69]–[75]. That is to say, that much effort has been made are within the context of extending link distances. These newly proposed schemes however may add further complexity to the transmitter and receiver hardware of the optical transmission systems.

In this section, several mainstream optical modulation formats such as NRZ, duobinary and 4-PAM are introduced. Their generation and properties are also discussed. It is worth noting that this research only focuses on intensity modulation and direct detection (IM/DD)-based formats due to their dominance in today's optical short range, access and metro networks. These modulation formats are also used as a base to generate more advanced higher-order schemes.

2.4.1 Non-Return-to-Zero (NRZ)

Non-return-to-zero (NRZ) has been the dominant modulation format for fibre-optical communication systems [48], [76]–[79]. The name of this modulation formats denotes two light amplitude states that are utilised to carry this binary data (i.e. On and Off). In the field of radio and cable telecommunications, this modulation format is synonymously known as binary amplitude shift keying (2-ASK). There are several reasons for using NRZ in the early days of optical communications. First, it requires a low electrical bandwidth for the

transceivers (compared to return-to-zero (RZ)); second, it is not sensitive to laser phase noise (compared to phase shift keying (PSK)); and last, it has the simplest configuration for the transmitter and receiver. Considering recent advancements in optical communication field, NRZ modulation format may not be the best choice for future high capacity optical networking systems. However, it has been widely deployed in field and due to its simplicity and its historic dominance, NRZ would be a good reference for the comparison.

The most common technique to generate the optical NRZ signal is externally modulating the laser signal from a LD using a MZM as depicted in Fig. 2.5 (intensity modulation). The MZM should be biased at quadrature point, and driven by an electrical NRZ signal. The optical NRZ signal can be merely detected and converted into electrical signal by using a single photodiode (PD) at the receiver [49], [80]–[82]. This is called direct detection. The measured eye diagram of binary NRZ is also shown in Fig. 2.6.

As an oldest binary modulation format, NRZ has a bandwidth equal to twice the bit rate ($2R_b$), where the bandwidth is defined as the null-to-null bandwidth of the main lobe spectrum. This results in a poor spectral efficiency and low tolerance to chromatic dispersion in comparison to the multilevel signalling that is discussed throughout this thesis.

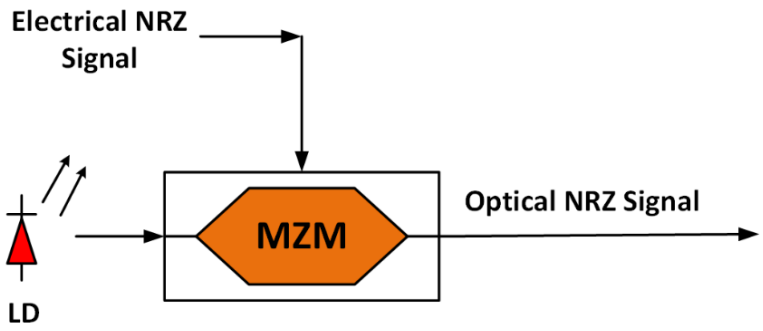


Figure 2.5: Structure of a MZM-based NRZ generation.

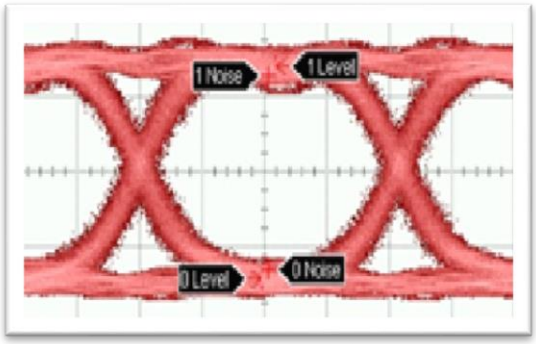


Figure 2.6: Measured NRZ eye diagram.

2.4.2 Duobinary

Waveform distortion due to fibre chromatic dispersion in optical communications systems is a vital problem. Optical duobinary scheme also known as phase-shaped binary transmission (PSBT) belong to a class of correlative coding formats is an effective way to avoid such distortions resulting in a significantly enhanced dispersion tolerance compared to NRZ signal [30], [45], [83], [84]. In fact, duobinary modulation is spectrally efficient because of the narrow occupied spectral bandwidth which is about half of the conventional binary NRZ [85]–[87]. It is thus beneficial for ameliorating the effects of fibre dispersion, as well as reducing adjacent channel crosstalk in dense wavelength-division multiplexing (DWDM).

A practical approach of generating electrical duobinary signal is shown in Fig. 2.7, which consists of a duobinary filter to convert the electrical binary NRZ signal into three-level signalling. A duobinary filter can be realised by an-either-or option. The first technique is to use a low-pass filter (LPF) with cut-off frequency of around $R_b/4$, where $R_b = 1/T$ and T is the symbol duration [9], [30], [83], [88]. This LPF acts as an analog converter, which simultaneously converts from binary to duobinary and trims high-frequency components in the duobinary signals spectrum. The second technique is to employ a delay and add block [37], [87], [89]. The correlation between the adjacent bits that is introduced by the delay and add circuit leads to a reduction in the bandwidth of the optical signal. Duobinary signal generated by the delay and add circuit generally enjoys an enhanced receiver sensitivity in B2B scenario since it has a

better eye opening while carefully selected LPF improves further the chromatic dispersion tolerance since it suppresses the optical spectrum side-lobes better than the delay and add method [29]. To generate an optical duobinary signal, a MZM biased at null and driven by the electrical duobinary signal. At the receiver, a simple NRZ decoder can be used to detect the received duobinary signal [87].

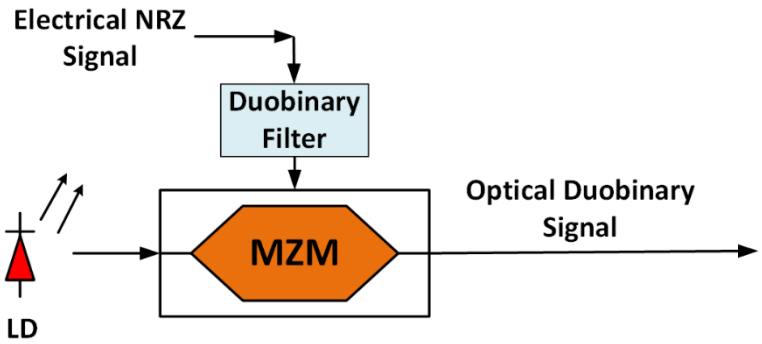


Figure 2.7: Principle of Duobinary modulation using MZM.

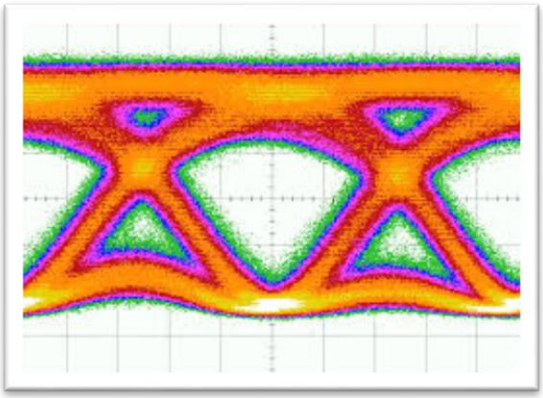


Figure 2.8: Measured Duobinary eye diagram.

The eye diagram of the duobinary signal is depicted in Fig. 2.8. The "narrow steep space valley" also known as "ripples" on the space level ('0') can give an indication about the B2B power penalty in comparison to its NRZ counterpart. This feature is discussed in detail in Chapter 7.

2.4.3 4-ary Pulse Amplitude Modulation (4-PAM)

With the ever increasing demand for higher line rates, multilevel modulation has been scrutinised as one of the approaches to scale the data rate of optical interfaces without increasing the number of wavelengths [8], [90]–[92]. Recently M-level pulse amplitude modulation (M-PAM), especially 4-PAM has attracted considerable interest for optical interconnect links as well as access networks as it can double the data rate [93]–[99]. In M-PAM, the number of levels required for each transmitted symbols is $M = 2^n$, where n is the number of bits transmitted for each symbol. If the number of bits transmitted for each symbol is two ($n = 2$), then an electrical 4-PAM signal is generated. This electrical 4-level intensity modulation can be used to drive an optical MZM that biased at the quadrature point resulting in the generation of an optical 4-level intensity modulation signal.

In practice a conventional electrical 4-PAM signal is generated by adding two electrical binary signals with unequal amplitude. In order to obtain an equally spaced electrical 4-PAM signal, the amplitude of one of the electrical binary NRZ signal is halved by using an electrical attenuator with 6 dB attenuation, then combined with second electrical binary NRZ signal via an electrical adder (or power combiner) as illustrated in Fig. 2.9.

An advantage of using optical 4-PAM signal is that it needs electrical and optical components operating at half the bit rate when compared to a binary NRZ signal operating at the same bit rate, which may reduce the cost of an optical transmission system. This cost reduction is because lower bandwidth devices are usually having lower cost.

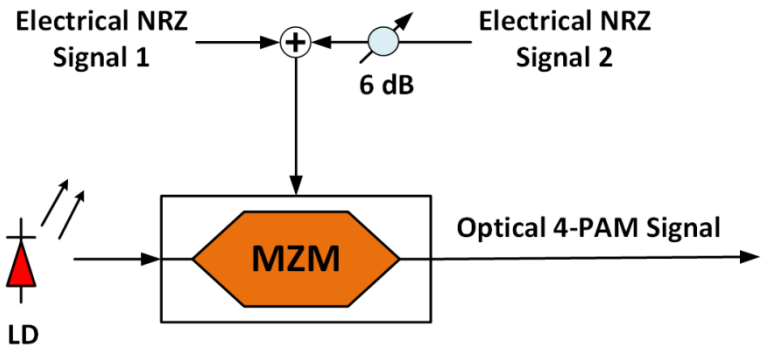


Figure 2.9: Optical 4-PAM generation based on MZM.

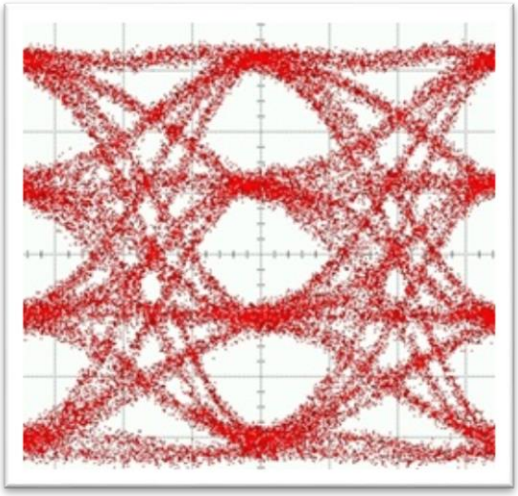


Figure 2.10: Measured 4-PAM eye diagram.

The measured eye diagram of 4-PAM is shown in Fig. 2.10 which consists of three smaller eye patterns (top, middle and bottom eyes). Since this is an intensity signalling, a single PD (direct detection) can be used at the receiver to convert the optical 4-PAM modulated signal into a 4-ary electrical signal. Different from NRZ and duobinary decoding, 4-PAM receiver requires a suitable decision circuit which to recover itself into two original transmitted NRZ signals for BER calculation. A more detailed explanation of this decoding algorithm is given in Chapter 3.

It is obvious that 4-PAM signal has a narrower spectrum than the NRZ signal resulting in an improved spectral efficiency and chromatic dispersion which can be useful in WDM optical networks. However the up-to-date results analysed in [100], [101] have revealed that 4-PAM is not superior to duobinary

signal with respect to the forbearance to fibre dispersion. In particular employing duobinary signal at the transmitter would be more effective in extending the transmission distance. This event could be attributed to the multilevel characteristics of 4-PAM signal as well as the fragmentation of the main eye diagram. At the same received optical power, these small eyes have different qualities; thus resulting in worst performances, which is not desirable in telecommunication systems. In fact, the top eye (symbols '2' and '3') is the factor that instigates higher system performance degradation which leads to low Q-factor as demonstrated in [43], [72].

Table 2.1: Comparison of NRZ, Duobinary and 4-PAM formats [101].

Modulation Format	Symbol Rate (bit/symbol)	Spectral Efficiency (b/s/Hz)	Dispersion Tolerance	Cost
NRZ	1	0.5	Low	Low
Duobinary	1	1	High	High
4-PAM	2	1	Medium	High

Table 2.1 summarises the key parameters of each modulation formats for comparison. Improving the dispersion tolerance as known as extending further the transmission distance for NRZ and 4-PAM is of great interest to researchers. The latter technique should be given preference since it could double the actual signalling rate compared with that of the former aiming for the next-generation high-speed extended-reach optical transmission systems. Next section introduces several techniques on mitigating the chromatic dispersion induced signal distortion for NRZ and 4-PAM schemes that have recently attracted great interest from both the research community and the commercial sector.

2.5 Chromatic Dispersion Compensation Techniques

The dispersion parameter of standard SMF, which represents the majority of deployed fibre in the field, is normally about 17 ps/(km.nm). The ISI caused by such a substantial amount of dispersion is certainly a limiting factor for transmitted data (*how fast*) or maximum link reach (*how far*). Consequently, CD compensation has been one of the most dynamic research fields in optical communications for a long time. This section considers three techniques to compensate the CD accumulation including one conventional method and two alternative approaches.

2.5.1 Dispersion Compensation Fibre (DCF)

The most common method to compensate for the chromatic dispersion is to cancel the accumulated dispersion after a certain SMF transmission length by mean of a particular kind of fibre, namely DCF [10], [11]. The DCF is characterised by a large negative dispersion and can be used for simultaneous compensation of several channels. Enabling the full dispersion cancellation of using DCF is straightforward by taking the advantage of linear nature of CD with the following rule:

$$D_{SMF}L_{SMF} = -D_{DCF}L_{DCF} \tag{2.20}$$

where D_{SMF} , D_{DCF} are the chromatic dispersion values of SMF and DCF, respectively. L_{SMF} , L_{DCF} are the lengths of these fibres. This rule can be executed by locating the DCFs in different positions within an optical link [45], [56].

Although DCF is widely used in commercial systems, it is expensive, bulky. It also lacks adaptability and introduces high attenuation losses which decrease the power budget of the system; therefore an optical amplifier is usually

needed for power loss compensation. However DCF still plays an important role in optical metro networks and long-haul transmission infrastructures [16], [63].

In the next subsection, two completely different approaches to compensate the fibre transmission impairments are presented. They are less costly and suitable solutions in current research on optical short-range and access networks on NRZ and 4-PAM signals.

2.5.2 Optical Equalisers

In DD systems, OEQs have been found not only to be more effective than electronic equalisers, but also to uniquely provide dispersion compensation across all wavelength channels in WDM systems since it deals directly with them in optical domain [15], [23], [102]–[104]. Simple colourless OEQs which were proposed in 2003 [105] still attract considerable research interest since it can alleviate the ISI in 40-Gb/s NRZ systems due to its narrow-band optical filtering, uncompensated dispersion as well as polarisation mode dispersion [102]. These devices have been used not only for equalising the waveform distortions due to the fibre dispersion and the bandwidth limitation of the MZM [106], the reflective semiconductor optical amplifier (RSOA) [104], [107]–[109] and the DML [15], [23], [103], [110] but also in reducing fibre nonlinearities such as self-phase modulation, cross-phase modulation and four-wave mixing [54], [111], [112]. More recent OEQ development includes monolithic integration with a silicon in-phase/quadrature (I/Q) modulator on the same chip that boosted the modulation bandwidth and enhanced the BER performance [113]. Latest research approach on optical equalisation technique is the utilisation of an optimised silicon micro-ring resonator (MRR) that integrated into the DML to optimise the extinction ratio and optically pre-compensate the dispersion [50]. Its fruitful results have been achieved with an error-free NRZ transmission over 2.5-km of SMF at 25-Gb/s [50]. It is promising that 4-PAM scheme would be the next target for doubling the link capacity in this system.

Table 2.2 summarises system demonstrations reported in the literature within the last five years with regard to the data rate per channel and modulation formats that employ OEQ as a technique to mitigate the dispersion-

induced signal distortions. It is worth noting that the OEQ is configured as an optical pre-equaliser, i.e. inserted right after the transmitter, whereas an OEQ configured as an optical post-equaliser if it is inserted right in front of the receiver as shown in Fig. 2.11.



Figure 2.11: The block diagram representing the placement of the OEQ to cancel the accumulated dispersion.

Table 2.2: Summary of transmission systems using optical equalisation techniques and DD receivers within the last 5 years.

Bit rate/λ (Gb/s)	Modulation Format	Modulation Optics	Ref	Year Published
10	NRZ	RSOA	[109]	2013
20	RZ 4-PAM	RSOA	[104], [107]	2016
25	NRZ	DML	[103]	2016
25	4-PAM	DML	[103]	2016
25	NRZ	VCSEL	[13]	2016
25	NRZ	DML	[15]	2017
25	NRZ	MZM	[114]	2017
25	NRZ	DML	[50]	2017
28	Duobinary	DML	[110]	2015
40	NRZ	DML	[115]	2014
40	NRZ	DML	[23]	2014
56	NRZ	MZM	[34]	2017

In order to elucidate the utility of OEQ in equalising the waveform distortions caused by fibre dispersion which resulting in the great extension of maximum transmission distance. The results of our OEQ study on duobinary signal are investigated and presented for the first time in Chapter 7.

2.5.3 Electrical Equalisers

This section discusses another possible solution for compensating fibre propagation impairments is the use of electrical equalisers (EEQ) as known as electronic equalisation, which has become increasingly attractive and been widely employed to assuage the dispersion effect in current research on optical transmission systems [51], [116]–[118]. EEQ in fact has been extremely studied in complementary metal-oxide-semiconductor (CMOS)-based chip-to-chip communications over high-loss electrical channels such as backplane to mitigate the effects of channel loss and other impairments and traditional communications systems (i.e. wireless and wireline system) [119]–[127].

EEQ was proposed to mitigate the effect of transmission impairments such as chromatic dispersion or polarisation-mode dispersion (PMD) in long-haul fibre-optic systems since early 1990s [128]. It has gained significant attention since it can improve the system performance at a small cost premium once they have entered large volumes and development cost is negligible [51], [70]. Latest research on the real-time implementation of EEQ in optical transmission has been demonstrated by a group of researchers from Bell Labs [129]. The authors experimentally applied and studied the on-chip adaptive EEQ, programmable input equalisation from Microsemi to compensate the dispersion effect in optical 4-PAM system at 20-Gb/s. Two other typical modulation formats: NRZ and Duobinary are also investigated in that work.

Another benefit of EEQ to be mentioned is the high adaptability. In general, an EEQ device is not designed to diminish a particular impairment. Its main task is to reduce the ISI effect and equalise the pulse sequence without knowing the causes of it. Hence several reports named this technique as adaptive equalisation [20], [130], [131].

Fig. 2.12 shows the generic arrangement of the EEQ at both the transmitting (pre-EEQ) and receiving side (post-EEQ). The former technique can also be called pre-emphasis or pre-distortion. By definition, pre-distorting the electrical signal in the transmitter pre-compensates the transmitted field for the accumulated dispersion of the transmission link to obtain a desired field at the receiver. The latter solution is currently of preeminent interest for NRZ, duobinary and 4-PAM [8], [9], [15], [24], [67], [97], [103], [116], [132]–[143]. The equalisation processes can also occur by sharing between the pre-emphasis and post-equalisation at the Tx and Rx side to maximise the transmission quality [144]–[147].

Since EEQ can also be implemented off-line based on DSP module [6], [132], [148], [149], therefore it is likely that electronic dispersion compensation is prevalently executed in almost transmissions even at very high data rate e.g. $>$ 100-Gb/s due to its simplicity. However considering the electronic limitations, it is troublesome for real-time EEQ demonstration in very high-speed optical transmission systems.



Figure 2.12: Arrangement of the electrical equalisers in optical transmission systems.

There are several types of EEQ techniques, which can be classified into the following categories. It should be noted that only the receiver-side EEQ is introduced due to its dominance in the recent literature.

- Feed forward equaliser (FFE): this is the most-widely-studied linear equaliser. The FFE filter method is based on a cascade of taped delay line of the input sample. Each tap spacing can be either symbol-spaced or fractionally-spaced. At each delay, the signal is weighted by the tap coefficients or as it is also called tap weights and then summed together to give the output sample. The filtering coefficients of the FFE can be adapted using least-mean square

(LMS) algorithm. Since a linear FFE boosts the noise, a pure FFE is usually less preferable.

- Decision feedback equaliser (DFE): this is a preferred technique to eliminate the post-cursors while using FFE before DFE to compensate the interference from the pre-cursors of the distorted signal. In other words, the equalised signal after FFE experiences further compensation at the DFE which consists of n coefficients and n delay taps. Details of FFE and DFE techniques for direct detection systems can be found in [51], [148], [150].

It is worth mentioning that a vital parameter in adaptive EEQ is the step size μ that is linked with the filter taps weight uploading. High value of μ means faster convergence but lower precision whereas low value of μ bring to slower convergence but higher precision. Also, the more of delay taps used, the more complex of the real-time electronic equalisers.

In Chapter 7, the use of EEQ in improving the transmission performance by equalising the ISI effect is experimentally studied.

2.6 Concluding Remarks

This chapter has covered the theory of optical transmission systems. Also described in this chapter are the generation and properties of those advanced modulation formats that gaining a lot of attention in the current research on IM/DD systems.

There are various performance metrics such as Q-factor, BER, chromatic dispersion, self-phase modulation, spectral efficiency and eye diagram have been comprehensively presented in order to evaluate and compare signal quality. Several dispersion compensation techniques including the conventional and the state-of-the-art ones have also been discussed in this chapter.

Chapter 3– AACC System Model and Performance Metrics

3.1 Introduction

This chapter presents comprehensively the transceiver structure, working principle and data recovery of the proposed multilevel modulation format namely AACC. In this chapter, the performance of AACC signalling with direct detection is analytically reported. Hereby the focus lies on the performance of the BER, noise contributions and spectral efficiency. This chapter also delineates the signal space model of AACC, where the average electrical and optical power expressions are derived for the first time. The signal space analysis is essential since it provides a convenient platform for representation and comparison between modulation formats. The proposed modulation format were also assessed numerically and compared to other well-known signalling such as NRZ at the same bit rate in a directly modulated vertical-cavity surface-emitting laser (VCSEL)-based transmission systems in order to validate the analytical performance. The comparison results show a clear advantage of AACC in achieving longer fibre delivery distance due to the higher dispersion tolerance.

The materials presented in this chapter have been published in:

N. Dong-Nhat, M. A. Elsherif, and A. Malekmohammadi, "Assessment of Absolute Added Correlative Coding in optical intensity modulation and direct detection channels," *Opt. Eng.*, vol. 55, no. 6, p. 66115, 2016.

3.2 AACC Transceiver Model

3.2.1 Transmitter Model

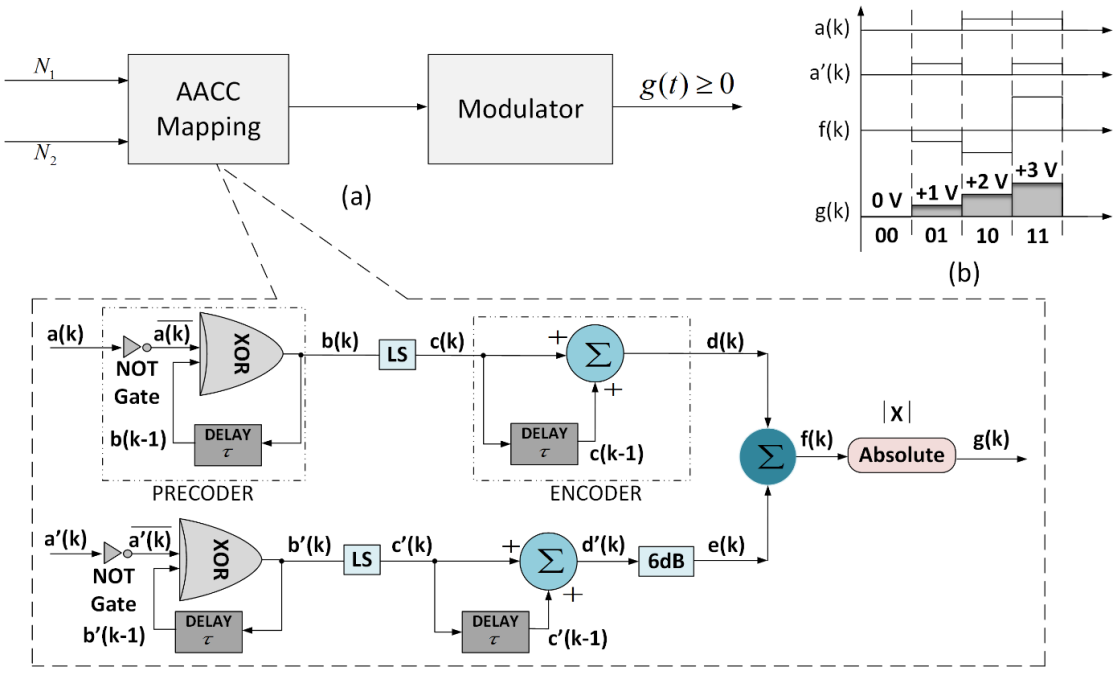


Figure 3.1: AACC concept (a) AACC transmitter model and (b) AACC symbols.

Fig. 3.1 (a) shows a general transmitter model of AACC format that based on partial response signalling (otherwise called as correlative coding) in electrical domain. In fact, the electrical AACC signal can be obtained by adding two unequal-amplitude duobinary tributaries via an electrical adder resulting in a multilevel bipolar signal which is symmetrical with respect to zero amplitude. The principle of duobinary generation has been discussed in Chapter 2. The process ends by taking the absolute value of the generated multilevel bipolar signal, which is a unique positive polarity symbol for each case by employing the absolute circuitry. By operating this way, the transmitted pulse is basically distorted, it is therefore promising that AACC signal enjoys the pre-distortion feature making itself robust to dispersion. In addition, having the knowledge of this unique approach of generating AACC signal, decision circuit and data recovery rules can be formed at the receiving side for BER estimation.

The transmitter is composed of two paths (N_1 and N_2) that comprise two binary data known as *a(k)* and *a'(k)*. The first path consists of a precoder, a level shifter (LS) and an encoder. The encoder at the transmitter side scrambles the original binary data; hence an electrical precoder which contains a logic NOT gate, a logic XOR gate with a one-bit delay/feedback loop is needed to avoid error propagation and eases hardware complexity for decoding at the receiver. The precoding function can be expressed as

$$b(k) = \overline{a(k)} \oplus b(k-1) \tag{3.1}$$

With

$b(k) = 1$ if either $\overline{a(k)}$ or $b(k-1)$ is 1

$b(k) = 0$ otherwise

where *a(k)* is the transmitted binary input bit stream, *b(k)* is the pre-coded binary sequence and $\oplus$ is the logic XOR gate.

The sequence *b(k)* is applied to the LS. All the output of the LS, *c(k)* is bipolar. In fact, if *b(k)* = 1 V or 0 V resulting in *c(k)* = 1 V or -1 V respectively. The sequence *c(k)* is then passed to an encoder which operates as an electrical one-bit delay-and-add filter. The main purpose of this encoding process is to convert an electrical binary signal to a normalised three-level electrical signal. The value of *d(k)* = 0 V if *a(k)* = 0 V and *d(k)* = $\pm$2 V if *a(k)* = 1 V. In other words, by implementing the addition of the current bit to the previous bit results in an electrical ternary voltage signals (-2 V, 0 V, 2 V). This relation is found as

$$d(k) = c(k) + c(k-1) \tag{3.2}$$

where *d(k)* is the encoded bipolar three-level signal and *c(k)* is the level-shifted binary stream.

A similar procedure is for the second path, but inserting a 6 dB electrical attenuator to reduce its power by half for achieving an equidistant 4-level

signalling. As illustrated in Fig. 3.1, the output voltage of AACC signal *g(k)* is given by

$$g(k) = |f(k)| = |d(k) + e(k)| \tag{3.3}$$

Table 3.1: Transmitted and received bit stream for AACC modulation.

k	-1	0	1	2	3	4	5	6	7
a(k)		0	1	0	1	1	0	0	1
$\overline{a(k)}$		1	0	1	0	0	1	1	0
b(k)	0	1	1	0	0	0	1	0	0
c(k)	-1	1	1	-1	-1	-1	1	-1	-1
d(k)		0	2	0	-2	-2	0	0	-2
a'(k)		0	1	0	1	0	0	1	1
$\overline{a'(k)}$		1	0	1	0	1	1	0	0
b'(k)	0	1	1	0	0	1	0	0	0
c'(k)	-1	1	1	-1	-1	1	-1	-1	-1
d'(k)		0	2	0	-2	0	0	-2	-2
e(k)		0	1	0	-1	0	0	-1	-1
f(k)		0	3	0	-3	-2	0	-1	-3
g(k)		0	3	0	3	2	0	1	3

Table 3.1 distinctly clarifies the transmitted and received bit pattern of AACC modulation. In fact, the process of how a binary input data (0 V, 1V) is converted to ternary levels (-2 V, 0 V, 2 V) and (-1 V, 0 V, 1 V) and then to quaternary-level signal (0 V, 1 V, 2 V, 3 V) is presented. The intensity levels are equidistant and nonnegative, which are favourable in intensity-modulated direct-detection links [151]–[154]. It is worth noting that the constellation point

of AACC is different to 4-PAM whose amplitude levels is (-3 V, -1 V, 1 V, 3 V). For differential precoding and encoding, a reference bit is vital to initiate the process. This reference bit could be arbitrarily set to either logic "1 V" or logic "0 V". In Table 3.1 the reference bit *b(k)* and *b'(k)* at the time instant k = -1 V were set to logic "0 V". Note that the impulse shaping used in the AACC transmission can be either NRZ or RZ Gaussian edge shapes which are represented as [155]

$$E_{NRZ}(t) = \begin{cases} e^{-(t/c_r)^2}, & 0 \le t \le t_1 \\ 1, & t_1 \le t \le t_2 \\ e^{-(t/c_f)^2}, & t_2 \le t \le T \end{cases} \tag{3.4}$$

$$E_{RZ}(t) = \begin{cases} 1 - e^{-(t/c_r)^2}, & 0 \le t < t_1 \\ 1, & t_1 \le t < t_2 \\ e^{-(t/c_f)^2}, & t_2 \le t < t_c \\ 0, & t_c \le t < T \end{cases} \tag{3.5}$$

where c_r and c_f are the rise time coefficient and the fall time coefficient respectively. The parameters t_1 and t_2 together with c_r and c_f are numerically determined so that pulses with the exact values of the rise time and fall time can be generated, and T is the bit period.

Fig. 3.1 (b) shows a waveform representation of the output signal for each block of the AACC transmitter. In other words, it illustrates two input bits are bound together to form a symbol, which then mapped to a unique voltage amplitude to form 4-level AACC signalling.

The signal is then modulated by a modulator for processing the electro-optical conversion and sending out the optical AACC signal ($g(t)$) into a dispersive optical channel which is single-mode fibre (SMF) or multi-mode fibre (MMF) links.

3.2.2 Receiver Model

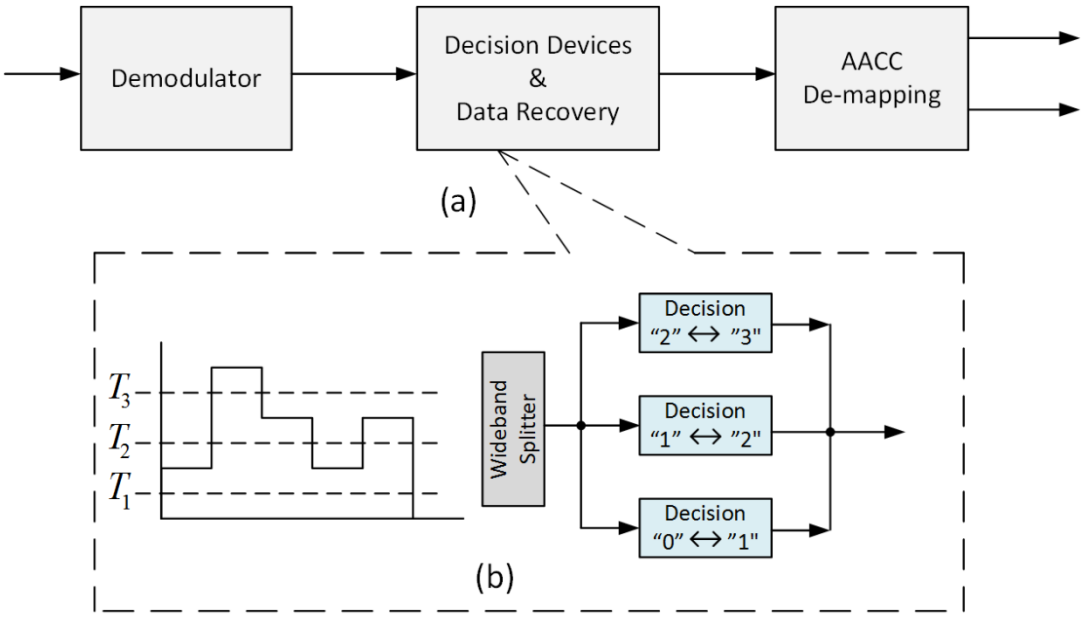


Figure 3.2: (a) AACC receiver and (b) Anatomy of a decision module algorithm.

As shown in Fig. 3.2 (a) once the optical AACC signal reaches its destination, it is then converted back to the electrical signal thanks to the demodulator which is the PIN or avalanche photodiode (APD) in real-world demonstration.

Since it is a 4-level intensity signal, three optimal threshold values are required in order to clearly determine its symbols prior to de-mapping it into two streams of binary data and compare with *a(k)* and *a'(k)* for BER calculation. Details of estimating the BER is discussed in Section 4.2.

3.2.3 Signal Space Model

AACC signal is a nonnegative four-level modulation scheme consisting of four symbols that depend upon one orthogonal time slot. Therefore it is often convenient to represent a set of finite-energy digital signals by a corresponding set of vector space components based on the Gram-Schmidt procedure [127]. Assuming that these signals are transmitted at every T_s seconds, where T_s is the

signalling interval (symbol duration). This means that in each second $R_s = {}^{1}/_{T_s}$ is transmitted, where R_s is called the signalling rate or symbol rate.

$$R_b = log_2 K \times R_s \tag{3.6}$$

where K is the number of levels of AACC-based signalling. For AACC modulation, K is equal to 4. In addition, AACC signal carries 2 bits/symbol; thus the bit interval T_b in which 1 bit of information transmitted is represented as

$$T_b = \frac{T_s}{2} \tag{3.7}$$

In optical intensity modulation and direct detection channels, the transmitted signal must satisfy the nonnegativity constraint. Hence the basis function for AACC can be expressed as

$$\phi_{AACC}(t) = \frac{1}{\sqrt{T_s}} rect\left(\frac{t}{T_s}\right) \tag{3.8}$$

where

$$rect(t) = \begin{cases} 1, if\ 0 \le t \le 1 \\ 0, otherwise \end{cases} \tag{3.9}$$

Because all signal points can be described in terms of one basis function, the constellation diagram is one-dimensional. The constellation diagram for AACC in IM/DD system is illustrated in Fig. 3.3, which consists of four equidistant points on the axis.

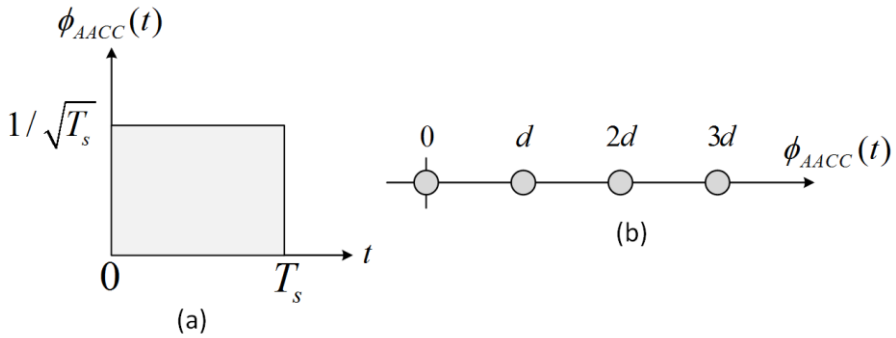


Figure 3.3: (a) Basis function and (b) signal space constellation geometry of AACC.

By employing vector presentation, it is worth noting that the Euclidean distance (d) indicates the degree of separation between any pair of signal points in the signal space can be expressed by

$$d = \frac{2\sqrt{T_s P}}{K-1} \tag{3.10}$$

where P is the average signal power.

3.2.4 Power Performance Metrics

In order to assess the performance of AACC power efficiency in IM/DD channels, the two important entities to discuss are the average electrical power and average optical power. This is unlike the conventional electrical additive white Gaussian noise (AWGN) channel, where the two standard power performance measures are average and peak electrical powers. These two measures are derived based upon the basis function and the constellation geometry in the following electrical and optical domain [84], [137], [151], [153]. Note that the average electrical and optical power of an intensity signalling scheme depends on the signalling interval as well. This is due to the fact that $\emptyset_{AACC}(t)$ in Eq. 3.8 is set to have unit electrical energy since detection is done in the electrical domain, as shown in Fig. 3.2. Therefore the average electrical

and optical power are dependent on T_s (symbol duration) which is specifically derived as follows.

3.2.4.1 Electrical Domain

The first evaluation metric is the average electrical power defined as

$$\overline{P_e} = \lim_{T\to\infty} \frac{1}{2T} \int_{-T}^{T} g^2(t)\, dt \tag{3.11}$$

Which can be simplified to

$$\overline{P_e} = \frac{E_{avg,e}}{T_s} \tag{3.12}$$

where $E_{avg,e}$ is the average electrical energy per signal constellation in the electrical domain and is equivalent to

$$E_{avg,e} = \frac{1}{K} \sum_{k=1}^{K} \|g\|^2 \tag{3.13}$$

For AACC signal, the energy in signal $g(t)$ can be expressed by

$$E_e = \|g\|^2 = T_s(A[k])^2 \tag{3.14}$$

where $A[k] \in \{0, 1, 2, 3\}$ and chosen uniformly. And the total average electrical energy AACC symbol is then given by

$$E_{avg,e} = \frac{T_s}{K}\sum_{k=1}^{K}\left(A[k]\right)^2 = \frac{T_s}{K}\left(1^2 + 2^2 + ... + \left(k-1\right)^2\right) \tag{3.15}$$

If all signals have the same energy, then $E_e = E_{avg,e}$. Therefore the average energy for transmission of 1 bit of information (average energy per bit) is

$$E_{avg,e/b} = \frac{E_{avg,e}}{\log_2 K} = \frac{E_e}{\log_2 K} \tag{3.16}$$

3.2.4.2 Optical Domain

The second evaluation metric is the average optical power defined as $\bar{P}_o = \lim_{T\to\infty}(v/2T)\int_{-T}^{T} g(t)\,dt$, where v is the electro-optic conversion factor in Watts/Ampere and $\bar{P}_o$ can be simplified to [151]

$$\bar{P}_o = \frac{E_{avg,o}}{\sqrt{T_s}} \tag{3.17}$$

where $E_{avg,o}$ is the average optical energy per signal constellation in the optical domain and $v = 1$ has been assumed, and it can be formed as

$$E_{avg,\mathrm{o}} = \frac{\sqrt{T_s}}{K}\sum_{k=1}^{K}\left(A[k]\right) = \frac{\sqrt{T_s}}{K}\left(1 + 2 + ... + \left(K-1\right)\right) \tag{3.18}$$

In order to have a fair comparison with on-off-keying (OOK) format whose spectral efficiency in a fixed bandwidth is 1 bit/s/Hz, the spectral efficiency of AACC on the intensity modulated channel is defined as

$$\eta = \frac{R_b}{B} = \log_2 K \text{ [bits/ s/ Hz]} \tag{3.19}$$

where $B = R_s$ is the first-null bandwidth of $g(t)$. This means that bandwidth of AACC modulation is lessened by half, compared to OOK at the same bit rate.

Apart from the use of NRZ pulse shape in AACC signal that has been discussed earlier, a variation of AACC for the IM/DD channel is RZ-AACC with duty cycle δ (δ-RZ-AACC). This is similar to NRZ-AACC scheme, except that the pulse width is taken for only a fraction $\delta \in (0,1]$ of the baud interval. The bandwidth for δ-RZ-AACC is

$$B = \frac{R_S}{\delta} \tag{3.20}$$

The AACC modulation with RZ pulse shape and different duty cycles is discussed further in Chapter 4.

3.3 Analytical Performance Evaluation

Although AACC has a completely different generation structure compared to 4-PAM, but from the optical domain signal perspective, AACC bears a resemblance to 4-PAM signal. Thus, the analytical BER of AACC and relative sensitivity to OOK can be expressed in the following sections according to Refs [10], [127].

3.3.1 Sensitivity and BER Calculation

Assuming that the noise is additive, white and stationary (e.g. when the thermal noise is dominating), the optical power penalty for using AACC expressed in dB, in comparison to OOK at the same baud rate, in terms of the required optical power to reach the same BER is $P_{pbaud} = 10log_{10}(K-1) \approx 4.8$ dB. The penalty is less when the bit rate is kept fixed due to the reduction of bandwidth. The optical power penalty for AACC, relative to OOK at the same bit rate P_{pbit} is [10], [127], is

$$P_{pbit} = 10\log_{10}\left(\frac{K-1}{\sqrt{\log_2 K}}\right) \tag{3.21}$$

This means that 3.3 dB more optical power is required for AACC in comparison to OOK signal at the same bit rate to reach the same BER. Prior to calculate the theoretical BER values for AACC system, it is important to firstly calculate the symbol error rate (SER) estimation. Under assumptions that all K symbols are equiprobable, the SER can be expressed as

$$SER = \frac{1}{K}\sum_{i=0}^{K-1}\sum_{j=0, j\neq i}^{K-1} P_{ij} \tag{3.22}$$

where P_{ij} is the probability of receiving symbols j when symbol i was transmitted and given by [10]

$$P_{ij} = \frac{1}{2}erfc\left(\frac{I_{th,j} - I_i}{\sigma_i\sqrt{2}}\right) - \frac{1}{2}erfc\left(\frac{I_{th,j+1} - I_i}{\sigma_i\sqrt{2}}\right) \tag{3.23}$$

where I_i is the photocurrent on the PIN photodiode at symbol i, and $I_{th,j}$ is the threshold current located between the subsequent symbols, and σ_i is the root mean square (RMS) value of the noise variance current for a symbol i.

The BER formula is dependent on the type of coding, where gray coding has a slightly improved performance in comparison to natural coding due to the less number of bits transition per symbol [57], [156], [157]. The BER then can be expressed as

$$BER = \frac{1}{K} \sum_{i=0}^{K-1} \sum_{j=0, j \neq i}^{K-1} \frac{d_{ij}}{\log_2 K} P_{ij} \tag{3.24}$$

where d_{ij} is the Hamming distance between the coding of symbols i and j. Table 3.2 shows two types of coding for AACC modulation.

Table 3.2: Gray and natural coding for AACC.

Intensity Levels (Symbol)	Gray coding	Natural coding
0	00	00
1	01	01
2	11	10
3	10	11

Assuming the thermal noise is dominating, all symbol levels are equally spaced and the decision thresholds are equidistant from adjacent symbols, the SER can be given as

$$SER = \frac{K-1}{K} erfc\left(\frac{I_{avg}}{(K-1)\sqrt{2}\sigma} \right) \tag{3.25}$$

where I_{avg} denotes the average photodetector current and $\sigma = \sigma_i$ for all i is the RMS noise current and dependent upon the received optical power P_o by $I_{avg} = R_r P_o$, where R_r is the photodiode responsivity. The BER then can be approximately estimated as

$$BER \approx d_H \frac{SER}{\log_2 K} \tag{3.26}$$

where d_H is the average Hamming distance between the labels of neighboring symbols. If gray coding is used, $d_H = 1$. In case of natural coding, $d_H = 2 - \frac{log_2 K}{K-1}$.

3.3.2 Total Noise Variance

The total current variance noise σ^2_{total} is given by

$$\sigma^2_{total} = \sigma^2_S + \sigma^2_T + \sigma^2_I = 2qI_{avg}\Delta f + \frac{4k_B T F_n \Delta f}{R_L} + I^2_{avg} N_{RIN} \Delta f \tag{3.27}$$

As discussed in [10], the three terms of Eq. 3.27 are shot noise, thermal noise and relative intensity noise (RIN) respectively. The values denoted by $q, \Delta f, k_B, T, R_L, F_n$ and N_{RIN} are respectively, the electron charge, receiver spectral bandwidth, Boltzmann constant, temperature in Kelvin, load resistance, electrical amplifier noise figure, and the average RIN spectral density. For simplicity, the photodiode dark current has been neglected due to its effect that is much less than the detected photodiode current. At a fixed bit rate of 10-

Gb/s, the bandwidth of OOK was set to 10-GHz and that of AACC was 5-GHz. Also, a set of values has been assumed, where F_n = 5 dB, T = 298 K, R_L = 50 Ω, N_{RIN} = -155 dB/Hz and R_r = 0.4 A/W.

Fig. 3.4 shows the theoretical BER for OOK and AACC based on Eq. 3.26, assuming gray coding and directly modulated laser used. At BER of 10^{-9}, OOK format has a sensitivity of about -15 dB, whereas the received optical power of AACC is approximately -11.7 dB, which is in the same agreement with results from Eq. 3.21. To further consolidate and verify the analytical BER performance of AACC modulation scheme, a corresponding simulation transmission setup at 10-Gb/s has been demonstrated and shown in Appendix A. More investigations on numerical performance of AACC and its related signalling is exhaustively discussed in chapter 4 and 5.

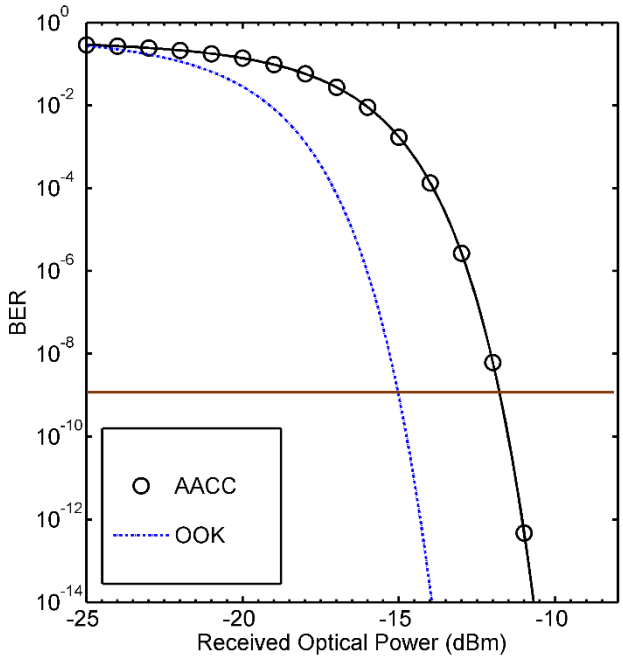


Figure 3.4: Theoretical BERs versus received optical power for OOK and AACC transmission formats at 10-Gb/s.

Figs. 3.5 and 3.6 illustrate the contribution of all noise sources based on Eq. 3.27, which are plotted against received optical power P_o and bit rate R_b respectively. As can be seen from Fig. 3.5, for the received optical power greater than 6.5 dB, the RIN and shot noises are stronger than the thermal noise. Thus, it is apparent that thermal noise is independent of the signal power and always

dominating in the system. Fig. 3.6 consolidates the robustness of the thermal noise in the performance of the link, by increasing the bit rate from 2 to 100-Gb/s, the thermal noise is still governing and almost overlapping the total noise, σ^2_{total}.

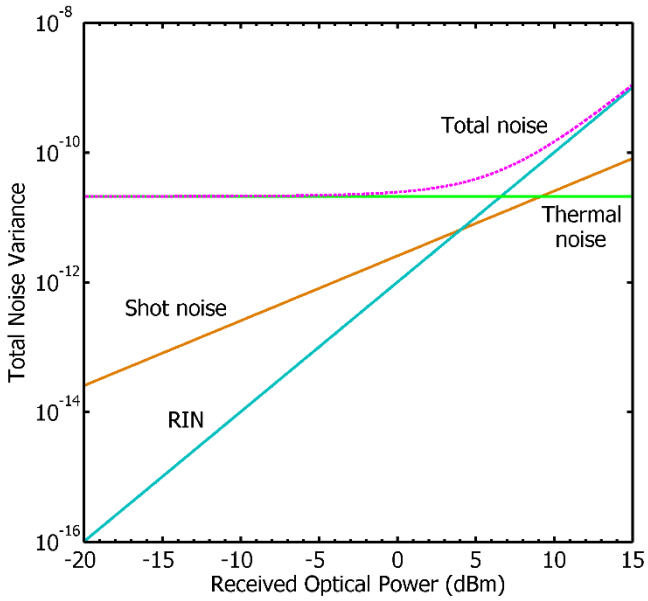


Figure 3.5: Contributions from shot noise, thermal noise, and RIN at a receiver bandwidth of 20-GHz for AACC.

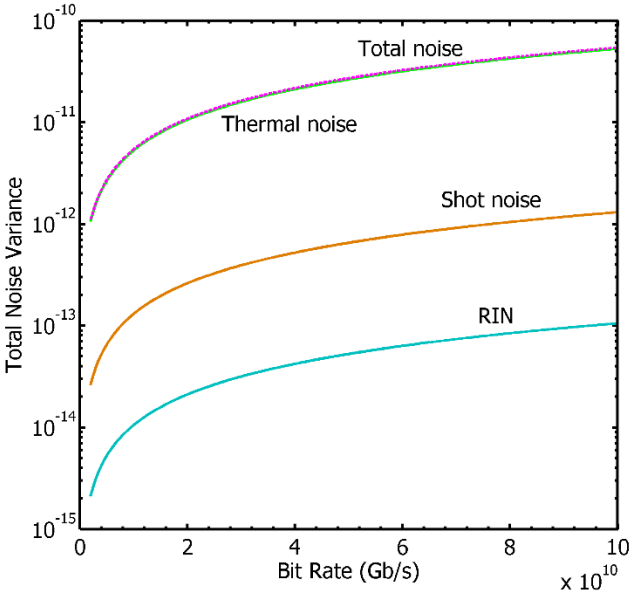


Figure 3.6: Contributions from shot noise, thermal noise, and RIN versus bit rate for AACC.

The effect of varying the spectral width on the total noise variance for OOK and AACC transmission formats is displayed in Fig. 3.7. Since the thermal noise is not signal-dependent, equally spaced levels and equidistant decision thresholds between the symbols of AACC signal are therefore used, as shown in Fig. 3.2 and constellation diagram in Fig. 3.3 in order to yield an optimised accurate theoretical results.

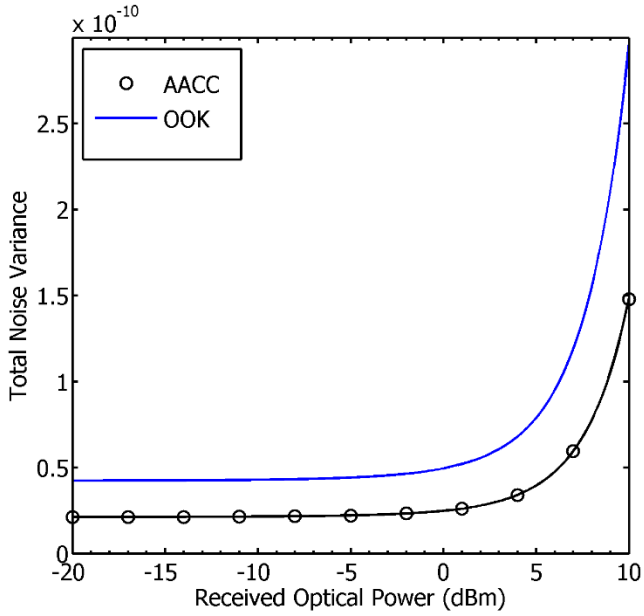


Figure 3.7: Total noise variance σ^2_{total} in $[A^2]$ versus the received optical power for OOK and AACC.

3.3.3 Impact of RIN on AACC

It is essential to show the effect of RIN, which is generated due to the fluctuation in the laser intensity on the sensitivity of a fibre optic communication link [151], [156]. Under certain circumstances, RIN can cause a significant degradation on the system performance. The effects of RIN can be evaluated analytically by taking into account the noise variance when calculating the BER.

Fig. 3.8 indicates the analytically calculated BER curves for OOK at the bit rate of 40-Gb/s and the RIN ranging from -155 to -115 dB/Hz. The BER

curves for AACC with various levels of RIN in the range of -155 to -126 dB/Hz, also at an aggregate bit rate of 40-Gb/s are displayed in Fig. 3.9. It was assumed that the decision thresholds are equally spaced from the adjacent symbol levels. As the RIN penalty increases, the BER curves start showing progressively higher error floors. It can be concluded that the RIN contribution does not remarkably degrade the link performance in comparison to the thermal noise.

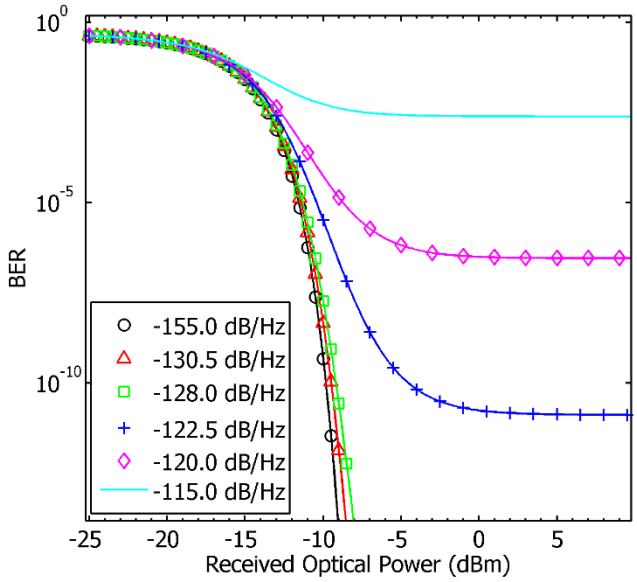


Figure 3.8: BER curves for various levels of RIN, shown for OOK at 40-Gb/s.

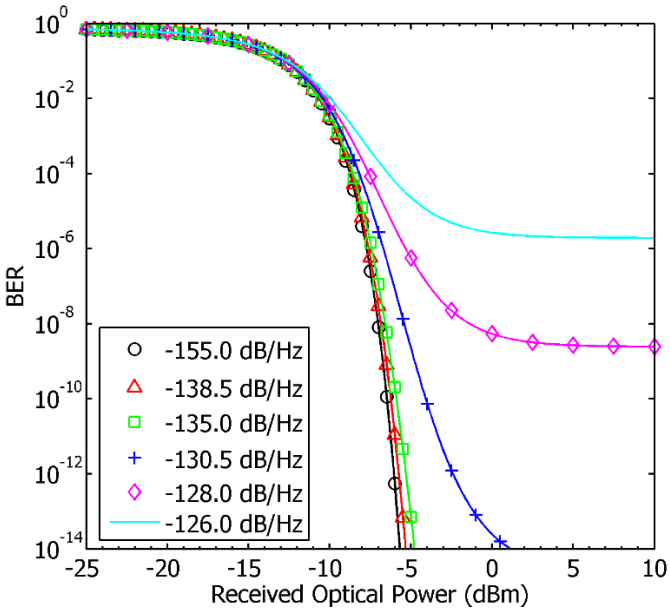


Figure 3.9: Influence of RIN on expected BER, shown for AACC at 40-Gb/s.

3.4 Concluding Remarks

Presented in this chapter is the novel transceiver structure, working principle, and data recovery of the AACC transmission system. The signal space model of the AACC modulation format has also been discussed, where the average electrical and optical power expression are derived. It is shown that proposed AACC can be used to double the transmission capacity. In addition, a development of the BER estimation based on threshold detection at the receiver has also been addressed.

Since AACC is a nonnegative multilevel intensity modulation format that based on partial response signalling (correlative coding); it is therefore favourable that the AACC signal is able to overcome the chromatic dispersion in single mode fibre as well as modal dispersion in multimode fibre transmission links. This is because AACC employs a bit correlation methodology which makes itself robust to the dispersion tolerance. It is noteworthy to mention that the use of bit correlation has successfully demonstrated in binary signalling e.g. duobinary and phase-shaped binary transmission. These two modulation

formats are still under research for high-speed optical access networks, data centre and long-haul transmission systems [37], [83], [103], [110], [135], [158].

Chapter 4– Numerical Performance Analysis of AACC-based Signalling

4.1 Introduction

This chapter gives a brief overview of the commercial optical system simulator that employed throughout in this study to assess the performance of optical fibre transmission systems. This chapter also presents several types of multilevel intensity signalling that based on the concept of AACC transmitter in different optical transport applications such as interconnects, short-haul and access networks. The generation of each related-AACC modulation format is described in specific with an evaluation of their performances according to numerical validated software OptiSystem 12 and MATLAB®. The comparison with other prevailing modulations such as NRZ, 33% RZ, 50% RZ, 67% carrier suppressed RZ (CS-RZ), duobinary, 4-PAM, RZ 4-PAM and 8-PAM is also investigated.

The materials presented in this chapter have been published in:

N. Dong-Nhat, M. A. Elsherif, and A. Malekmohammadi, Investigations of high-speed optical transmission systems employing Absolute Added Correlative Coding (AACC)," *Opt. Fiber Technol.*, vol. 30, pp. 23–31, 2016.

N. Dong-Nhat and A. Malekmohammadi, "RZ-absolute added correlative coding (AACC) transmission system featuring improved receiver sensitivity for high-speed optical transport," *Electron. Lett.*, vol. 52, no. 8, pp. 639–641, 2016.

N. Dong-Nhat, L. Nguyen, and A. Malekmohammadi, "75 Gbit/s transmission over single mode fibre links using 8-PAM and 8-AACC modulations," *Electron. Lett.*, vol. 53, no. 5, pp. 326–328, 2017.

4.1.1 Numerical Simulation Software

The simulation of optical fibre transmission systems involves realistic modelling of the generation, propagation and reception of the transmitted signals. The trade-off of any simulation is between accuracy and time. Thanks to the availability of commercial optical system simulators, with sophisticated simulation algorithms and easy-to-use graphical user interfaces, it was decided

to use one of such packages. It was chosen OptiSystem from Optiwave Systems Inc. Several key reasons have concurred for this option as follows.

- OptiSystem (http://www.optiwave.com) is a high-end and innovative optical communication system simulation package that has been commercial for more than 20 years for professional engineering and advanced research. It is a stand-alone system-level simulator that does not rely on other simulation frameworks. Its capabilities can be extended easily with the addition of user components, and can be seamlessly interfaced to a wide range of tools.

- Besides the software can also interacte with MATLAB® programming language, so the users are able to design and model their own electrical and optical components. This valuable feature has enabled to develop and evaluate the performance of AACC-based signalling and equalisers.

- Another reason should be mentioned to consolidate the competence of OptiSystem is that it satisfies the demand of recognised optical telecommunication services providers and also well-known research universities [10] [22]. Especially it offers an affordable price for academic institutions.

4.2 AACC

4.2.1 Simulation Setup

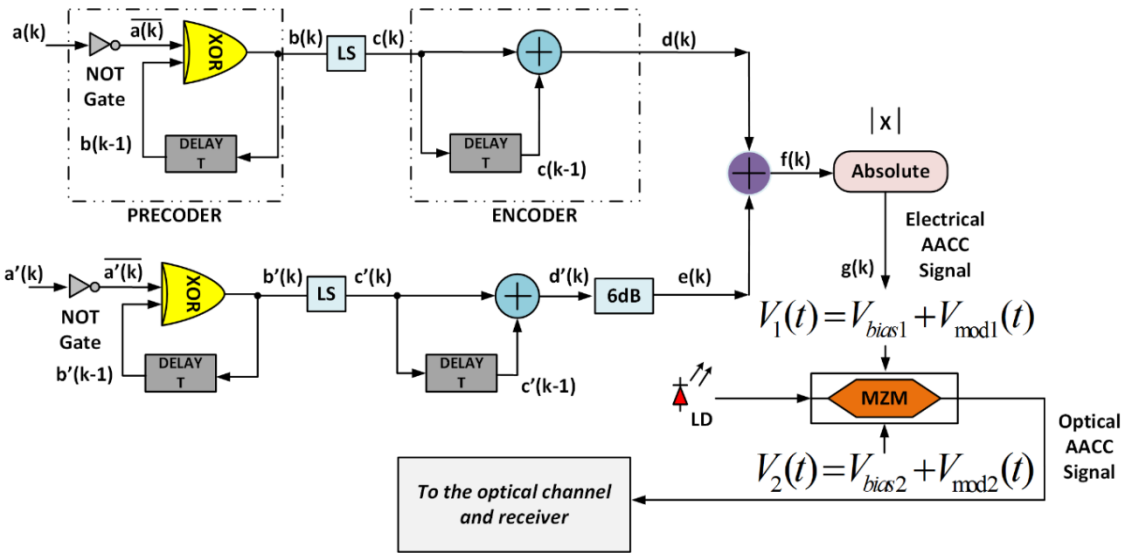


Figure 4.1: Schematic of the AACC transmitter for numerical evaluation.

Fig. 4.1 shows the simulation setup of optical AACC transmitter. The generation of AACC which denoted as $g(k)$ in electrical domain has been presented in Chapter 3. A dual-drive MZM is used to modulate the optical carrier wave which emitted from a continuous wave LD with the four-level electrical AACC drive signal. The MZM consists of an input Y-branch splitter, two electrical drive voltages and an output Y-branch combiner. The total optical field is, to a good approximation, the sum of the fields at the outputs of the two arms. If the splitting ratio (SR) of the input and output Y-branches are identical, the optical signal is expressed by [58], [72], [159]:

$$E(V_1, V_2) = \frac{E_0}{1+SR}\left[SR\exp\left(-\left(\frac{\Delta\alpha_0(V_1)}{2}+j\Delta\beta(V_1)\right)L\right)\right.$$
$$\left.+\exp\left(-\left(\frac{\Delta\alpha_0(V_2)}{2}+j\Delta\beta(V_2)\right)L-j\phi_0\right)\right]$$
$$\equiv \sqrt{I(V_1V_2)}\exp(j\phi(V_1,V_2) \quad (4.1)$$

where $SR = P_1/P_2$ is the Y-branch power splitting ratio; $\Delta\alpha_0/2$, attenuation constant; $\Delta\beta$, phase constant; L is the interaction length of the modulator arm; ϕ_0, 0 radians for a conventional modulator and π radians for a π phase-shift modulator; V_1, V_2 are the voltages applied to arms 1 and 2, respectively; I, intensity of the optical signal and ϕ is the phase.

For $i = 1, 2$

$$V_i(t) = V_{bi} + V_{modi}v(t) \quad (4.2)$$

where V_{bi} is the bias voltage; V_{modi}, peak-to-peak modulation voltage and $v(t)$ is the modulation waveform with a peak-to-peak amplitude of one and an average value of zero. The dependence of the attenuation and phase constants on the applied voltage is obtained for a straight section of waveguide cut from one arm of a modulator. Note that for a dual-drive MZM module, the absorption ($\Delta\alpha_0$) and the phase difference ($\Delta\beta$) are nonlinear functions of the applied bias voltage as illustrated in Fig. 4.2.

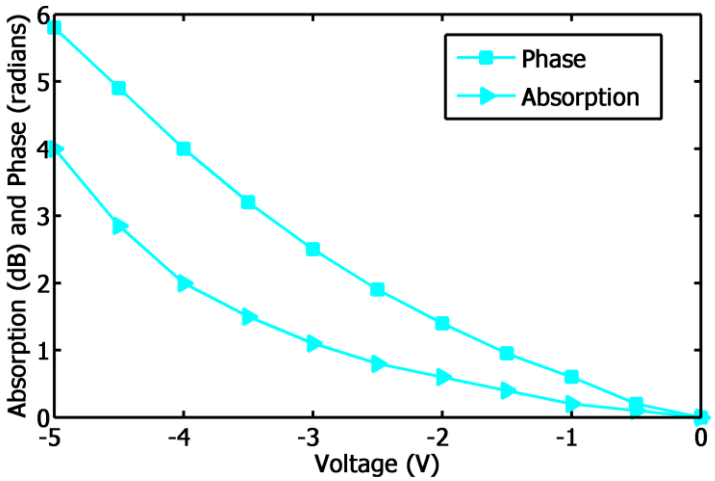


Figure 4.2: Characteristics of absorption ($\Delta\alpha_0$) and phase difference (Δ_β) in the simulated optimised dual-drive MZM [58].

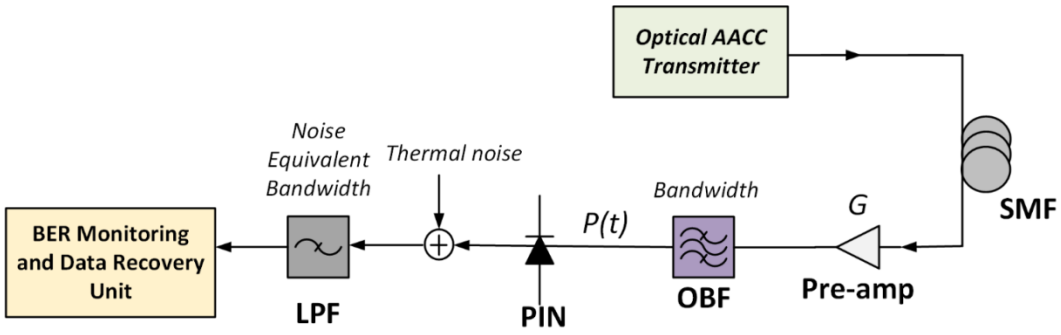


Figure 4.3: Simulation setup.

The lightwave full link system under study is depicted in Fig. 4.3. The aggregate bitrate is 40-Gb/s (2 x 20-Gb/s) with pseudo-random binary sequence (PRBS) of $2^{10}-1$. The NRZ-AACC signal is used to modulate the CW laser at ~1550 nm wavelength by a dual-drive MZM with the splitting ratio of 1, the modulating voltage of 1.3 V and the bias voltages V_{b1} and V_{b2} of -0.9 V and -2.3 V, respectively. The gain of the optical pre-amplifier was set as 30 dB while the noise figure was taken to be 6 dB. The optical AACC is transmitted to the standard single mode fibre (SMF). A variable optical attenuator (VOA) is inserted after the SMF to vary the received optical power. A pre-amplifier which is the EDFA to amplify the generated signals and offset the transmission loss. A Gaussian optical bandpass filter (OBF) with an optimal bandwidth B_o is used to shape the signal and eliminate the amplified spontaneous emission (ASE) noise.

The larger OBF bandwidth degrades the system performance since more ASE noise is collected by the OBF. This aspect is specifically shown in Section 4.2.2.1 (Fig. 4.5).

At the receiving end, this optical 4-intensity level signal can be easily detected by a simple direct detection technique as OOK or 4-PAM signals without any modification that results in a reduced complexity in implementation [9], [44], [84], [85], [95], [134], [156], [160]. In fact, it is passed through the PIN photodetector, which is a square-law detector and used to convert the optical signal to electrical signal. The contribution from the thermal noise σ_{th}^2 was also added. The subsequent electrical signal is transmitted to a Gaussian LPF which is considered to have an optimal bandwidth that associated to the null-to-null bandwidth in order to eliminate the photodiode noises and avoid introduction of ISI on the transmitted signal. The received signal is then fed into the MATLAB®-based module for the BER estimation and data recovery unit.

In fact, all of the sampled values taken at the sampling point (S_Δ) displayed in Fig. 3.2 (b) are passed into the decision devices in order to compare against three threshold levels T_1, T_2 and T_3. Table 4.1 shows the truth table (data recovery rules) that explains the functionality of this receiver completely. Fig. 4.4 shows the sample of the received 4-level intensity eye diagram and its Gaussian probability densities. The red and blue regions display the probability of incorrect identifications. The total BER can be calculated taking into account the probability density functions (PDFs), which correspond to the incorrect identifications of AACC symbols. Given in the table, there are four symbols denoted as S_0, S_1, S_2 and S_3 corresponding to the four pairs of bits as “00”, “01”, “10” and “11”. A symbol error is detected when transmitting a symbol S_i while receiving a symbol S_j, where i is not equal to j. The conditional probability of receiving S_j when S_i was transmitted is symbolised as P_{ij}.

Table 4.1: Data recovery rules at the receiver.

Rules	Decision on Path 1 (N_1)	Decision on Path 2 (N_2)	Intensity Level (Symbol)
If $S_\Delta < T_1$	0	0	0
If $T_1 < S_\Delta < T_2$	0	1	1
If $T_2 < S_\Delta < T_3$	1	0	2
If $S_\Delta > T_3$	1	1	3

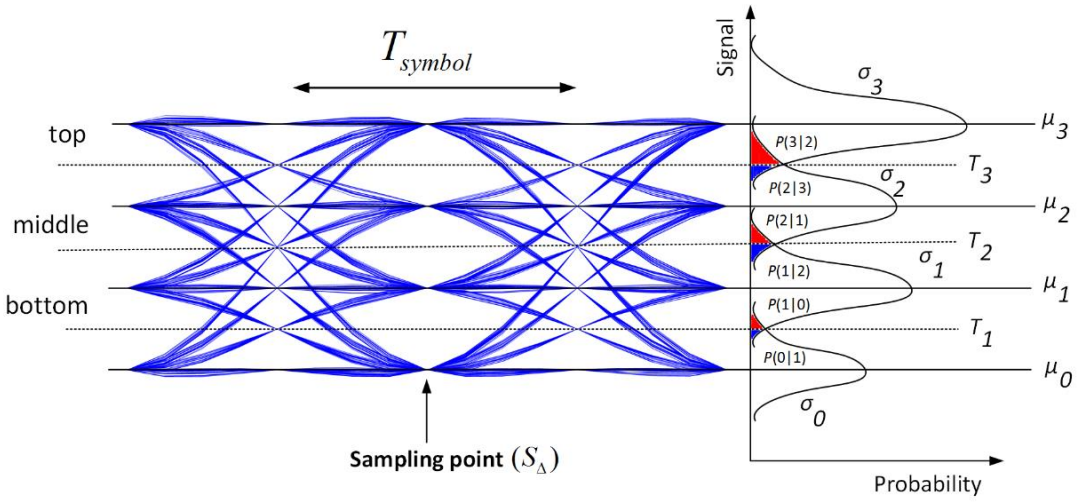


Figure 4.4: Sample of 4-level intensity eye diagram and its conditional probability density functions with Gaussian noise.

Specifically, regarding to the bottom eye diagram, an error occurs at the receiver side of the system when a sampled value of a "1" in N_2 (Path 2) is lower than decision threshold T_1 or the sampled value of a "0" in N_1 (Path 1) is higher than the decision threshold T_1. With a probability of an incorrect decision when a "1" is received (P_{01}) and the probability of an incorrect decision when a "0" is received (P_{10}), they can be written as

$$BER_1 = \frac{1}{2}(P_{01} + P_{10}) \tag{4.3}$$

For the middle eye diagram, note that P_{12} and P_{21} are weighted double due to the susceptibility to noise from the upper and lower PDFs. Therefore the BER_2 can be calculated as

$$BER_2 = \frac{1}{2}[2(P_{12} + P_{21})] \tag{4.4}$$

While the BER_3 measurement at the decision level T_3 is given by

$$BER_3 = \frac{1}{2}(P_{23} + P_{32}) \tag{4.5}$$

Consequently the aggregate BER can be calculated as

$$\begin{aligned} BER = BER_1 + BER_2 + BER_3 &= \frac{1}{2}(P_{01} + P_{10} + 2P_{12} + 2P_{21} + P_{23} + P_{32}) \\ &= \frac{1}{2}erfc\left(\frac{Q_1}{\sqrt{2}}\right) + erfc\left(\frac{Q_2}{\sqrt{2}}\right) + \frac{1}{2}erfc\left(\frac{Q_3}{\sqrt{2}}\right) \end{aligned} \tag{4.6}$$

where $erfc$ is the complementary error function. While the Q-factors are obtained from

$$Q_1 = \frac{\mu_1 - \mu_0}{\sigma_1 - \sigma_0}, Q_2 = \frac{\mu_2 - \mu_1}{\sigma_2 - \sigma_1}, Q_3 = \frac{\mu_3 - \mu_2}{\sigma_3 - \sigma_2} \tag{4.7}$$

where $\mu_0, \mu_1, \mu_2, \mu_3$ and $\sigma_0, \sigma_1, \sigma_2, \sigma_3$ represent the mean and the variance (standard deviations) corresponding to the PDFs respectively.

4.2.2 Results and Discussion

A Gaussian OBF was used with an optimal bandwidth B_o and transfer function of $H_o(f)$ tuned to cut-off frequency of 45-GHz. The photodiode with the responsivity and dark current of 0.8-A/W and 10-nA, respectively. The electrical AACC signal then launched into a Gaussian electrical LPF, with the electrical bandwidth B_e of 13-GHz. Fig. 4.5 shows B2B receiver sensitivity as a function of electrical and optical filter bandwidth. Filter bandwidths ranging from 40 to 60-GHz and 13-GHz to 21-GHz were tested for optical and electrical filter, respectively. As illustrated in Fig. 4.5 the bandwidth of 45-GHz and 13-GHz were found as an optimum bandwidth for optical and electrical filter, respectively. Thus, the optical filter bandwidth was fixed to 45-GHz and electrical bandwidth was fixed to 13-GHz in the following calculation, for eliminating the photo- diode noises and optical noises, respectively.

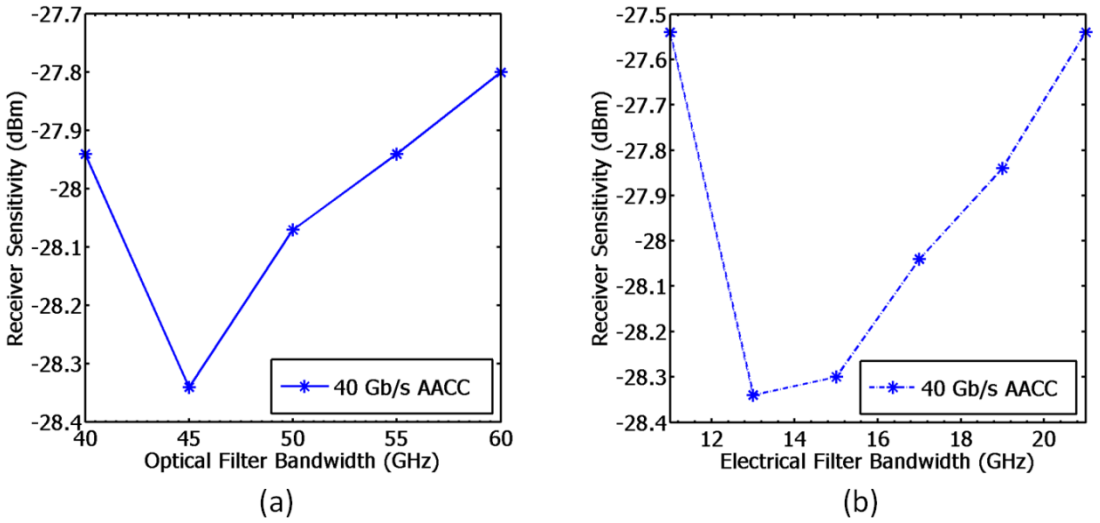


Figure 4.5: Receiver sensitivity as a function of (a) optical filter bandwidth and (b) electrical filter bandwidth.

4.2.2.1 Receiver Sensitivity

Fig. 4.6 shows the BER curves for the three AACC received eye diagrams (top, middle and bottom) with respect to the received optical power of the signal. The corresponding AACC eye diagram is shown as inset of Fig. 4.6. The bottom eye diagram, which represents the amplitude levels "0" and "1" dominates the overall BER in all three cases. Its received optical power at BER of 10^{-9} is about -30.2 dBm. At the same calculated BER, middle and top eye diagram experience ~1.2 dB and ~3 dB penalty with respect to bottom eye diagram, respectively.

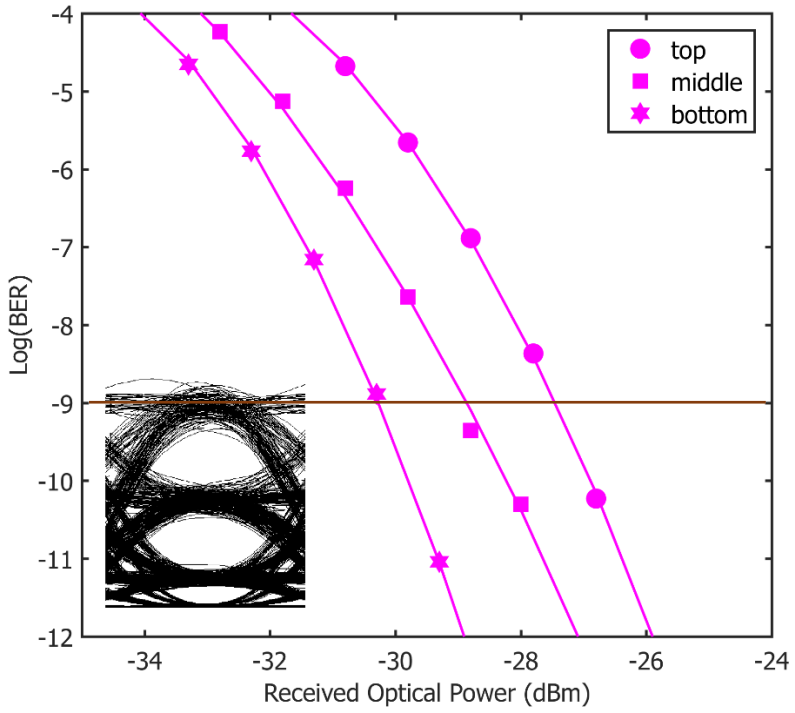


Figure 4.6: BER curves for the three received eyes of AACC (top, middle and bottom) in B2B scenario. Inset is the corresponding eye diagram.

This can be explained by approaching the noise powers associated with each symbol at the receiver. It is approximately given by [78], [84], [161]

$$\sigma_n^2 = 2(c_2 R_s N_{ASE})^2 I_2 + 4P_n G c_1 c_2^2 R_s^2 N_{ASE} B_{oe} + \sigma_{th}^2 \qquad (4.8)$$

where P_n is the average power of level n ($n = 0, 1, 2, 3$). The coefficient c_1 and c_2 are the input and output coupling losses of the optical pre-amplifier which is the EDFA, respectively. The noise bandwidth of the ASE-ASE beat noise is measured through I_2. R_s is the responsivity of the optical receiver while G is the amplifier gain at the operating wavelength of an optical preamplifier. B_{oe} is a measure of the noise equivalent bandwidth of the combined optical and electrical filtering process, expressed as [162]

$$B_{oe} = \int_{-\infty}^{\infty} |H_e(f)|^2 |H_o(f)|^2 df \tag{4.9}$$

The one-sided power spectral density of the ASE noise, per polarisation, can be written as [78], [155], [163]

$$N_{ASE} = (G - 1) h\nu n_{sp} \tag{4.10}$$

where $h\nu$ is the photon energy. The variance (power) of the random variables is derived

$$\sigma^2 = P_{ASE} = (G - 1)\, h\nu n_{sp} B_o \tag{4.11}$$

From the signal-dependent noise power (Eq. 4.8) and its interrelation to BER-Q-factor estimation in Equations 4.6 and 4.7, it can be observed that due to the higher noise power, the Q-factor of top eye diagram (symbols 2 and 3) is lower compared to middle and bottom eye diagrams, which consequently results in higher performance degradation compared to other two eyes.

As illustrated in Fig. 4.6, owing to the different variation of variance (standard deviations) and means at each level at the same received power, eye with minimum variations of noise has the best performance and vice versa. It should be noted that in order to minimize the performance variation between

different eyes, dual-drive MZM with optimised voltage biases is therefore employed.

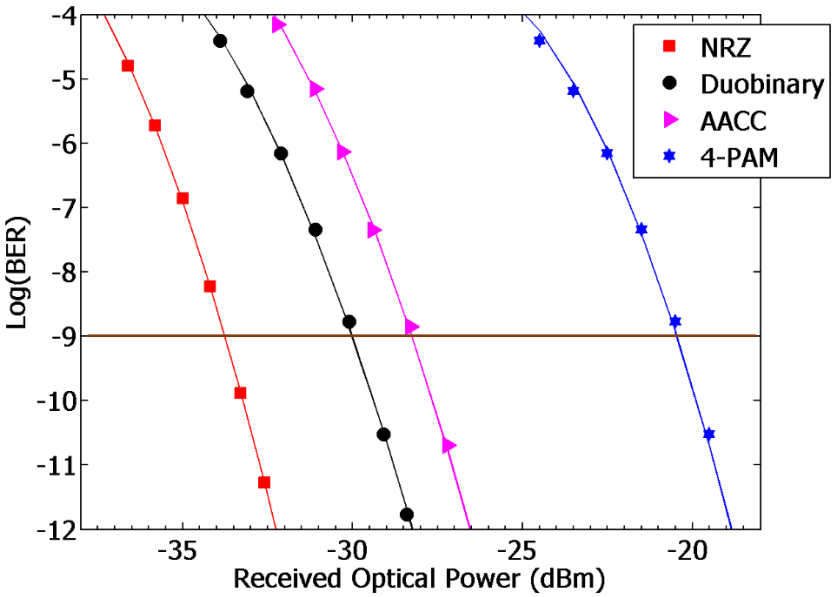


Figure 4.7: B2B receiver sensitivity of AACC, 4-PAM, duobinary and NRZ.

Based upon the BER calculation discussed earlier, Fig. 4.7 depicts the calculated mean BER versus received optical power for the B2B scenario of AACC in comparison to NRZ, 4-PAM and duobinary, respectively. It can be seen that at the same capacity of 2 bits per symbol, AACC shows much better performance compared to 4-PAM in terms of receiver sensitivity due to the utilisation of optimised MZM. More details of this optimisation technique can be found in Appendix B. By employing the same methodology (optimised eye opening distribution), a better performance for 4-PAM is also expected. In comparison to duobinary, although AACC offers double of transmission capacity but it suffers from ~1.8 dB power penalty, due to its multilevel nature.

The receiver sensitivity of AACC is downgrade in comparison to NRZ which is dominant due to the less intensity levels. 50% RZ and CS-RZ enjoy a ~1-2 dB advantage over NRZ in ASE noise-limited systems due to an inherent tolerance of the RZ pulse shape to ISI in the receiver [56], [80], [81].

4.2.2.2 Spectral Efficiency

The transmission bandwidth of 4-PAM is a factor of $1/log_2 M$ less than conventional binary scheme, where M is the number of levels in the M-ary PAM signal [156], [164], [165]. As shown in Fig. 4.8 (d), considering the null-to-null bandwidth, the optical spectral width of AACC is 40-GHz, which is in equivalence to 4-PAM. The resulting AACC spectrum has a central lobe, which is nearly identical to the 4-PAM single-lobe spectrum as well as several first sidelobes as can be seen in Fig 4.8 (e). Hence, AACC and 4-PAM result in a spectral efficiency of 1-b/s/Hz. The spectral width of AACC in association with number of generated levels ($\boldsymbol{L}$) can be defined as

$$Spectral\ width = 2 \times \frac{aggregate\ bit\ rate}{\boldsymbol{L}-2} \tag{4.12}$$

While that of NRZ, 50% RZ and 67% CS-RZ are 80, 160 and 120-GHz corresponding to the spectral efficiency of 0.5, 0.25 and 0.33-b/s/Hz. This is because AACC is produced based on partial-response signalling, that makes use of bit correlation in order to narrow the spectral width, which is about half of the NRZ bandwidth. This amount of saving in the spectral width is significant which results in better chromatic dispersion tolerance and enabling the implementation of future spectrally-efficient WDM transport networks. It is noteworthy to state that the optical spectral width of these simulated data formats has a strong agreement with experimentally verified optical spectra in [29], [86].

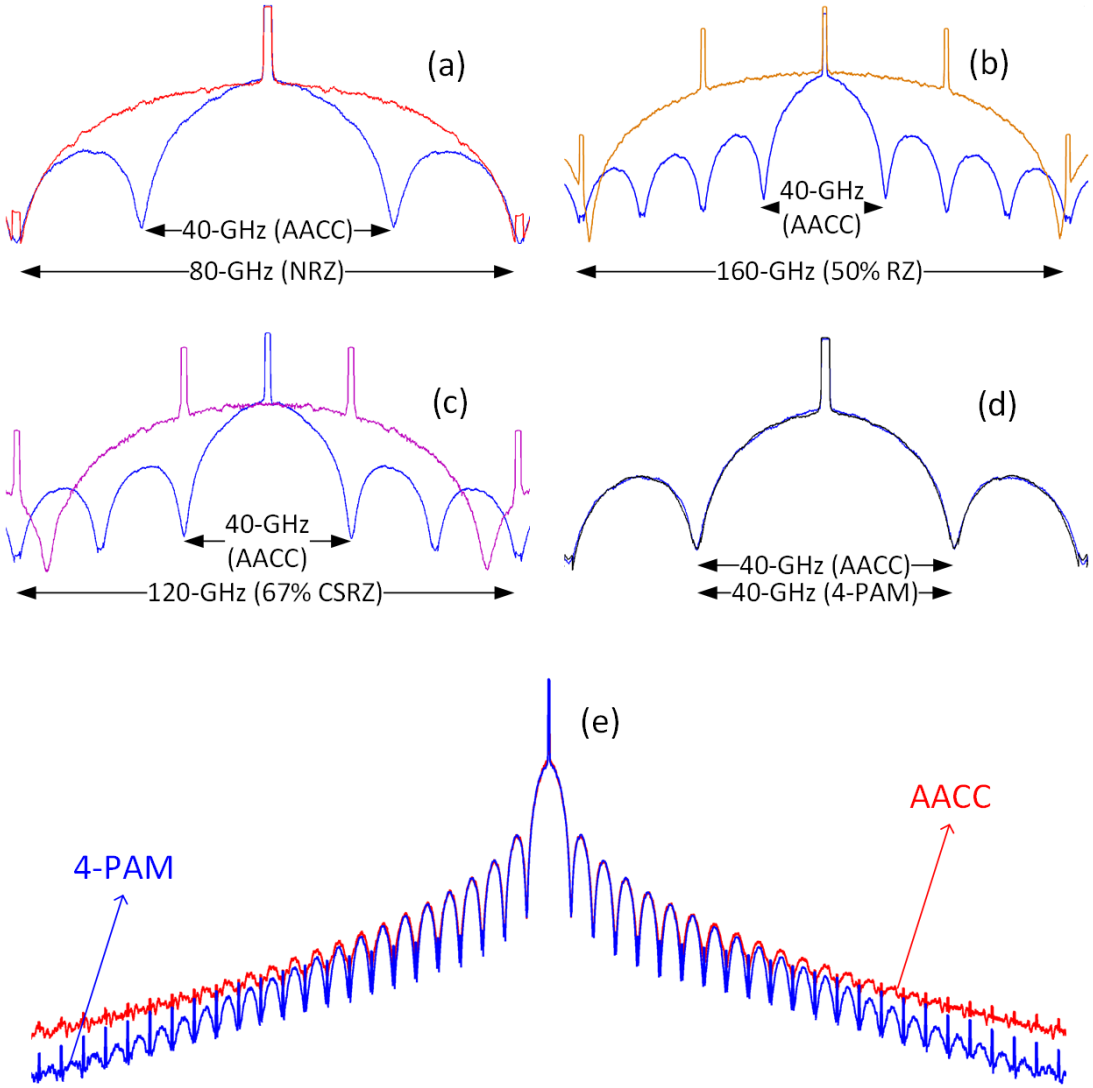


Figure 4.8: Spectral width of AACC in comparison to (a) NRZ (b) 50% RZ, (c) 67% CSRZ, (d) null-to-null spectral width 4-PAM and (e) full spectrum 4-PAM, all at the same aggregate bitrate of 40-Gb/s.

4.2.2.3 Chromatic Dispersion Tolerance

The AACC signal is simulated in a dispersive transmission medium in order to evaluate its tolerance towards fibre dispersion. Higher dispersion tolerance can reduce the adjacent channel crosstalk. In fact, when operating at higher bitrates over long lengths of fibre, the chromatic dispersion causes broadening of a single transmitted pulse which is known as ISI that producing distortions in the received signals. As a consequence, the relation between the maximum

dispersion length L_D (ps/nm) and the null-to-null spectral width Δf (GHz)can be written as follows

$$L_D = \frac{c}{R_b D \lambda^2 \Delta f} \tag{4.13}$$

where c is the speed of light (c = $3 \times 10^8\ m/s$), R_b is the bitrate (b/s), D is the dispersion parameter (ps/(km.nm)) and λ is the central wavelength (nm). It is evident that the spectral width is inversely proportional to both the dispersion parameter and the transmission length. Therefore the signal with narrower spectral width delineates better chromatic dispersion tolerance.

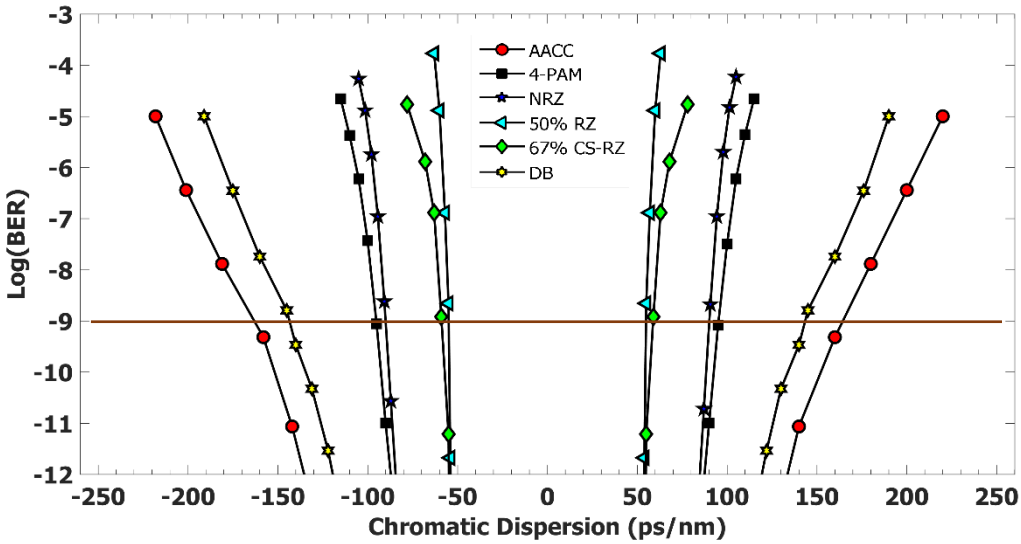


Figure 4.9: Measured BER versus chromatic dispersion. DB: Duobinary.

Fig. 4.9 shows the chromatic dispersion tolerance of AACC compared with 4-PAM, 50 % RZ, 67 % CS-RZ, NRZ and duobinary. It is evident that the AACC and 50% RZ display the best and worst tolerance of around 336 ps/nm and 104 ps/nm at the BER of 10^{-9}, respectively. The slightly degraded dispersion tolerance of ~26 ps/nm is observed when comparing duobinary to NRZ-AACC. This degradation can be explained by the imperfections of duobinary transmitter which consisting of a differential phase shift keying (DSPK) transmitter and a fifth-order Bessel electrical low-pass filter with cut-off

frequency of 11.2-GHz (i.e. 28% of the 40-Gb/s data rate). In the previous work reported in [166], a chromatic dispersion tolerance of ~200 ps/nm for NRZ-AACC was shown due to the unavailability of OBF whose characteristics can greatly reduce the effect of the ASE noise on the system performance and control the chromatic dispersion in fibre [74], [81], [167].

In comparison to 4-PAM, in spite of having the same null-to-null bandwidth, NRZ-AACC shows better dispersion tolerance. This can be explained by considering a *1 0 1* bit pattern of *a(k)* and *a'(k)* which corresponding to time constant *k* of *1 2 3* in Table 3.1, after being encoded as *2 0 -2* and *1 0 -1*, the two *2*-bit and *1*-bit pulses spread into the *0*-bit due to dispersion, the encoders let them interfere destructively, which results in a low *0*-bit level whereas NRZ format in 4-PAM let the pulses interfere constructively, which leads to a raising *0*-bit level and closes the eyes. The closing of the eye is a measure of degradation in receiver performance and is associated with a corresponding increase in the BER. In order to firm up the superior resilience against the fibre dispersion of AACC over 4-PAM modulations, it is essential to refer to Fig. 4.8 (e). It is found that the AACC shows larger suppression (more than 10 dB) for the optical spectrum sidelobes which produces greater dispersion improvement as well as better tolerance to SPM effect. Whereas 4-PAM spectrum has obvious power attenuation at the high frequency components, which make itself sensitive to dispersion and therefore limit the system performance [30], [83], [89], [168].

Since researchers are now interested in scaling the bit rate up to 100-Gb/s in a single channel for optical interconnects and data centres applications, it is required to use the powerful electrical equalisers and forward error correction (FEC) coding at the receiver to reduce the errors; therefore the region of $10^{-6} < \text{BER} < 10^{-2}$ is more concerned [16], [20], [115], [140], [141], [169]–[171]. As can be seen from Fig. 4.9 NRZ-AACC features higher slope dispersion tolerance than other modulation formats even at $10^{-6} < \text{BER} < 10^{-2}$ which can be expected to be an interesting technique for higher data rate systems.

To consolidate the robust performance of AACC signal, a post-compensated transmission system is modelled, the set-up mostly based on Fig. 4.3. The transmission link now consists of SMF and DCF without an inline EDFA, the dispersion of the SMF was perfectly compensated. Detailed fibre parameters are presented in Table 4.2. The effect of nonlinearities in both SMF

and DCF are negligible as the launch power to both DCF and SMF are much below the threshold. This effect is investigated in Chapter 5.

Table 4.2: Fibre parameters used in the schematic [10].

SMF parameters		
D	Dispersion	+17 ps/nm/km
S	Dispersion Slope	0.075 $ps/nm^2/km$
A	Attenuation Coefficient	0.2 dB/km
A_{eff}	Effective Area	80 μm^2
L	SMF Length	30, 60, 90 km
DCF parameters		
D	Dispersion	-100 ps/nm/km
S	Dispersion Slope	-0.3 $ps/nm^2/km$
A	Attenuation Coefficient	0.5 dB/km
A_{eff}	Effective Area	12 μm^2
L	DCF Length	5.1, 10.2, 15.3 km

Fig. 4.10 displays the measured sensitivities as a function of the transmission distance. The advantage of AACC system rendering for longer fibre reach with reference to its higher dispersion tolerance over 4-PAM, has been clearly shown. Despite the advantage in received optical power over 30- and 60-km SMF observed at BER = 10^{-9}, AACC maintains good receiver sensitivity after 90-km SMF delivery whereas 4-PAM could not reach that distance and occurs an error-floor of 10^{-5}.

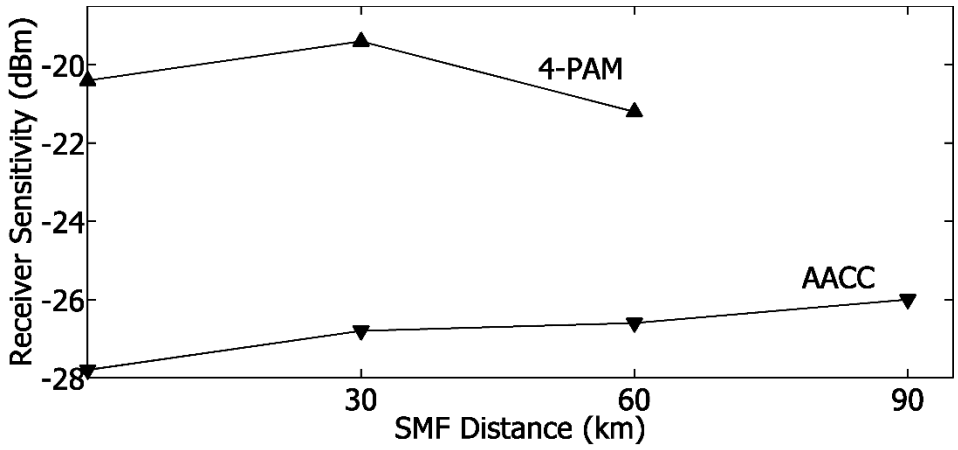


Figure 4.10: Optically preamplified receiver sensitivity measured as a function of SMF transmission distance for AACC and 4-PAM systems at 10^{-9} BER .

4.2.2.4 Performance Comparison of AACC and 4-PAM in Optical Access Networks

As another set of simulations, at the same capacity of 2 bits per symbol, an extensive performance investigation and comparison of 40-Gb/s and 100-Gb/s is examined for both AACC and 4-PAM. This is to realise their potential application in future optical access networks. The transmission configurations is simplified by removing DCF and pre-amplifier EDFAs. The output optical power of the modulator is approximately -2 dBm for each transmission scenario. In order to have a fair comparison between AACC and 4-PAM, standard single-drive MZM is used.

The simulation result of receiver sensitivities for AACC and 4-PAM without utilisation of pre-amplifier at an aggregate bit rate of 40-Gb/s is presented in Fig. 4.11, for the B2B case (circles), and after transmission over 5-km SMF (triangles) and 10-km SMF (squares). Due to the use of single-drive MZM which is not optimised for AACC system, both modulation formats show almost the same performance in the B2B scenario, however by extending the transmission distance up to 5-km of SMF, AACC signal precisely shows 2 dB better sensitivity in comparison to 4-PAM. Note that 5-km is also the maximum reach of 4-PAM taking at BER = 10^{-9}. By increasing the transmission distance

to 10-km, it can be observed that 20-Gbaud/s AACC system performs much better than 4-PAM system.

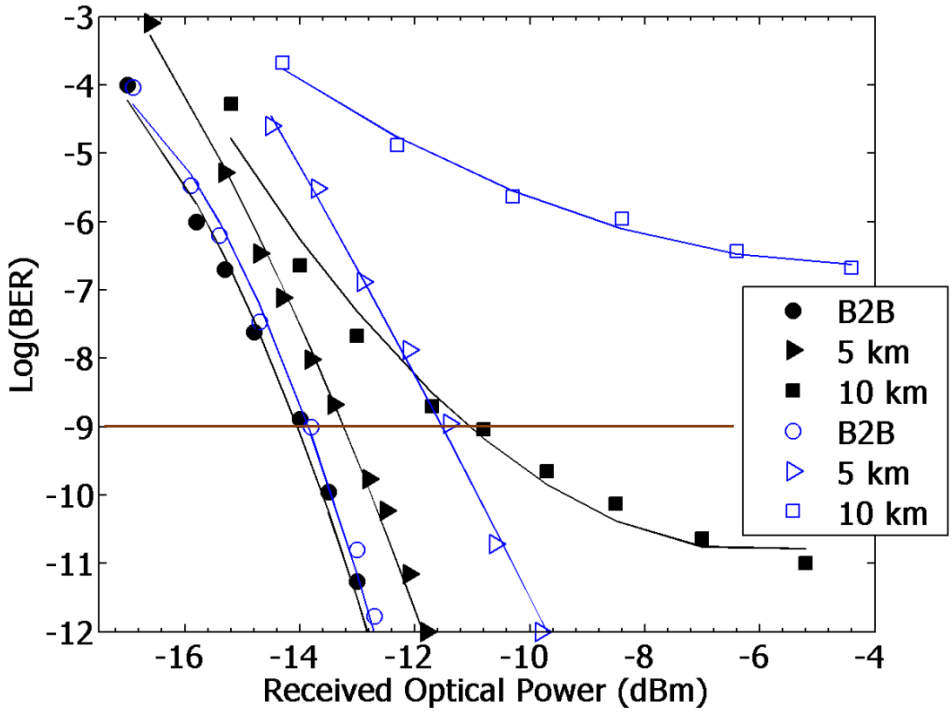


Figure 4.11: BER versus received optical power over different lengths of SMF for AACC (black curves, solid markers) and 4-PAM (blue curves, hollow markers) at an aggregate bit rate of 40-Gb/s in EDFA-free DCF-free configuration.

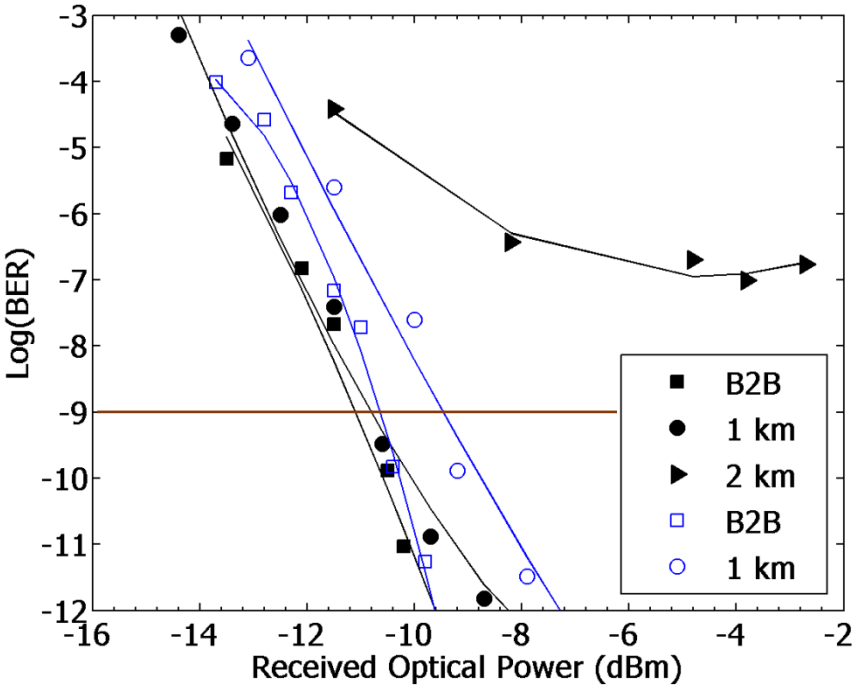


Figure 4.12: BER versus received power for AACC (solid symbols) and 4-PAM (hollow symbols) for B2B, 1-km and 2-km at 100-Gb/s data rate in EDFA-free DCF-free transmission scheme.

Fig. 4.12 depicts the performance comparison of AACC (solid symbols) and 4-PAM (hollow symbols) for 100-Gb/s transmission systems. Performance of both AACC and 4-PAM are severely degraded in comparison to their performances in Fig. 4.11 (at 40-Gb/s). At 100-Gb/s and after transmission over 1-km of SMF it can be seen that AACC has around 0.7 dB penalty compared to its B2B performance at BER of 10^{-9} while 4-PAM is downgrade by ~2 dB penalty. This degradation is attributed to the low tolerance to fibre dispersion of 4-PAM as shown in Subsection 4.2.2.3. For longer distances such as 2-km, error floors arise for both 4-PAM and AACC.

Finally, results in this work divulge that the performance of the proposed multilevel system (AACC) outperforms 4-PAM in terms of required sensitivity and maximum reach. It's also worth to note that in case of experimental demonstration, by utilising an optical equaliser at the optical links or electrical equaliser at the receiver, the maximum transmission distance of AACC signal can be extraordinarily increased. These equalisation techniques have been recently exploited to compensate fibre dispersion of VCSEL or DML systems and realising optical short-range and access networks in the OOK and 4-PAM

transmission systems [9], [13], [23], [97], [103], [104], [116], [132], [134], [148], [172]–[174].

4.3 RZ-AACC

4.3.1 Simulation Setup

In this section, the bit rate of 40-Gb/s is demonstrated for all modulation formats. Assuming that unchirped RZ-AACC signals are generated utilising a cascade of two MZM, as shown in Fig. 4.13. A complex baseband electric field is denoted as $E(t)$. At each MZMs ($i = 1, 2$), the input and output electric fields are described mathematically by the relation

$$E_{1,out}(t) = E_{1,in}(t)\, sin\left(\frac{\pi V_i(t)}{2V_\pi}\right) \tag{4.14}$$

where $V_i(t)$ represents the algebraic difference between the two drive voltages, which are complementary to produce zero chirp. V_π denotes the change in $V_i(t)$ that is required to swing the intensity from minimum to maximum.

The process of generating optical AACC signal via the first MZM is specifically discussed in Section 4.2. It is subsequently transmitted to second MZM (MZM2) which is known as pulse carver with a sinusoidal driving function of $V_2(t)$

$$V_2(t) = Acos(2\pi f_c - \pi\theta) \tag{4.15}$$

where A is the amplitude, f_c is the frequency of $V_2(t)$, and θ is the phase offset.

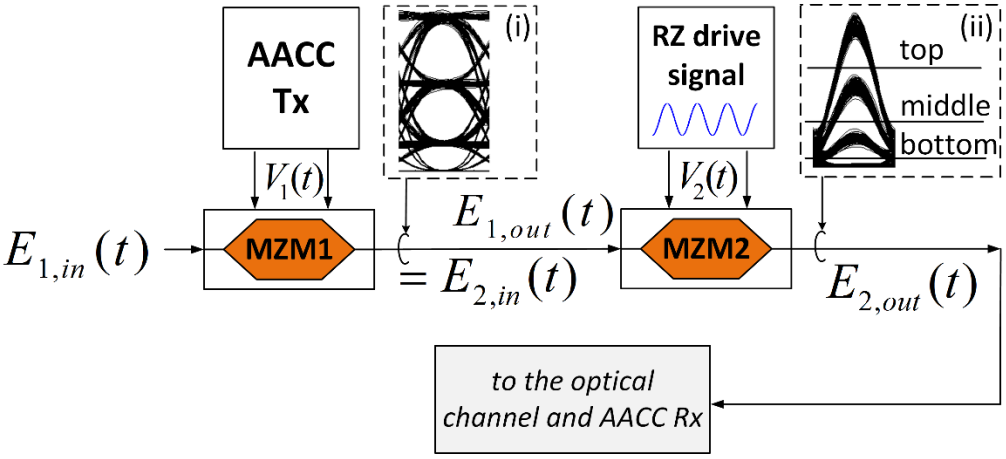


Figure 4.13: Schematic diagram for RZ-AACC Tx. Insets: (i) Simulated eye diagram of optical AACC signal and (ii) optical RZ-AACC signal at 40-Gb/s.

As visualised in Fig. 4.14, the graphical representation gives an overview of different ways in driving the MZM2 to produce 33%, 50%, and 67% RZ-AACC signal. In fact, sinusoidally driving the MZM2 at the baud rate between minimum and maximum transmission results in optical pulses with a full-width at half-maximum (FWHM) of 50% of the bit duration (50%-duty cycle RZ-AACC).

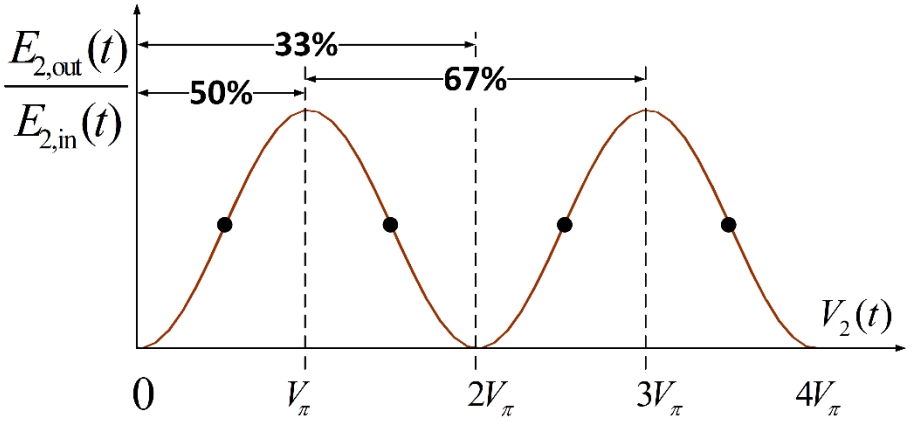


Figure 4.14: Transfer charateristics of the MZM2, indicating the excursion of drive waveform $\boldsymbol{V_2(t)}$ for generating RZ-AACC with different duty cycles (black circles: MZM quadrature point).

The duty cycle therefore can be mathematically expressed by the ratio of the FWHM of the pulse intensity to the time duration of the entire bit slot (T_B):

$$d_c = \frac{T_{FWHM}}{T_B} \tag{4.16}$$

Sinusoidally driving the MZM2 at half the baud rate between its transmission minimum and its transmission maxima realises 33% and 67% RZ-AACC, respectively. The latter modulation format can be also called carrier-suppressed RZ-AACC (CS-RZ-AACC). Note that the optical transmission link and detection technique at the Rx of RZ-AACC modulation remain unchanged as presented in Section 4.2. The motivation of proposing this RZ-AACC format is to further improve the receiver sensitivity and optical power budget in simplified optical access networks which not employing optical amplifiers.

It is also worth noting that in practical demonstration of modulation formats that using RZ pulse shape. In order to ease the complexity of the transmitter due to the use of clock generator and MZM2 as a pulse carver, a cost-effective NRZ-to-RZ converter has been well introduced recently in [104], [107].

4.3.2 Results and Discussion

Optical power spectra and eye diagram of RZ-AACC (with different duty cycles) after the modulation process is depicted in Fig. 4.15 and Fig. 4.13 (inset (ii)), respectively. It has been shown that the duty cycle and the null-to-null bandwidth are inversely proportional.

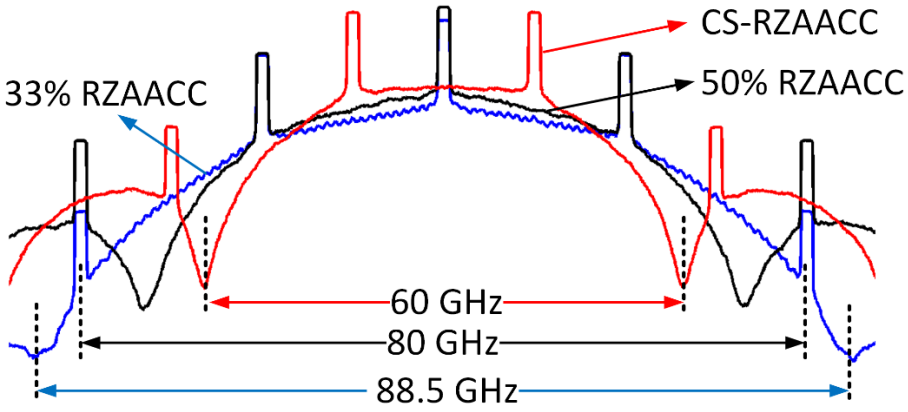


Figure 4.15: Optical spectra of 33%, 50% and 67% RZ-AACC for 40-Gb/s bit rate.

In order to assess the performance, RZ-AACC with other prevailing modulation formats such as 50% RZ and RZ 4-PAM at the same aggregate bitrate of 40-Gb/s are performed and compared. 50% RZ is selected because it is the most common used modulation format in the deployed optical transmission systems. While RZ 4-PAM has similarities to the proposed technique RZ-AACC such as 4-intensity levels signalling, the information rate is 2-bits/symbol as well as direct-detection receiver; especially it has lately attracted much research in high-speed optical transmission system [104], [107] and in full-duplex radio over fibre (RoF) systems for alternative wired and wireless access [93]. Fig. 4.16 exhibits the spectral width of 50% RZ-AACC which is shrunk to half of that of 50% RZ and equivalent to RZ 4-PAM due to the utilisation of partial-response signalling.

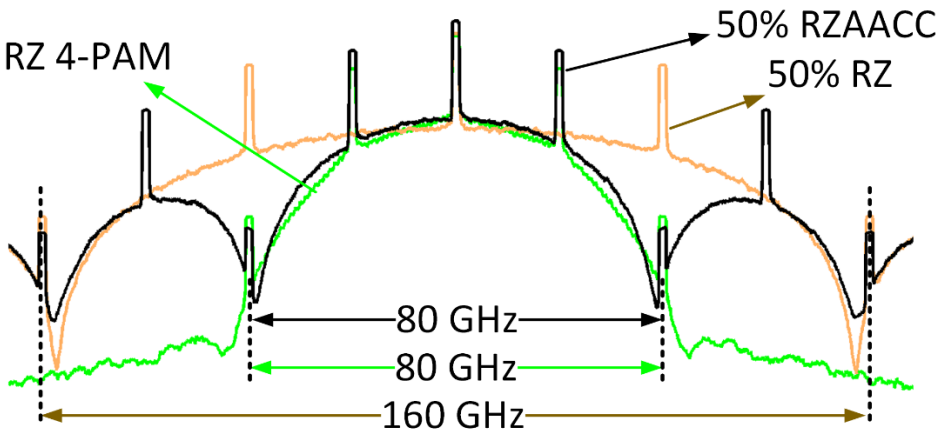


Figure 4.16: Comparison of optical spectra of 50% RZ-AACC to RZ 4-PAM and standard binary 50% RZ signals at 40-Gb/s.

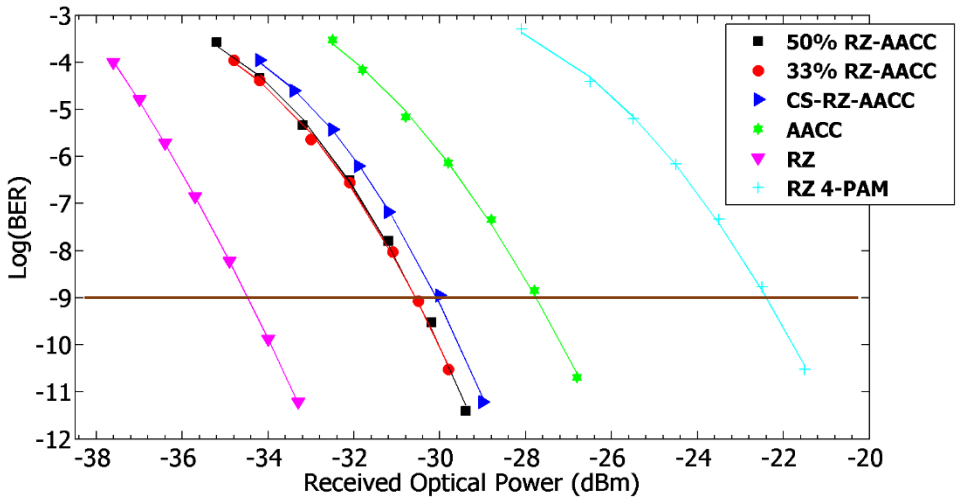


Figure 4.17: BER curves for 50% RZ-AACC, 33% RZ-AACC, CS-RZ-AACC, AACC, RZ and RZ 4-PAM formats in B2B configuration at 40-Gb/s.

The proper BER averaging of RZ-AACC is performed and depicted in Fig. 4.17 to represent the mean BER of the received pattern. As can be clearly seen, the receiver sensitivity of RZ-AACC is enhanced by ~2.5 dB and~8 dB in comparison to AACC and RZ 4-PAM at the BER of 10^{-9}, respectively. More investigations on the comparison between NRZ and RZ-AACC is in Chapter 5. It is worth mentioning that binary RZ signal is best in terms of receiver sensitivity because a superior sensitivity is obtained when the optical pulses take up only a fraction of the bit duration (RZ shape).

Table 4.3 summarises and compares the key performance characteristics of the most commonly used modulation formats for 40-Gbit/s transmission. From this investigation, it is evident that AACC is more robust to dispersion which is of help to extend the transmission distance in optical IM/DD systems.

Table 4.3: Comprehensive comparison between MZM-based advanced optical modulation formats reported recently at 40-Gb/s (BER = 10^{-9}) [29], [44], [72].

Modulation Format	Information Capacity (bits/symbol)	Positive CD Tolerance (ps/nm)	Spectral Efficiency (b/s/Hz)	Complexity
NRZ	1	+85	0.5	Low
33% RZ	1	+52.5	0.17	Medium
50% RZ	1	+55	0.25	Medium
67% CSRZ	1	+58	0.33	Medium
Duobinary	1	+145	1	High
MMT	4	+137	1	High
4-PAM	2	+96	1	High
AACC	2	+168	1	High

4.4 8-AACC

4.4.1 Simulation Setup

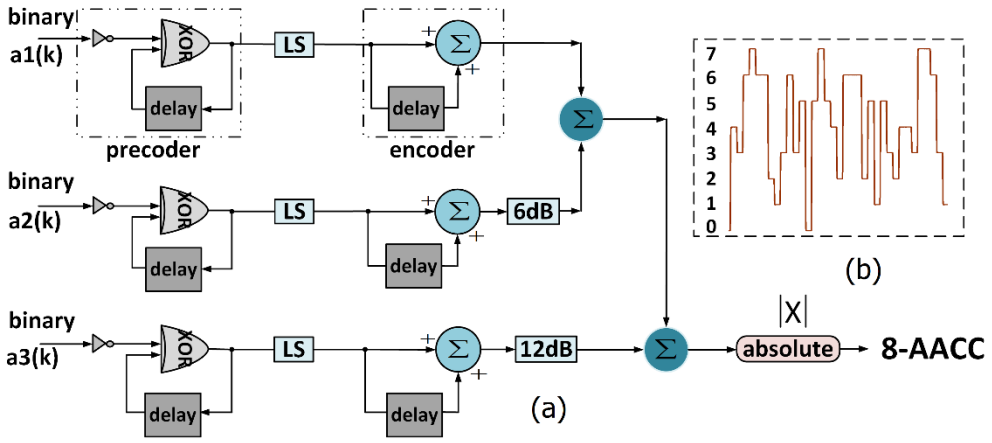


Figure 4.18: The electrical 8-AACC signal. (a) 8-AACC encoding and (b) 8-AACC waveform.

The block diagram of 8-AACC in electrical domain is illustrated in Fig. 4.18 (a) that consists of three duobinary tributaries. The output achieves eight equally-spaced intensity levels by attenuating the second tributary by 6 dB and the third by 12 dB. The passive power combiners combine the three tributaries to generate a 15-level bipolar signal that is symmetrical about zero. The absolute circuit converts the 15-level bipolar signal to eight unique positive polarity symbols {0, 1, 2, 3, 4, 5, 6, 7} as shown in Fig. 4.18 (b).

Fig. 4.19 describes the 8-AACC transmission setup operating at bit rates of 30-Gb/s, 60-Gb/s and 75-Gb/s. The optical 8-AACC signal was generated using a single-drive multiple quantum-well MZM to modulate the optical carrier from a LD operating at ~1550 nm. A PRBS of length $2^{10}-1$ was used to generate the signals. The output of the MZM was then launched into different lengths of standard SMF with chromatic dispersion and attenuation of 17 ps/nm/km and 0.2 dB/km, respectively. A VOA adjusts the received optical power into the PD that has a responsivity of 0.8-A/W. A Gaussian LPF rejects the noise at the detector output that is outside the signal bandwidth; the filter

bandwidth was set at 80% of the symbol rate. The error analyser module was implemented in MATLAB® for data recovery and calculating the BER. Both 8-AACC and 8-PAM modulation formats have seven decision thresholds that are chosen as the midpoint between two adjacent symbol levels. The aggregate BER was determined from the bit errors according the recovery of symbols by comparing the filtered signal with the 8-AACC and 8-PAM threshold levels. It is worth mentioning that this transmission setup is considered as a short-reach links or data centre interconnections. The motivation of proposing 8-AACC is because of the nature of 8-PAM signal, increasing the number of level also leads to increased ISI. In other words, 8-PAM is more sensitive to CD and therefore would reduce the fibre transmission length as reported in [97], [175].

Insets (i) and (ii) in Fig. 4.19 display the B2B electrical eye diagram and optical null-to-null spectra of 8-AACC. For a fair comparison, the transmission setup for 8-PAM was similar to 8-AACC. It is observed that both 8-AACC and 8-PAM signals have the same spectral bandwidth, hence the same spectral efficiency, as shown by inset (ii).

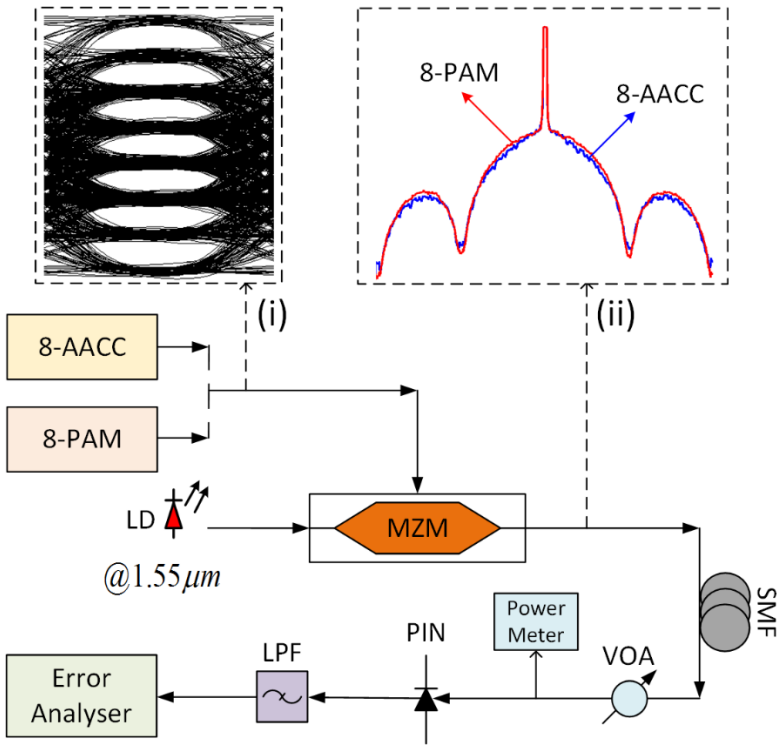


Figure 4.19: 8-AACC and 8-PAM transmission setup. Insets: (i) B2B eye diagram of 8-AACC and (ii) Optical spectra.

4.4.2 Results and Discussion

Fig. 4.20 depicts the receiver sensitivity at 30-Gb/s, 60-Gb/s and 75-Gb/s for 8-AACC (solid markers) and 8-PAM (hollow markers). At 30-Gb/s, the B2B sensitivity at 10^{-9} BER was around -9.5 dBm for both 8-level signalling. The plots show a power penalty of about 1.5 dB and 2 dB as the bit rates increase to 60-Gb/s and 65-Gb/s, respectively. The BER performance agrees very well with the 8-PAM results from the IEEE 802.3bm Fibre Optic Task Force at 75-Gb/s which plotted in dotted straight line in Fig. 4.20 [164].

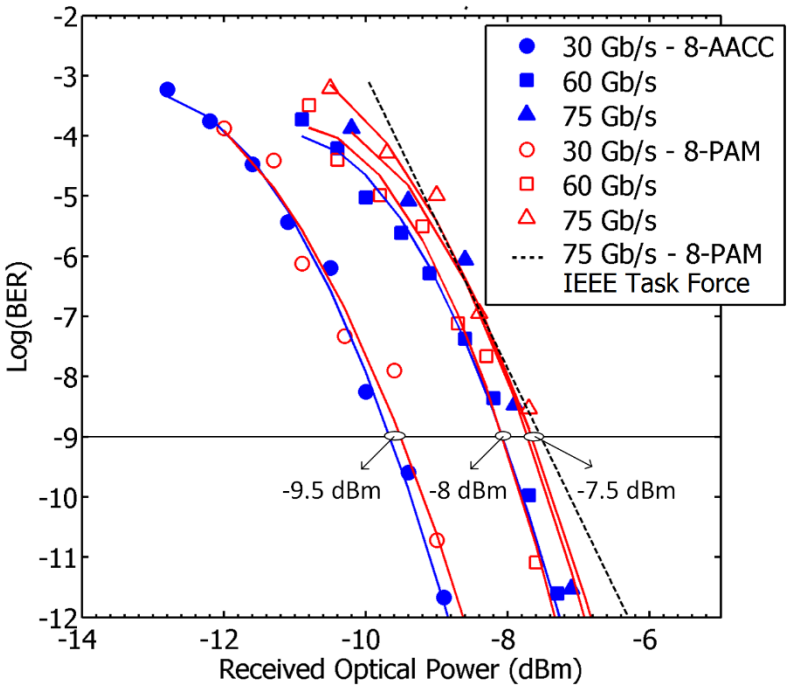


Figure 4.20: Receiver sensitivity at 30-Gb/s, 60-Gb/s and 75-Gb/s in B2B configuration for 8-AACC (solid markers) and 8-PAM (hollow markers).

Fig. 4.21 compares the BER performance at 75-Gb/s over 2-km and 3-km of SMF for 8-AACC and 8-PAM. The plots show that for the BER of 10^{-9}, the receiver sensitivity of 8-AACC is around -6.8 dBm, which is about 1.4 dB better than that of 8-PAM. As the transmission distance increased to 3-km, the performance of 8-PAM degrades noticeably having reached a BER floor of 2×10^{-6}, compared to about 2.6 dB of power penalty for the 8-AACC. The results

from Fig. 4.21 would suggest that 8-AACC is capable of reaching a BER floor of 1×10^{-8} over a transmission length exceeding 3-km.

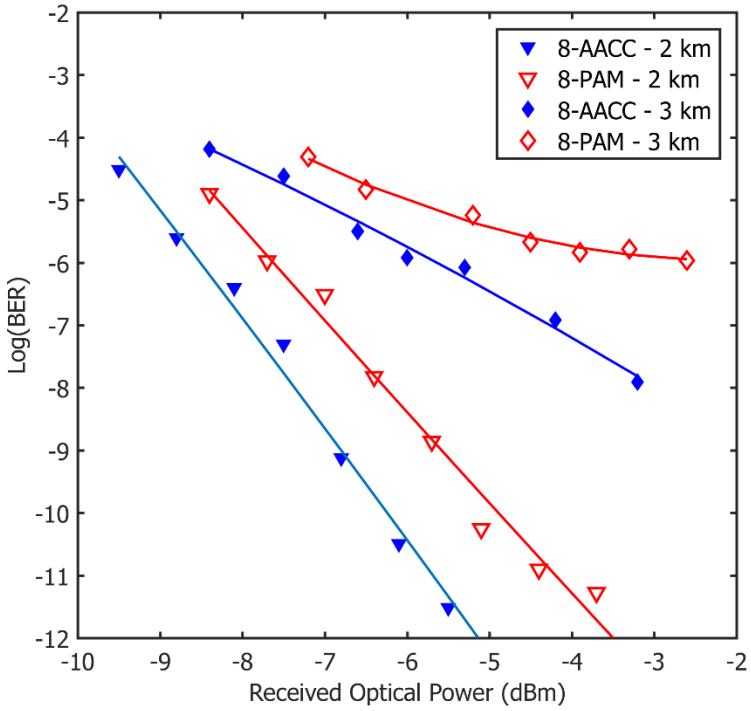


Figure 4.21: Receiver sensitivity at 75-Gb/s over 2-km and 3-km of SMF.

Fig. 4.22 compares the received eye diagrams of 8-AACC and 8-PAM after 2-km and 3-km of SMF delivery for qualitative comparison. While the eight amplitude levels in the eye diagrams are virtually uniform, the closures of the upper eyes are evident with 8-PAM compared to 8-AACC, reflecting a degradation in the receiver sensitivity and corresponding to an increase in the BER. In addition, the narrowing of the eye diagrams with transmission distance is indicative of the effect of dispersion-induced ISI. 8-AACC based on duobinary signalling is more resilient to dispersion compared to 8-PAM which is NRZ-based scheme.

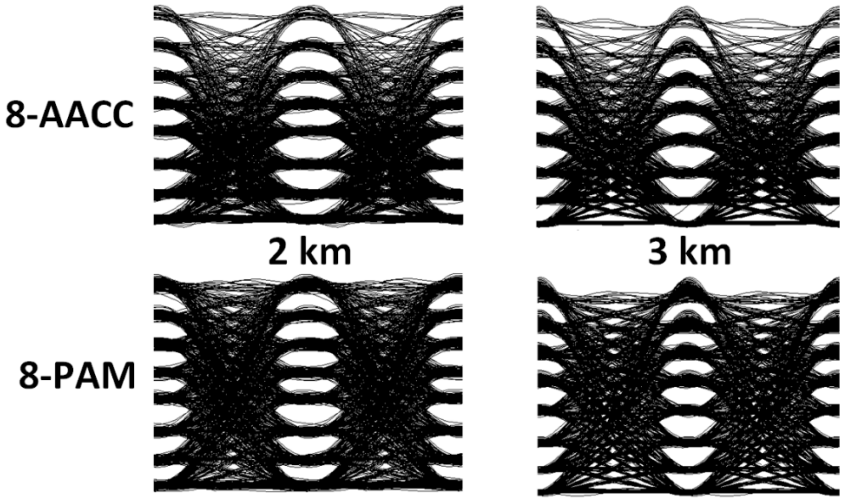


Figure 4.22: Eye diagrams of 8-AACC and 8-PAM at 75-Gb/s after transmisison over 2-km and 3-km of SMF.

4.5 Concluding Remarks

In this chapter, the novel higher-order modulation format, called AACC, which is an extrapolation of the partial-response signalling family are numerically demonstrated. The results show a clear advantage of the proposed AACC technique over NRZ, 50% RZ and 67% CS-RZ in terms of spectral efficiency and dispersion tolerance.

The performance of AACC in comparison to 4-PAM whose characteristics are fairly similar to AACC e.g. same number of levels, capacity of 2 bits/symbol as well as direct-detection receiver. It is shown that at 40-Gb/s and BER of 10^{-9} AACC signal can be transmitted over 10-km of SMF whereas 4-PAM can only reach to 5-km. Moreover using this proposed technique, two lanes can be carried over the same WDM channel which consequently resulting in the capacity utilisation of the networks can be increased at tolerable penalty.

A new modulation scheme utilising RZ format over absolute added correlative coding (RZ-AACC) is also presented and evaluated. Considerable receiver sensitivity improvement of 2.5 dB and 8 dB has been obtained in comparison to conventional AACC and RZ 4-PAM, respectively at 40-Gb/s.

AACC with eight levels has also been proposed and demonstrated numerically at bit rates of 30-Gb/s and 60-Gb/s, and up to 75-Gb/s over 2-km and 3-km of SMF using a MZM targeting short-range optical interconnection applications. The performance has been evaluated and compared to the conventional 8-PAM in terms of the BER and received electrical eye diagrams. The results show that 8-AACC has better receiver sensitivity and is more resilient to dispersion-induced ISI than its 8-PAM counterpart.

It is promising that AACC-based signalling can be used as an alternative modulation format in the next-generation optical IM/DD transmission systems.

Chapter 5– Comparison of NRZ versus RZ Pulse Shapes over AACC in Linear and Nonlinear Transmission Medium

5.1 Introduction

It is obvious that for any optical modulation format, one of the decisive dependent parameters in system design and performance optimisation is the pulse coding format. For practical reason, this choice is often between RZ and NRZ impulse shaping, with possible variation in duty cycles [80], [88], [89]. In the last decades, many reports have continuously centred on the comparative study of impulse coding of NRZ and RZ for binary schemes e.g. OOK [48], [80], [81], differential phase shift keying (DPSK) [48], [76] and duobinary [88], [89] whereas the multilevel signalling such as 4-PAM [93], [107] and differential quadrature phase shift keying (DQPSK) [176] has recently received considerable attention.

Such researches have yielded critical conclusions. In specific that modulation formats with RZ impulse shaping are more similar to a soliton transmission, having a ~2 dB advantage in performance over NRZ pulse in ASE noise-limited systems. This is because of an inherent tolerance to ISI of the RZ pulse shape. In other words, reported in 1977 Personick pointed out that of the received pulse energy is constant, a superior sensitivity is obtained when the optical pulses take up only a fraction of the bit duration (RZ impulse coding) [161]. The aim of this section is to present a direct comparison between NRZ and RZ pulse shaping in AACC transmission whether the same conclusions hold true for AACC. A numerical analysis of externally-modulated direct-detection on NRZ-AACC and RZ-AACC system in dispersive transmission medium with different conditions. Moreover the impact of fibre nonlinearity e.g. SPM on the performance of AACC is also investigated.

The materials presented in this chapter have been published in:

N. Dong-Nhat, M. A. Elsherif, H. Le Minh, and A. Malekmohammadi, "NRZ versus RZ over Absolute Added Correlative Coding in optical metro-access networks," *Opt. Commun.*, vol. 387, pp. 30–36, 2017.

5.2 System Model and Performance Settings

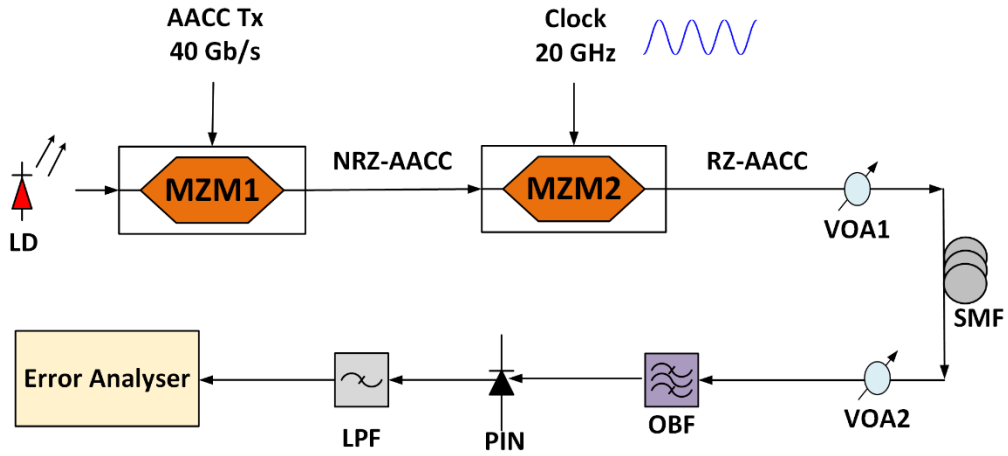


Figure 5.1: Schematic configuration of NRZ-AACC and RZ-AACC transmitter and direct detection used in the simulation.

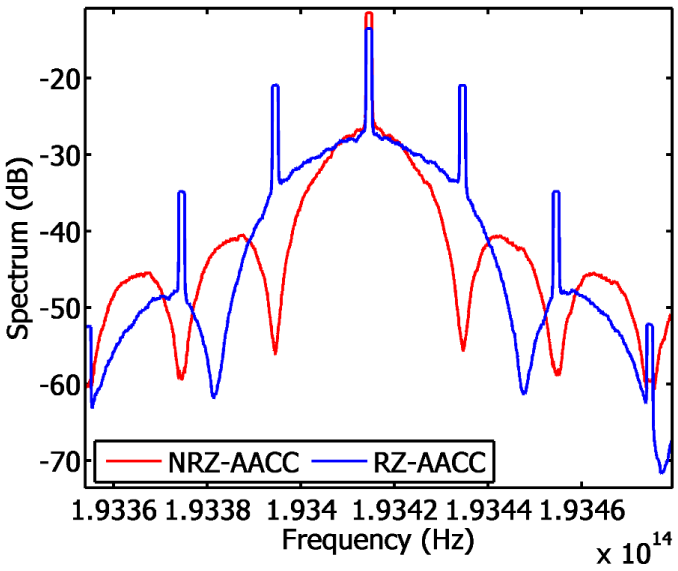


Figure 5.2: Optical spectral width of NRZ-AACC and RZ-AACC measured at 20-Gbaud/s. The spectrum analysers are placed right after the modulators.

The simulated systems are displayed in Fig. 5.1. The optical NRZ-AACC signal was produced by modulating the light from a LD which radiates an optical carrier wave at ~1550 nm with a $2^{10}-1$ PRBS at an aggregate bitrate of 40-Gb/s using a single-drive multiple quantum-well MZM (MZM1). The bias voltages V_{b1}, V_{b2} and the modulation voltage V_{mod} of the MZM1 were set at -1V, -2.3V and 1.3V respectively. Thanks to these parameters, it is expected to obtain the optimal receiver sensitivity since it satisfies the relationship, $V_{mod} = V_{b1} - V_{b2}$ [58]. After producing NRZ-AACC signal, a periodic RZ pulse train with 50% duty cycle was generated by driving a lithium niobate MZM (MZM2), which was biased at quadrature, with 20-GHz clock signals from a sine generator. For the case of MZM2, modulating signals were applied to both electrodes in a push-pull configuration. The voltages applied to arm 1 and 2 were fixed at -2 V and 2 V respectively. The bias voltages were $V_{b1} = 0$ V and $V_{b2} = 2$ V. The modulated NRZ- and RZ-AACC signals were then transmitted to a VOA1, which controls the LP into a standard SMF with variable lengths, the dispersion coefficient was set to 17 ps/nm/km. A second VOA (VOA2) was used to vary the received optical power. A 2nd order Gaussian OBF with bandwidth of 85-GHz, which are typical of WDM networks employing the International Telecommunication Union (ITU) 100-GHz grid, was used to reduce the deleterious effects on the system performance [177], [178]. Finally the signals were detected using a PIN photodetector with responsivity equal to 0.8-A/W, followed was a 13-GHz Gaussian 4th order LPF.

Fig. 5.2 illustrates the 40-Gb/s optical NRZ- and RZ-AACC spectra. It is apparent that RZ-AACC spectrum exhibits a wider null-to-null bandwidth. Indeed, the spectral width of RZ-AACC is 80-GHz resulting in a spectral efficiency of 0.5-b/s/Hz while that of NRZ-AACC is halved to give a spectral efficiency of 1-b/s/Hz. This is because the first-null bandwidth of RZ-AACC with duty cycle $\tau = 0.5$ is defined as $B = R_s/\tau$, where R_s represents the signalling rate (or baud rate) as discussed in Chapter 3.

5.2.1 Comparison of the Transmission Performance in Erbium-Doped Fibre Amplifier (EDFA)-free and Dispersion Compensation Fibre (DCF)-free Configuration

As a first set of simulation, the forbearance of the two multilevel intensity signalling to the chromatic dispersion was investigated. As the transmission distance without amplifiers are extended, fibre chromatic dispersion causes severe ISI which becomes an important factor limiting the system reach. To ensure a fair comparison between NRZ and RZ impulse shaping, the LP into SMF is decreased to a relatively low value about 0 dBm.

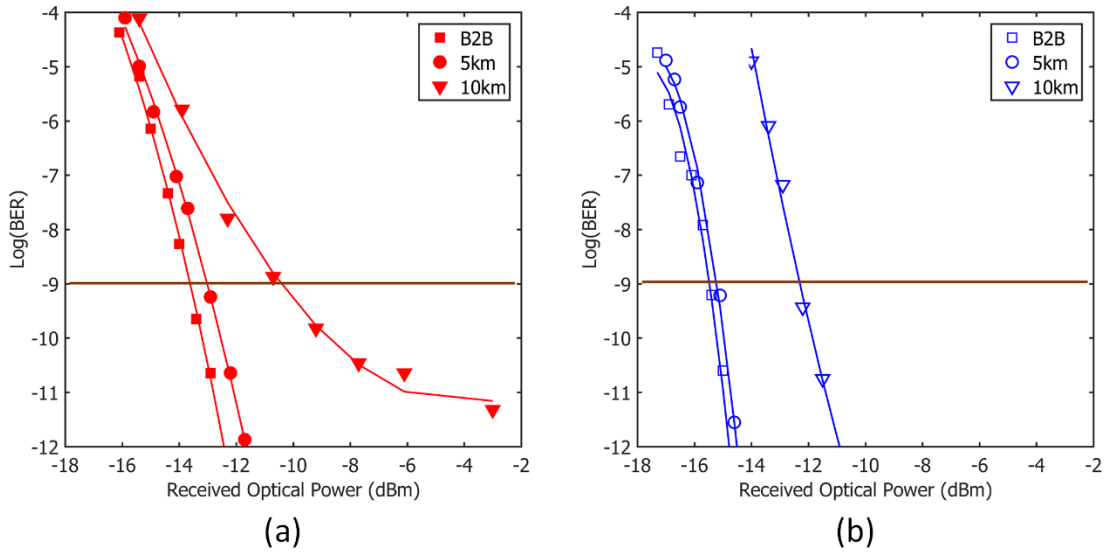


Figure 5.3: Calculated BER performance in optical access networks using (a) NRZ-AACC and (b) RZ-AACC data.

Fig. 5.3 (a) and (b) indicate the BER curves of NRZ-AACC and RZ-AACC respectively. The overall BER performance comparison indicates that the latter outperforms the former by at least 1.5 dB which matches our theoretically aforementioned conjecture. In fact, the B2B receiver sensitivity of NRZ-AACC was found around -13.8 dBm whilst that of RZ-AACC was ~-15.2 dBm. An

adequate average BER after 10-km SMF transmission can be acquired at an optical received power of ~-10.4 dBm for NRZ pulse shape resulting in a power penalty to B2B condition in such case was 3.4 dB. On the other hand, -12.4 dBm receiver sensitivity for the same SMF transmission distance was observed for RZ coding in Fig. 5.3 (b). The minimal power penalty of 2.8 dB was discovered as well in this case.

It is worth noting that for NRZ-AACC signal, an error floor was observed at 10^{-11} after 10-km transmission, while RZ-AACC was able to maintain a good sensitivity at BER of 10^{-12} at that distance. This could be interpreted based upon the RZ pulses which can benefit from its soliton-like transmission to perform better than NRZ-AACC during propagation in SMF. However the performance of NRZ-AACC could be improved as long as the LP is accurately monitored as discussed in the following section [80], [89].

5.2.2 Comparison of Self-Phase Modulation (SPM) Tolerance as a Function of the Residual Dispersion

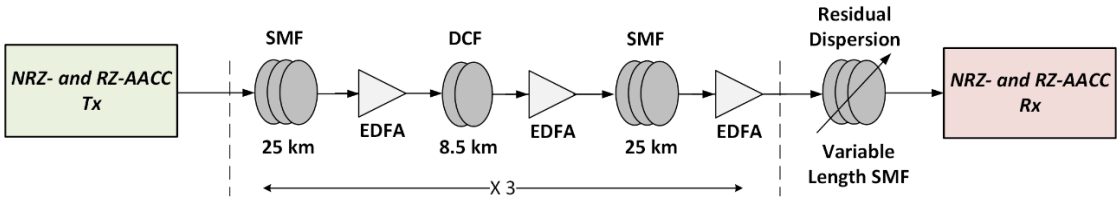


Figure 5.4: Setup for scrutinising SPM effects and residual dispersion of optical NRZ- and RZ-AACC transmission systems.

In this section, another set of simulations is generated in order to examine the tolerance of the NRZ- and RZ-AACC transmission at 40-Gb/s in the presence of Kerr effect which results in SPM nonlinearity. To examine the signalling format resilience to SPM, various LPs ranging from -5 to 10 dBm are considered into three spans of 2×25-km SMF link as shown in Fig. 5.4. Dispersion-compensating methods and EDFAs are inevitably required in >100-km

transmission systems. Hence the overall fibre dispersion of the SMF for each span was fully compensated by using a DCF module of 8.5-km. The SPM effect in the DCF module is negligible since its LP was adjusted to less than 0 dBm. Each fibre is followed by an in-line EDFA with a noise figure of 6 dB to amplify the generated signals and offset the transmission loss. A post SMF was used to adjust the residual dispersion.

The fibre parameters such as dispersion coefficient (D), dispersion slope (S), attenuation, effective area (A_{eff}), nonlinear index of refraction (n_2) and nonlinear coefficient (γ) are indicated respectively in Table 4.2. The receiver were remained the same as in Fig. 5.1. It should be noted that the accumulated amplified spontaneous emission (ASE) noise is the major noise source that generated over several EDFAs in cascade that would degrade the signal quality. However shrinking the OBF bandwidth would reduce the effects of ASE noise and improve the system performance [88], [101].

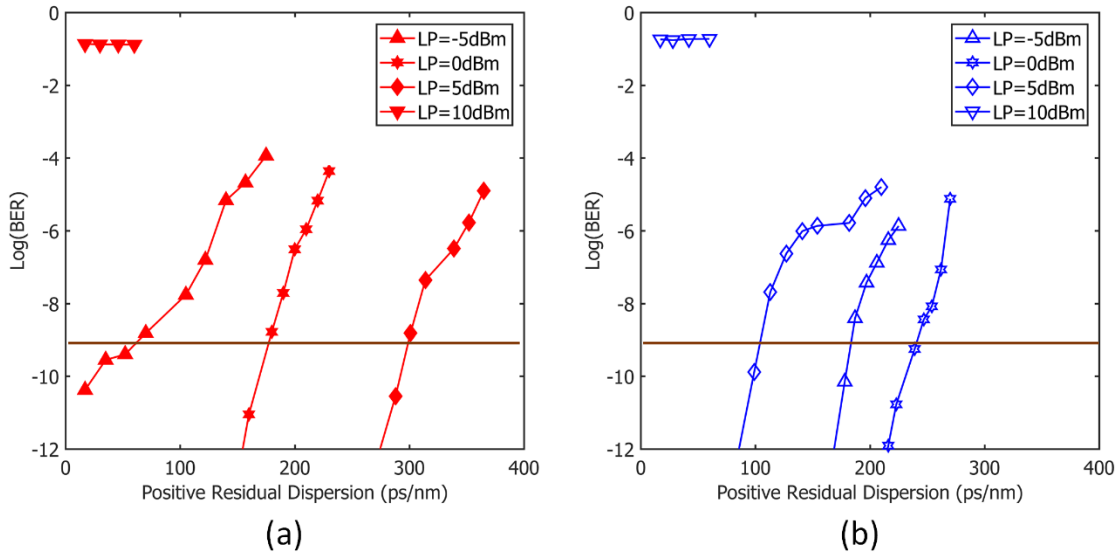


Figure 5.5: BER versus simulated positive residual dispersion using (a) NRZ-AACC and (b) RZ-AACC data.

Fig. 5.5 (a) and (b) depict the BER versus positive residual dispersion for corresponding NRZ and RZ pulse shapes with LP were set to -5, 0, 5 and 10 dBm at the output of transmitter. There are several interesting features in the data. For the NRZ-AACC signal, the residual dispersion was set from 0 to 400

ps/nm. From Fig. 5.5 (a), as LP was increased from -5 to 0 dBm, the dispersion tolerance was relatively improved from ~60 ps/nm to ~160 ps/nm which is equivalent to a better residual distance of about 5.8-km. At a high LP of 5 dBm, the optimum NRZ-AACC performance is obtained with the tolerance to residual dispersion of roughly 300 ps/nm. If LP was set to 10 dBm, the dispersion resilience was severely degraded by the pulse distortion because of the weak SPM tolerance.

For the RZ-AACC signals, the positive residual dispersion was varied from 0 to 300 ps/nm as shown in Fig. 5.5 (b). In LP set to -5 and 0 dBm, the attained dispersion was 180 and 240 ps/nm respectively, which highlight its superiority to NRZ-AACC. In contrast to NRZ coding, SPM clearly affects the residual dispersion tolerance even at a reasonably modest LP of 5 dBm. The dispersion was found about 100 ps/nm which is one-third of that for NRZ format circumstance. In other words, NRZ-AACC signal could offer longer signal propagation with a residual distance of nearly 12-km SMF in comparison to RZ-AACC. An error-floor also occurred when increasing the LP up to 10 dBm.

These simulated results interpret that the SPM nonlinearity can be actually used to improve the NRZ-AACC system performance, as long as the LP is properly controlled.

5.2.3 Comparison of the Transmission Performance in Optical Metro Networks

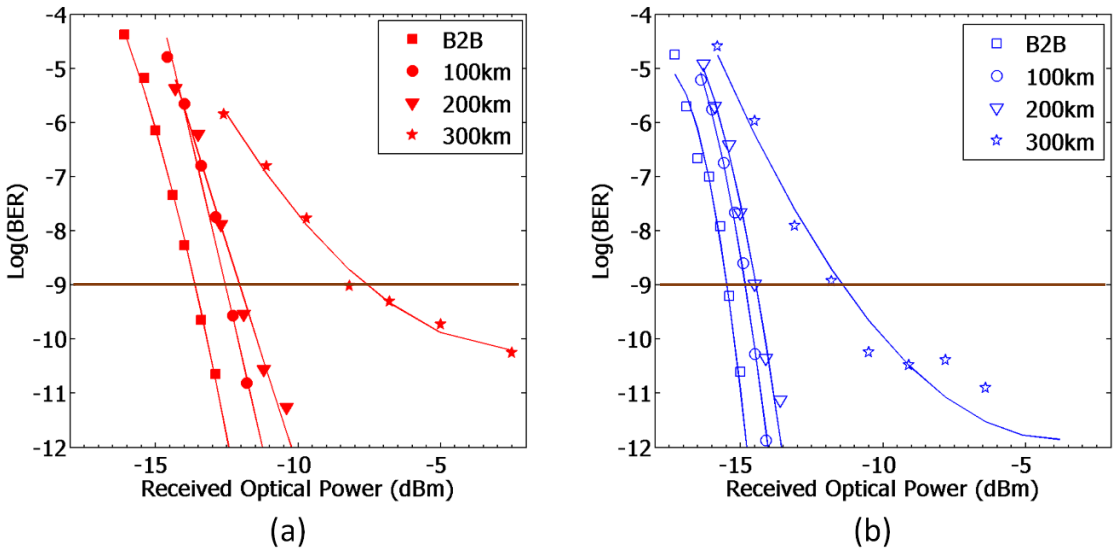


Figure 5.6: Calculated BER characteristics as a function of the transmission distance in optical metro networks using (a) NRZ-AACC and (b) RZ-AACC.

Fig. 5.6 illustrates the BER performances for NRZ-AACC and RZ-AACC transmission for B2B, 100-km, 200-km and 300-km of SMF at 40-Gb/s. For a fair comparison between these two multilevel signalling, the LP was fixed at 0 dBm for both cases. The number of spans in the simulation setup was increased to six spans which can be considered to be an optical metro network. All parameters and BER estimation technique were kept the same as in the previous simulation.

It is shown that the overall comparison in terms of power penalty between RZ-AACC and NRZ-AACC for B2B scenario or after different transmissions was typically 1-2 dB. For example, with regard to Fig. 5.6 (a), it is capable to achieve a receiver sensitivity of ~-11.8 dBm after 200-km SMF transmission for NRZ impulse while that of RZ impulse was ~-13.8 dBm as displayed in Fig. 5.6 (b). Extending the transmission up to 300-km of SMF, revealed a similar penalty.

5.3 Concluding Remarks

In this chapter, a numerical investigation on 40-Gb/s NRZ- and RZ-AACC modulation formats using a binary direct detection receiver in optical access and metro networks has been presented. AACC using the NRZ and RZ pulse shapes has been thoroughly compared in terms of fibre chromatic dispersion, residual dispersion and SPM tolerance as well as receiver sensitivity.

It is shown that, for AACC transmission, the NRZ impulse shaping is superior in comparison to RZ in spectral efficiency, residual dispersion and SPM tolerance. However RZ-AACC experiences a ~1-2 dB advantage in receiver sensitivity over NRZ-AACC for B2B configuration as well as after 300-km SMF delivery which agrees the aforementioned theoretical analysis.

Chapter 6– AACC Experimental Verification

6.1 Introduction

This chapter discusses the experimental implementation of AACC by presenting the commercial components that able to be used to generate the AACC signal. In fact, various possibilities is discussed in order to form the AACC transmitter and then producing its electrical signal. This experiment took place in KAIST, Korea. A DSP-based module to produce AACC signal is also developed.

6.2 Options to Construct the AACC Transmitter

For the electrical AACC mapping structure, one might be concerned that the complexity of the AACC transmitter was higher than other systems. Nevertheless, as presented in the previous chapter AACC transmitter is mostly based on duobinary transmitter. Work on duobinary technology in the aspects of integrated circuit (IC) has now reached to the stage where cost-effective commercial products are being readily developed [85], [179], [180]. As a matter of fact, major components required by electrical AACC transmitter were the delay and add block which is the high-speed differential precoder IC modules and full-wave rectifiers [179] which have been successfully introduced back in 1997.

Two years later, same research group fruitfully demonstrated the fabrication of the electrical duobinary IC transceiver based on indium phosphide (InP) material and performed at 40-Gb/s optical transmission [181].

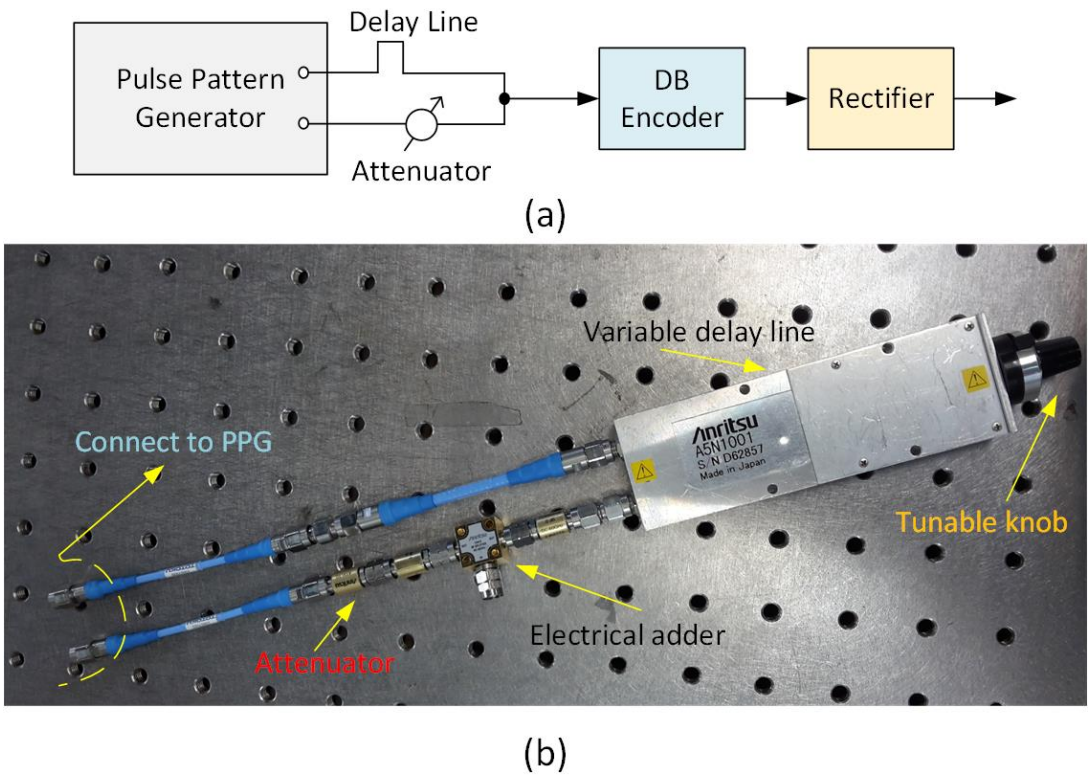


Figure 6.1: (a) AACC experimental schematic and (b) AACC components.

Fig. 6.1 (a) and (b) display the block diagram and the necessary components to build the electrical AACC transmitter. Most the components are commercialised by Anritsu, Marki Microwave, Midwest Microwave Solutions and Weinschel. They are linked by using sub-miniature version A (SMA) connectors.

As specifically discussed in Chapter 2 and 3, electrical AACC transmitter is actually a duobianary encoder which can be realised by either a delay and add block or the electrical low-pass filter having 3 dB bandwidth of $^1/_4$ of the bit rate [29] [83]. These filters are typically manufactured by Anritsu, Tektronix and Hewlett Packard.



Figure 6.2: Low-pass filters.

Another effective and compact method for electrical AACC generation is the use of electronic test equipment arbitrary waveform generator (AWG) instead of creating the transmitter based on aforementioned components. In fact, this is a powerful tool that can flexibly generate complex signals by loading a *.txt file which is developed by MATLAB®-based DSP module. Due to this significant advantage, AWGs have been widely used in current experimental demonstration [61], [118], [141], [182]. AWGs are capable to produce any arbitrarily defined shape by jumping from sample to sample or utilise any kind of interpolation to connect the consecutive points.

Figs. 6.3 shows the AWG from Tektronix and Keysight companies (formerly known as Agilent). The former is used in the experiment testbed later. The former with an integrated LCD display allows for the generation of arbitrary electrical signals with a sampling rate of 12-GSa/s. With the aid of *interleaving* mode, the sampling rate can be doubled. The drawback of such generators is the very high cost which could reach tens of thousands of US dollars.

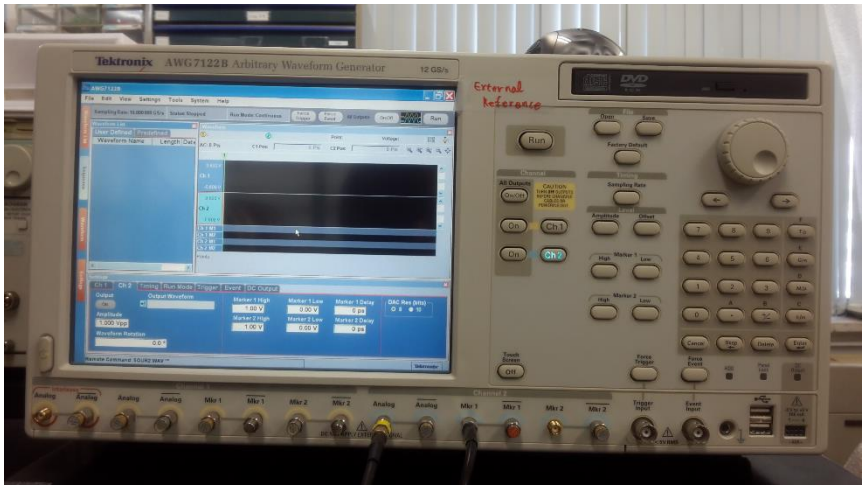


Figure 6.3: Tektronix arbitrary waveform generator (AWG7122B).

6.3 DSP-based AACC Generation

Due to the availability of the Tektronix AWG at that time, a transmitter DSP-based AACC is developed and then performed transmission at the data rate of 5-Gb/s as a proof of concept to the numerical results.

Fig. 6.4 shows the DSP flow chart for AACC signal. Two PRBS patterns with length of $2^7 - 1$ bits were used for bit-to-symbol mapping and generation of the AACC. The purpose of using a short PRBS pattern is to reduce the computing time during the execution of the DSP transmitter. The tributaries were up-sampled by a factor of 2 to fulfil the Nyquist criterion since the AWG setting is in normal circumstances with the sampling rate of 12-GSa/s. Note that one of the bit streams was 24-bit delayed and halved in amplitude for decorrelation. The upsampling signals were subsequently transmitted to the correlative coding algorithm unit. First task of this module was to convert the binary streams (0, 1) to (-1, 1), then embedded to the duobinary pulses to generate ternary-level signalling which is symmetric with respect to '0'. Two streams of bipolar signal then added to form a 7-level signal and sent to the rectifier to produce a nonnegative signal with normalised intensities as (0, 1, 2, 3). After that, the electrical AACC waveform was saved into *.txt file and transferred to the AWG (Appendix C).

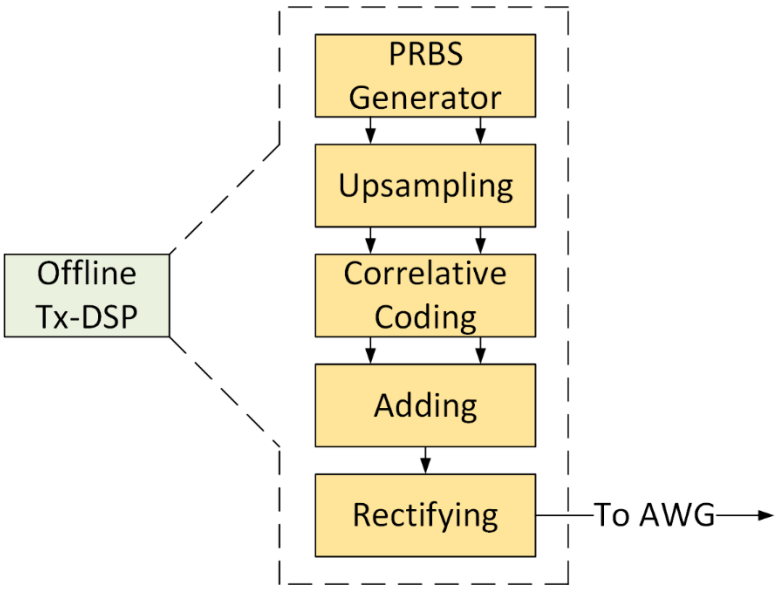


Figure 6.4: Offline DSP stack employed at the transmitter.

The DSP-based AACC signal was then tested by performing an electrical B2B transmission. The generated signal was captured by means of Keysight digital communication analyser (DCA) as shown in Fig. 6.5. It is clear to recognise that the AACC eye diagram exhibited on the DCA is in good agreement with the numerical analysis presented in Chapter 4 (Inset of Fig 4.6). In fact, due to the unique generation, the clear eye openings for AACC signal – especially the upper eyes has been achieved which reveals an improvement in receiver performance and corresponds to a reduction in the BER. This is because the upper eye in the eye diagram usually causes higher system performance degradation or by other words, its quality factor is lower as shown in Equation 4.8. Fig. 6.6 shows the measured optical spectra of AACC signal using Anritsu optical spectrum analyser.

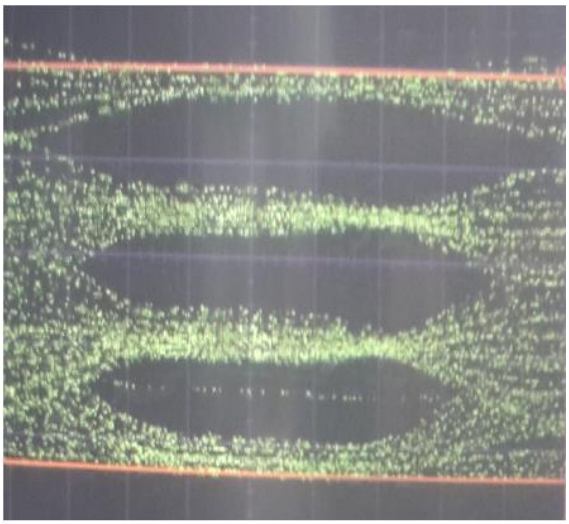


Figure 6.5: AACC eye diagram displayed on the digital communication analyser.

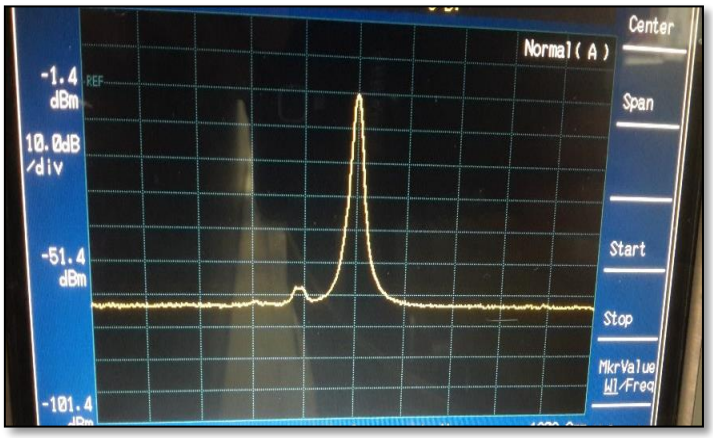


Figure 6.6: Optical spectra.

6.4 Concluding Remarks

With the full support from the lab at KAIST, Korea, it is presented in this chapter the essential components to construct the electrical AACC transmitter for future implementation. All of the components in fact were introduced back in 1997 and have been extensively commercial. No unreal components are needed which enabling AACC as a cost-efficient solution to real-life applications.

A DSP-based module has also been developed to generate the electrical AACC signal. Thanks to the use of the AWG and DCA, the experimental results have been verified. It qualitatively matches the presented numerical analysis as a proof of concept.

With the developed DSP module, it is promising to apply AACC in any experimental transmission systems.

Chapter 7– Alternative Dispersion Compensation Techniques

7.1 Introduction

In this chapter, extended works are proposed to present two state-of-the-art alternative techniques for mitigating the fibre dispersion that causes signal distortion. Two techniques namely OEQ (optical domain) and EEQ (electrical domain) is comprehensively reported in numerical simulations and experiments, respectively.

The materials presented in this chapter have been issued in *OSA Advanced Photonics – Signal Processing in Photonic Communications* (USA) *and OSA IONS* (Japan) as follows:

N. Dong-Nhat, L. Nguyen, and A. Malekmohammadi, "Combining filtered antipodal signaling and optical equalization for extended-reach access networks," in *Advanced Photonics - Signal Processing in Photonic Communications*, USA, 2017, p. SpM2F.1.

N. Dong-Nhat and A. Malekmohammadi, "28-Gb/s PAM-4 transmission over 50-km of SSMF using a Mach-Zehnder modulator and linear equalizers," in *IONS – Okinawa*, Japan, 2017.

7.2 Optical Equalisers

In this work, a simplified optical access networks without having optical amplifiers, filters and dispersion compensation fibre is considered at 25-Gb/s and 50-Gb/s. The main motivation is to extend the transmission distance without adding any devices at both electrical transmitter and receiver for dispersion compensation. The transmission reach and BER are actually improved with optical duobinary signalling using 1^{st} and 2^{nd} OEQs for dispersion compensation for the first time in pre-equalisation scenario. Note that NRZ signalling with identical OEQ configurations is also demonstrated for qualitative comparison.

It has been reported that duobinary is not effective when combining with adaptive electronic compensation or EEQ as discussed in Ref. [183]. Therefore the integration of duobinary and OEQ is demonstrated for the first time in this work.

7.2.1 Simulation Setup

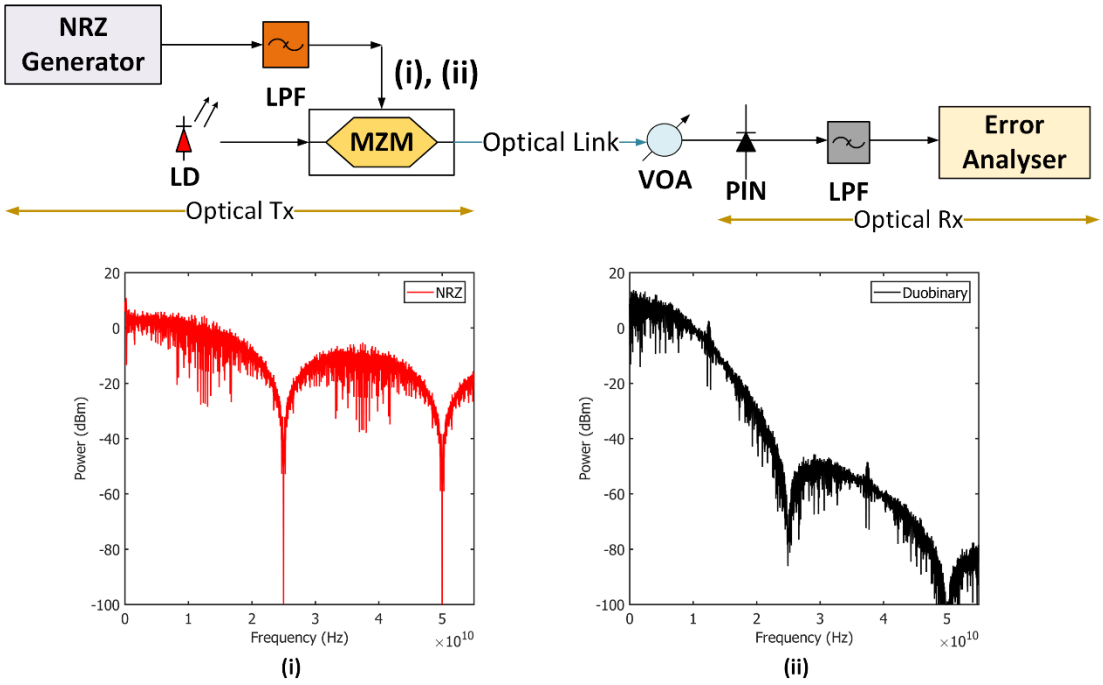


Figure 7.1: Simulation setup at 25-Gb/s. Insets (i) and (ii) are the electrical spectra of NRZ and duobinary respectively.

Fig. 7.1 illustrates the simulation setup for the 25-Gb/s duobinary transmission in simplified access networks. To generate duobinary signals, the NRZ intensity signals were filtered by a 5^{th}-order Bessel filter with a 3 dB bandwidth of about 25% of the bit rate. Insets (i) and (ii) show the electrical spectra for conventional NRZ signals and duobinary respectively. The duobinary signal having a substantially reduced bandwidth can be expected to show more resilience than NRZ signal to fibre dispersion, thereby achieving a longer SMF transmission distance. The electrical duobinary drive signal modulates the optical carrier wave from the LD operating at ~1550 nm with a $LiNbO_3$ MZM biased at null

[37]. The MZM insertion loss is 2 dB. $V_1(t) = V_2(t) = 4$ V nominally are the modulating RF electrical voltage. V_{b1}= 0 V and V_{b2}= 4 V are the bias voltages applied to upper and lower arms of the MZM, respectively. The MZM switching or half-wave voltage V_π is set at 4 V and γ is the power splitting ratio, which can be expressed as $\gamma = (1 - \frac{1}{\sqrt{10^{ExtinctionRatio/10}}})/2$. The dc extinction ratio is about 50 dB in order to obtain a balanced modulator ($\gamma = 0.5$). Next, the 25-Gb/s duobinary signal is launched over an optical link, which consists of a standard SMF.

Fig. 7.2 (a) configures the 1st order OEQ as pre-equaliser whereas Fig. 7.2 (b) similarly configures the 2nd order pre-OEQ. The 1st order OEQ construction is a two-tap feed-forward linear equaliser. The 2nd order OEQ, a cascade of two 1st order OEQs, is a three-tap equaliser [109], [184]. The OEQs in our setup perform high-pass filtering by having the relative optical path delay of one-half of the bit rate. The devices have 0^o phase shifters, 0.5 coupling coefficients, and insertion loss of about 2 dB and 4 dB for the first- and second-order OEQ, respectively. The optical receiver employs a VOA that adjusts the received optical power into a PD having a responsivity of 0.8 A/W, followed by a 4^{th}-order Bessel LPF with the bandwidth of approximately 70% of the bit rate. Note that the receiver noise sources such as shot noise and thermal noise are accounted in this simulation study. The filtered output signal was then applied to a MATLAB®-based error analyser for BER calculation. All system parameters were kept equivalent to the experimental setup for both NRZ and duobinary transmission, with the output power of the MZM maintained at +0 dBm.

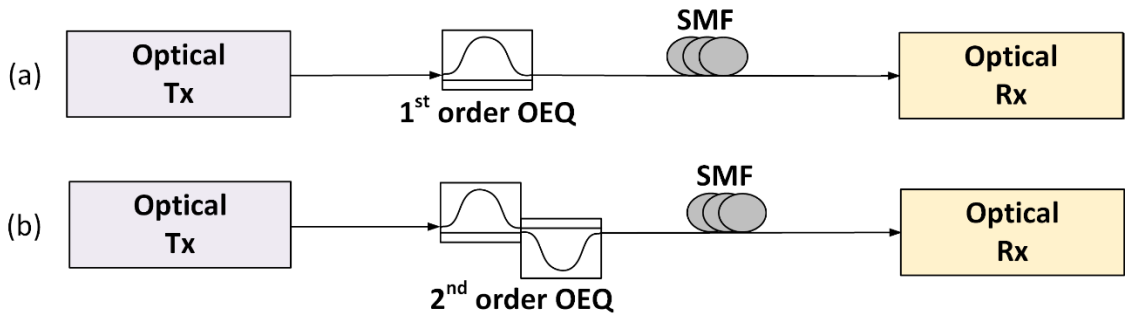


Figure 7.2: SMF links with (a) 1st order OEQ pre-equalisation and (b) 2nd order pre-equalisation.

7.2.2 Performance at 25-Gb/s without OEQs

The link performance was evaluated in terms of BER, power penalty and eye diagrams. In the BER plots, solid and hollow symbols denotes NRZ and duobinary transmissions, respectively.

First the duobinary performance without OEQs is presented and compared with conventional NRZ signal. Fig. 7.3 displays the BER for B2B configurations and various link distances. For the B2B scenarios, the receiver sensitivity at 10^{-9} BER for NRZ and duobinary, are about -14.8 dBm and -13 dBm, respectively, which leads to about 1.8 dB in power penalty for duobinary. This is in good agreement with the IEEE 802.3bm Fibre Optic Task Force [164]. Compared to B2B, the power penalty is about 0.8 dB for NRZ over 5-km SMF, but less than 0.2 dB over 10-km for duobinary. Notice that NRZ is subjected to an additional power penalty of 1.1 dB over 10-km SMF.

NRZ performance was found to degrade severely over longer distance, reaching a 8×10^{-4} BER floor over 15-km. Meanwhile duobinary was able to maintain a good performance over the same distance, while reaching a 10^{-9} BER over 30-km with about 5.5 dB of power penalty. This resultant penalty can be attributed to the overshoot on the level '1' of the eye diagram as can be seen in Fig. 7.5.

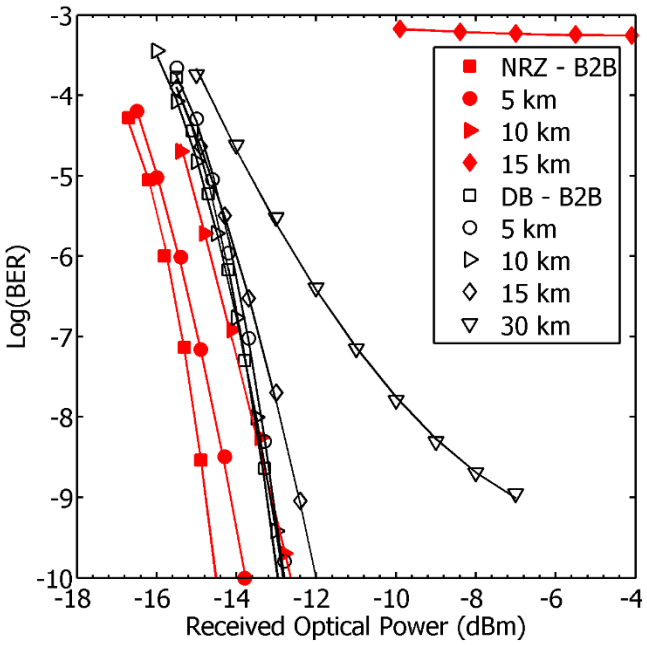


Figure 7.3: NRZ and duobinary performance without OEQ for various SMF link distances at 25-Gb/s.

Figures 7.4 and 7.5 show the corresponding eye diagrams for NRZ and duobinary that exemplify the dispersion-induced ISI. It is worth noting that the eye diagrams are relatively noisy due to the effect of noise sources at the receiver such as shot and thermal noises. The difference on the space levels ('0') between the two eye patterns, the "narrow steep space valley" also known as "ripples" of duobinary, contributes to its B2B power penalty. Over longer link distance, both eye diagrams gradually close and distort on the mark levels ('1'), indicating the effect of chromatic dispersion. However, duobinary eye diagrams are consistently more robust than NRZ over the same distance. The results in Fig. 7.3 verifies the resilience of duobinary to chromatic dispersion in short reach network, owing to its narrow bandwidth.

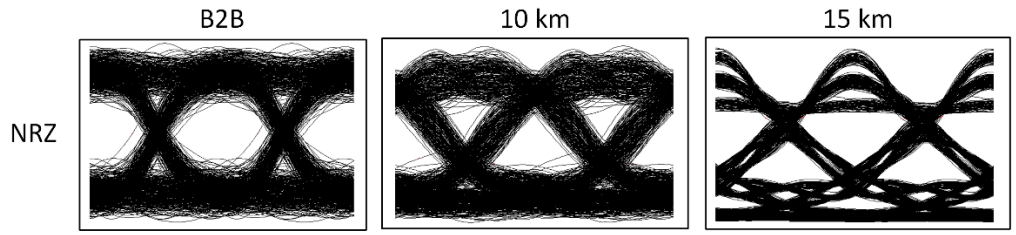


Figure 7.4: NRZ eye diagrams w/o OEQ over various link distance.

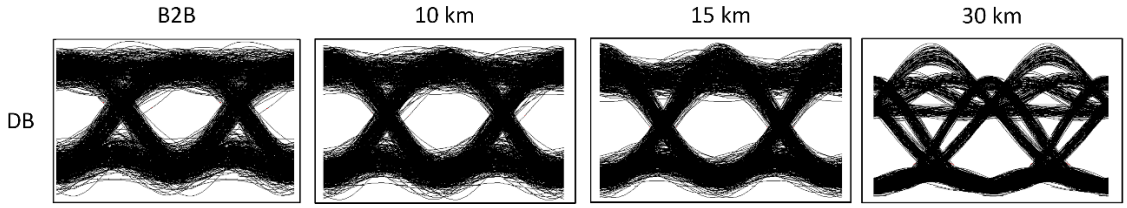


Figure 7.5: Duobinary eye diagrams w/o OEQ over various link distances. DB: duobinary.

7.2.3 Performance at 25-Gb/s with OEQs

Figure 7.6 displays the BER for the two different OEQ configurations over various link distances. The plots show that the OEQ improved the link performance compared to the results in Fig. 7.3. For example, it can be seen from Figs. 7.6 (a) that with the 1st order OEQs the NRZ error floor over 15-km is much lower at about 10^{-5} BER, while the pre-OEQs have improved the duobinary performance by 5 dB to nearly B2B performance at 10^{-9} BER over 30-km, and could extend the link to 35-km as well. Figures 7.6 (b) verifies that the cascade, 2nd order OEQs further compensate for the residual dispersion from the 1st order OEQs in Fig. 7.6 (a) over the same distance, while further extending the duobinary link distance from 35-km to 40-km. Notice that the receiver sensitivity of duobinary with 2nd order OEQ is better over 35-km than the B2B performance, suggesting that the OEQ may have also contributed to some measure of duobinary signal equalisation.

The overall results confirm that pre-OEQ with the 2nd order equalisation device are being more effective in mitigating dispersion induced ISI and waveform distortions. In practice, pre-OEQs have been found to achieve a better

equalising gain compared to the post-OEQ signal which are subjected to the fibre non-linearity while the pre-OEQ signal is largely free of the detrimental effects from the transmission medium [102], [106], [112].

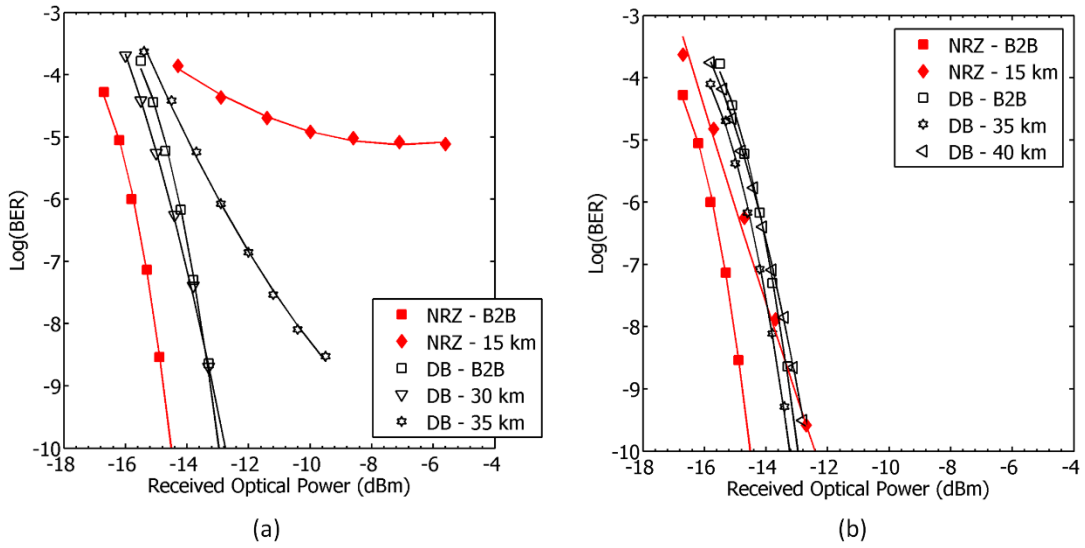


Figure 7.6: NRZ and duobinary performance at 25-Gb/s for (a) 1st order OEQ pre-equalisation and (b) 2nd order OEQ pre-equalisation.

Fig. 7.7 compares the eye diagrams of NRZ and duobinary links with 1st and 2nd order OEQs under pre-equalisation. For the 15-km NRZ link in Fig. 7.7 (a), the 1st order OEQ sharpened the distortion considerably on the mark level but is less effective on the space level, resulting in a poor BER as seen in Fig. 7.6 (a) and (b). The 2nd order OEQ for the same 15-km NRZ link in Fig. 7.7 (b) improved the eye openings clearly with almost no distortion on the marks and spaces.

For the 30-km duobinary link, Fig. 7.7 (a) shows that the 1st order pre-OEQ has reduced the "overshoot" distortion on the mark level in comparison to the non-equalised waveform in Fig. 7.5. However, the distortion returns as the duobinary link distance increases to 35-km. The 2nd order pre-OEQ in Fig. 7.7 (b) is shown to successfully compensate for the distortion at 35-km link distance and beyond at 40-km.

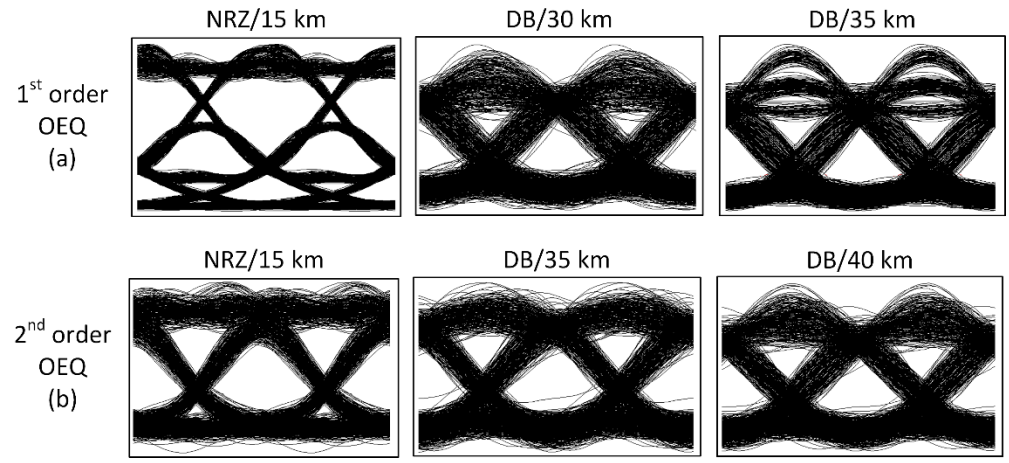


Figure 7.7: Received NRZ and duobinary eye diagrams at 25-Gb/s (a) 1st order pre-OEQ and (b) 2nd order pre-OEQ.

The eye diagrams illustrate that the signal waveforms are restored as the OEQs compensate for the distortion. This can also be observed by comparing the optical spectra, for example, the 25-Gb/s duobinary signal as shown in Fig. 7.8 with and without 1st and 2nd order pre-OEQs. While both OEQs appreciably boost the modulation spectra compared to the non-equalised condition, the 2nd order OEQ further reshape the signal by suppressing spectral nulls and sidelobes, further improving the equaliser gain.

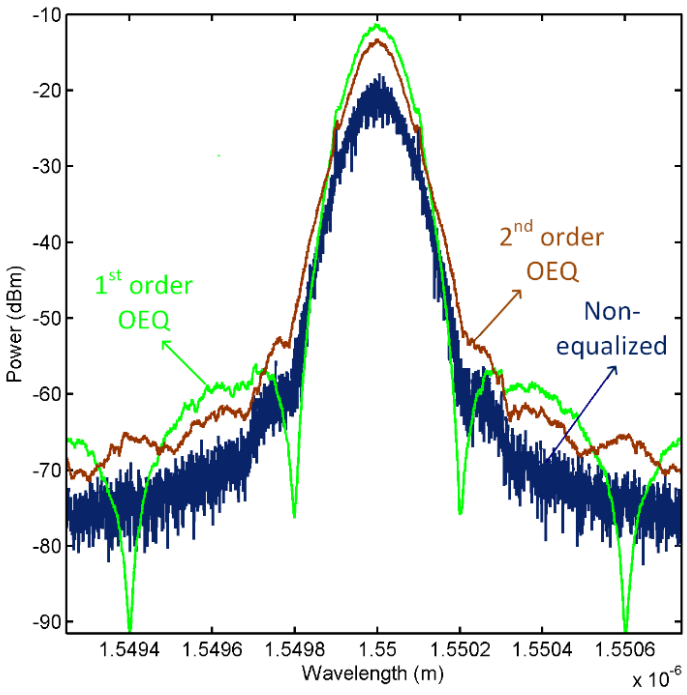


Figure 7.8: Optical spectra of duobinary signal with and without 1st order and 2nd order pre-OEQs at 25-Gb/s.

7.2.4 Performance at 50-Gb/s

The bandwidth of optical signal increases with the symbol rate, worsening the signal distortion due to fibre dispersion, which would limit the transmission distance. The speed increment translates into escalated electronic signal processing sophistication, hardware implementation and power consumption, while optical signal processing turns out to be relatively static since its power consumption remains roughly constant [106]. This section presents the performance of the optical access networks operating at 50-Gb/s.

Fig. 7.9 plots the BER performance without OEQ at various link distances for NRZ and duobinary signals at 50-Gb/s. While the B2B power at 10^{-9} BER increases by about 1.8 dB and 1.3 dB, respectively, from the 25-Gb/s results in Fig. 7.3, the power penalty at 50-Gb/s increases severely with distance. For examples, at 50-Gb/s, in the case of B2B, NRZ has a 10^{-3} BER floor (similar to transmission over 15-km SMF at 25-Gb/s) and duobinary has a receiver sensitivity of – 9 dBm at 10^{-9} BER over 5-km in Fig. 7.9.

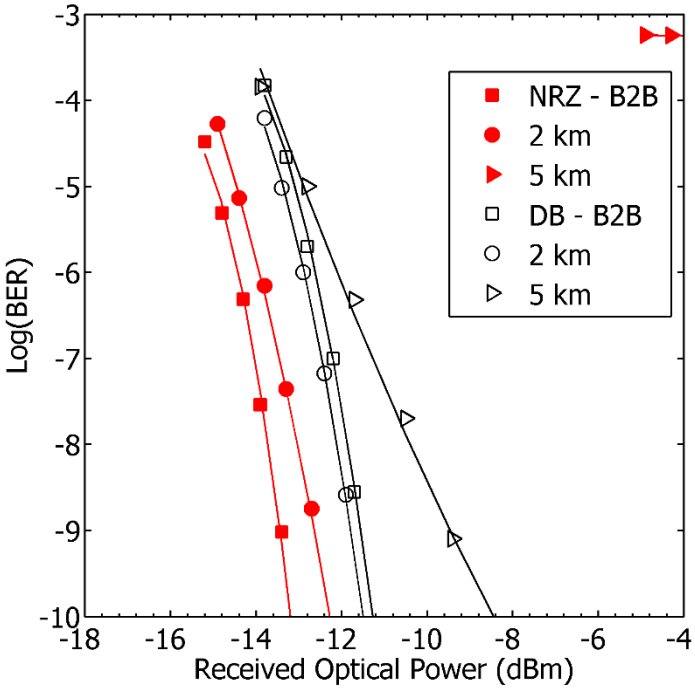


Figure 7.9: NRZ and duobinary performance without OEQ for various link distances at 50-Gb/s.

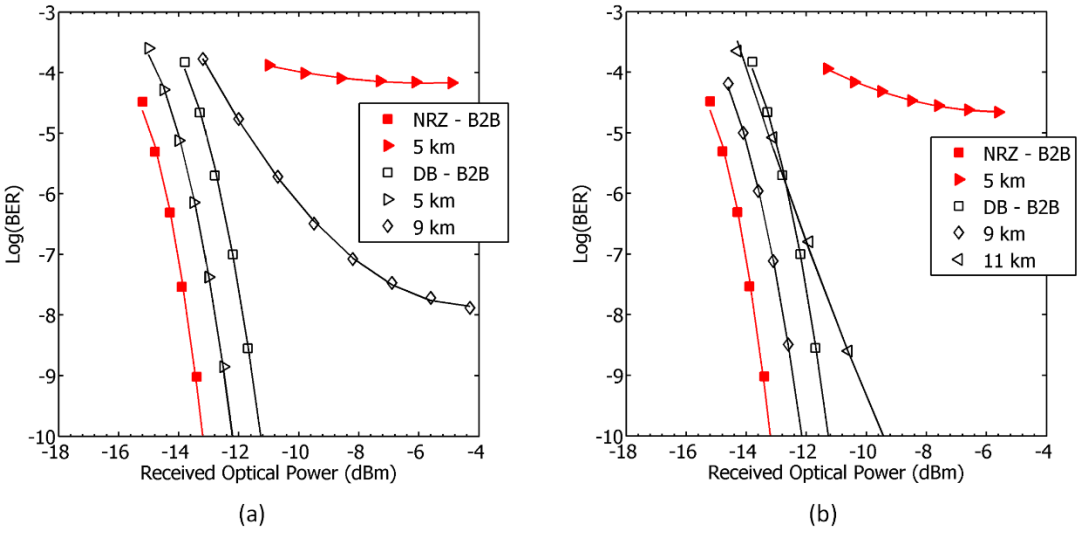


Figure 7.10: NRZ and duobinary performance (a) 1st order OEQ pre-equalisation and (b) 2nd order OEQ pre-equalisation.

Figure 7.10 displays the BER performance of the 50-Gb/s system incorporating the two pre-OEQ configurations. The plots show that unlike the 25-Gb/s NRZ results in Fig. 7.6, even the 2nd order OEQ was unable to compensate NRZ

signals for fibre dispersion at 5-km distance. The results in Fig. 7.10 also demonstrate that the duobinary integrated with 2nd order OEQ having the best performance.

However, as similar to other dispersion compensation techniques in optical domain such as DCF, IDF and FBG, OEQ is fairly expensive and has the major disadvantage of high insertion loss which could fall to 8 dB [63], [105], [108], [173], [184]–[186]. This may seriously degrade the system power budget and thus require the use of integrated low-cost semiconductor optical amplifier (SOA) and PIN detector for loss compensation [187]. The sensitivity degradation can be fully compensated by employing the APD in lieu of PIN [66], [103], [188]. It is worth mentioning that APDs are preferred over pre-amplified receivers attributable to their much lower power consumption [14], [189]. With the rapid developments of large-scale photonic integrated circuit (PIC) technology whose advantages are low packaging cost, more robust, higher functionality and low manufacturing cost (in large volume), it is promising that in the near future the OEQ device is commonly integrated with MZM or DML onto the same chip with the size of several millimetres, which surely introduce a moderately lower insertion loss than the conventional technique [6], [7], [35], [142], [158], [171], [190]–[192]. Another drawback of the OEQ is that parameters itself such as time delay and initial phase shift have to be manually adjusted depending on the data rate to achieve the proper dispersion compensation, which makes the optical performance monitoring time-consuming and inefficient.

7.3 Electrical Equalisers

This study was also carried out in experiments during the exchange at Photonics Systems Research Lab at KAIST, Korea in late spring, 2017. Fig. 7.11 displays the overview of the experimental space in the lab. In order to clearly realise the capability of EEQ in compensating the ISI effect. An experimental setup with a high data rate delivering over a short distance of SMF and detected with a low-bandwidth PIN detector is proposed. No optical amplifiers or dispersion compensation modules are used in the system. This demonstration was meant

to introduce a massive ISI effect to the received signal. The performance efficiency is evaluated based on the eye opening.



Figure 7.11: Working space to carry out the experiments at KAIST, Korea.

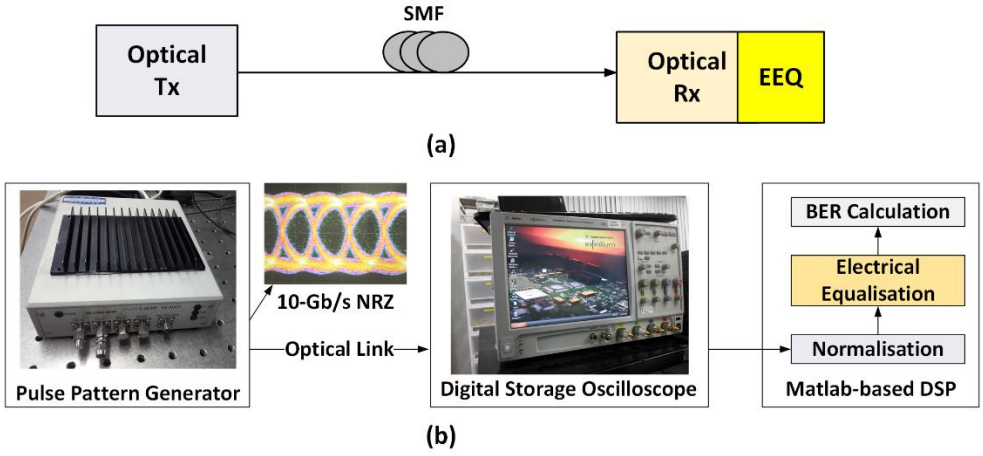


Figure 7.12: (a) System schematic and (b) Demonstration of EEQ in equalising the waveform distortion. Inset is the electrical eye diagram at the Tx.

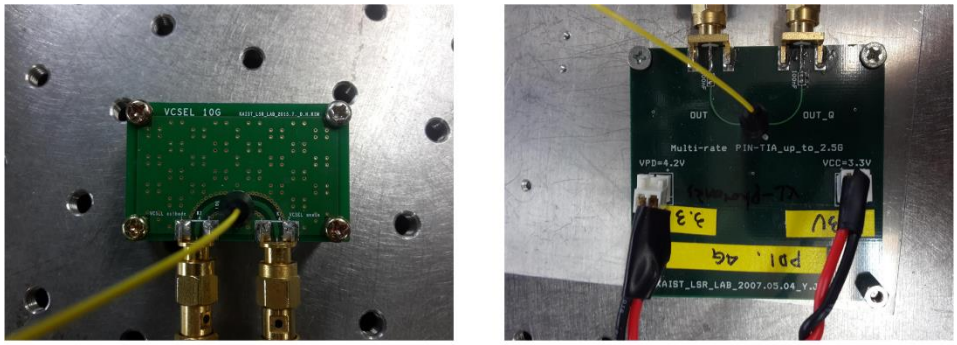


Figure 7.13: (a) 10-G VCSEL and (b) 2.5-G PIN.

Fig. 7.12 shows the 10-Gb/s NRZ signal which is generated by using a Multilane pulse pattern generator (PPG) with a PRBS length of 2^{15}-1. Inset is its electrical eye diagram. The generated electrical signal is loaded onto the 10-G VCSEL packaged in a TO-can (transistor-outline can) without temperature control as displayed in Fig. 7.13 (a) to achieve optical NRZ signal. A bias of 8 mA, which is sufficiently higher than the threshold current (1.2 mA), was applied to the laser, and the output power of the measured laser was 0.5 dBm. After transmission and detection by a 2.5-G-class photodiode (Fig. 7.13 (b)), the signal was then captured by a digital storage oscilloscope (DSO) with grab-and-store real-time. The scope used was an Agilent DSO90804A series with 50-GSample/s. This is because the data rate is 10-Gb/s and this allows for an integer number of samples per second to be recorded. The scope has a single shot approach to sampling – once triggered the scope writes a *.txt file containing the requested number of samples. This was transferred to a personal computer (PC) where off-line digital signal processing (DSP) is completed utilising MATLAB® program. The breakdown of the DSP module is also shown in Fig. 7.12. It usually consists of 5 main stages: re-sampling, synchronisation, normalisation, equalisation and BER calculation. Errors calculation for low data rate transmission could also be achieved in real-time by using BER testers supported from Anritsu, Keysight or SHF communication technologies [15], [137], [138], [193].

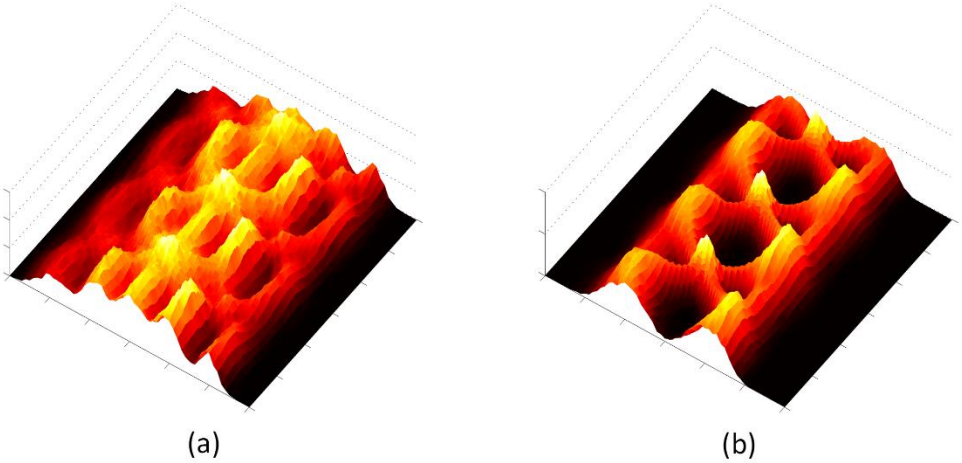


Figure 7.14: Received 3D eye diagrams (a) w/o EEQ and (b) w/ EEQ.

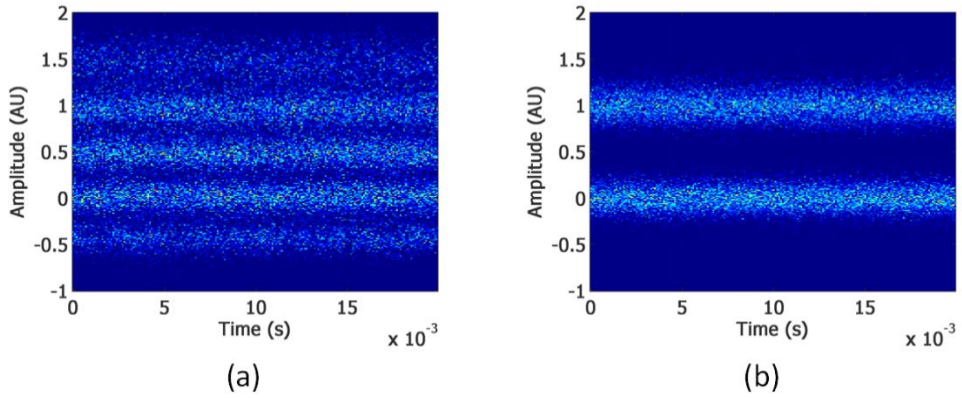


Figure 7.15: Corresponding signal levels (a) before and (b) after equalisation.

A combination of the bandwidth limitation of PIN photodiode and also the chromatic dispersion of the standard optical fibre undoubtedly exacerbates the effect of ISI on the transmitted NRZ signal. It is therefore anticipated that the received signal is severely distorted which corresponds to a completely closed 3D eye pattern and undistinguishable 'space' and 'mark' levels as can be seen in Fig. 7.14 (a). It is then post-processed with a powerful EEQ having 17-tap FFE followed by a 7-tap DFE for waveform distortions compensation on a set of 65534 bits where the first 32767 have been used to train the EEQ, and the last 32767 to evaluate the system performance. LMS algorithm was used to adaptively update tap weights in order to compensate time-varying impairment effects. Note that the iteration of this post-equalisation process is five. As

indicated in Fig. 7.14 (b), the signal quality is evidently enhanced with an open eye diagram. The two symbol levels '0' and '1' are clearly distinguishable as illustrated in Fig. 7.15 (b).

Off-line DSP-based EEQ has become a prevalent method for compensating for the dispersion-induced waveform distortion and provide a superior solution in many respects in high-speed optical communications systems. It can also be used to further relax device requirements in transmission setups as they have no inherent insertion loss. However it also has a number of major limitations both in terms of product development and experimental demonstration. Using off-line EEQ for restoring the signal generated even at very high baud rate could be hardly acceptable since they are highly computationally complex and resulting in PC-time consuming and heating. However it would even be more troublesome for practical real-time EEQ demonstration; in other words on-line error measurements due to the unavailability of high-speed BER testers. This equipment necessitates sophisticated hardware implementation and power-hungry electronic processing circuitry making it a high power consumption device and hence cost.

7.4 Concluding Remarks

The NRZ and duobinary signalling in simplified optical access transport networks with the aid of OEQs to mitigate the waveform distortion caused by fibre dispersion have been demonstrated. The results showed that optical equalisation can improve the performance significantly, with 2^{nd} order OEQ yielding the best performance with duobinary, owing to its resilience to dispersion compare to NRZ. The BER performance and the link distance have been greatly enhanced. Duobinary at 25-Gb/s can reach 40-km with the receiver sensitivity of - 13 dBm while at 50-Gb/s it has a receiver sensitivity -10 dBm over 11-km. Note that without optical equalisation techniques, duobinary can only be transmitted to the maximum distance of 30-km and 5-km, at bitrate of 25-Gb/s and 50-Gb/s respectively. It is also interesting to know that duobinary signal does not register any consistent improvement following the implementation of the linear electronic equaliser.

Adaptive EEQ or electronic dispersion compensation is a cost-effective and widespread solution to overcome transmission restriction due to the chromatic dispersion-induced ISI and correct for the transmission impairments of an optical signal. It is experimentally demonstrated the transmission of 10-Gb/s NRZ using VCSEL as a transmitter. The signal distortion caused by the bandwidth limitation of the PD device and the chromatic dispersion of the optical fibre is compensated with 17-tap FFE followed by a 7-tap DFE.

When considering the IM/DD-based WDM systems, OEQ can be placed in front of the WDM de-multiplexer and operate simultaneously on multiple channels that are affected by similar impairments. In contrast, EEQ always acts on the optical intensities of an individual channels after square-law photo-detection, and are therefore inherently per-channel devices. Another downside of real-time EEQ results from the fact that the electronics techniques have to rely on electronic circuits which suffer from the inherent speed and bandwidth limitation.

Chapter 8– Conclusions and Future Works

8.1 Thesis Conclusion

Having performed such a plethora of simulations and experiments, it is straightforward to comprehend that all the researches developed in this thesis are interconnected by a mutual point. That is the goal of reducing the fibre dispersion impairment for purposely increasing the transmission distance in optical IM/DD systems by mean of several techniques that implemented at the electrical transmitter (AACC), optical link (OEQ) and electrical receiver (EEQ).

In Chapter 3 and 4, first analytical report on a novel multilevel intensity signalling – AACC with focus on the format properties, transceiver design, system applications and its BER estimation method is studied. The signal space of AACC is also discussed, where the average electrical and optical power expressions are derived. AACC signal can be used to double the bit rate, especially extend the dispersion-limited transmission distance which is receiving much attention nowadays in metro data centre interconnects or transport links between data centres. Numerical demonstration is then investigated for this proposed modulation format in optical access networks. The performance of AACC is examined and compared against other prevailing OOK and multilevel modulation formats at an aggregate bit rate of 40-Gb/s e.g. NRZ, 50% RZ, CS-RZ, duobinary and 4-PAM in terms of receiver sensitivity, spectral efficiency and dispersion tolerance. Calculated receiver sensitivity at a BER of 10^{-9} and CD tolerance of the proposed system are ~-28.3 dBm and~336 ps/nm, respectively. The performance of AACC is delineated to be improved by 7.8 dB in terms of receiver sensitivity compared to 4-PAM in B2B scenario. The comparison results also show a clear advantage of AACC in achieving longer fibre transmission distance due to the higher dispersion tolerance. This is because the existence of the differential encoders that distort the transmitted pulse realising a pre-distortion technique which make itself tolerant to dispersion.

In the third part of Chapter 4, a systematic study on the transmission performance of RZ with different duty cycles over AACC format is presented. It is shown that the proposed RZ-AACC signal with duty cycle of 50% can approximately enhance the receiver sensitivity by 2.5 and 8 dB in comparison

to conventional AACC and RZ 4-PAM respectively at 40-Gb/s. While in the fourth part of Chapter 4, eight-level AACC scheme named as 8-AACC in optical interconnects applications to overcome the drawback of 8-PAM signal which is the ISI effect due to the increment of signal levels itself is also presented. In Chapter 5, a comparative investigation of AACC transmission using NRZ and RZ pulse shapes with a binary receiver considering the linear and nonlinear impairments such as CD and SPM in 40-Gb/s optical metro-access networks is shown. Then in Chapter 6, the proposed multilevel modulation format is verified by presenting the commercial components to construct its electrical transmitter. AACC signal based on DSP is also developed to enable AACC real-time transmission in almost every experimental labs in the future.

In Chapter 7, the capability of OEQ and EEQ as alternative techniques in mitigating the ISI effect for duobinary and NRZ signals is studied. The signal quality enhancement is observed via the received eye diagrams.

In a nutshell, Fig 8.1 illustrates the advancement of advanced modulation formats that have been demonstrated over the years in the literature. The use of optical and electrical equalisation techniques is indispensable for dispersion compensation in optical NRZ transmission systems. 4-PAM is a spectrally-efficient modulation which is beneficial for ameliorating the effects of fibre dispersion but its structure of having four intensity levels making itself more sensitive to dispersion-induced ISI effect. Therefore either OEQ or EEQ is essential in 4-PAM transmission. These equalisation techniques are uncommon for duobinary demonstration thanks to its typical characteristic. A similar conclusion also goes to AACC scheme due to its unique operation that realising the pre-distortion feature which provide a dispersion-tolerant transmission. It is therefore concluded that optical transmission system using AACC would enjoy a cost-efficient feature since neither of OEQ and EEQ employed.

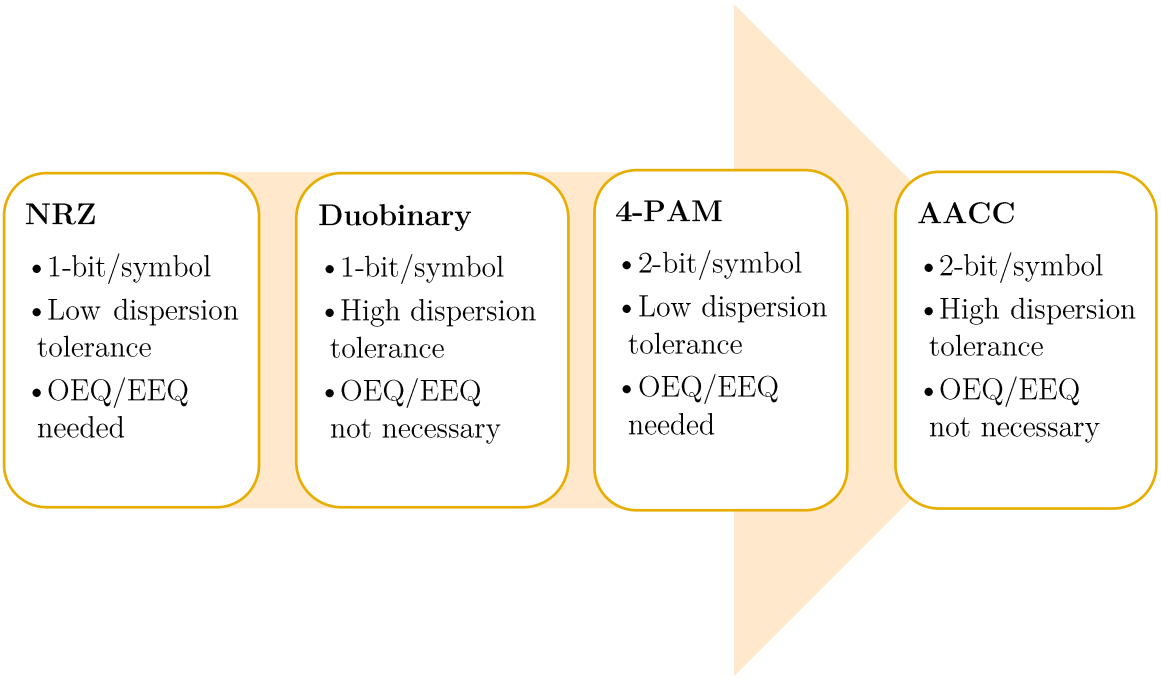


Figure 8.1: Progression of advanced modulation formats integrated with equalisers.

8.2 Future Works

The research topics presented in this thesis laid the firm foundations and framework for a number of possible paths that are worthy for further investigation. They are enumerated as follows:

1. Even though AACC format is robust to fibre dispersion; however it would be outstanding if further numerical simulation is the combination of AACC signal and optical or electrical equalisation techniques to substantially extend the transmission distance in optical IM/DD systems.

2. Enabling a cost-effective optical transmission system is an important concern at the moment. AACC is known as a cost-benefit transmitter since it is based on the commercial devices and also detected by a simple DD receiver. It is interesting to generate the optical AACC signal using DML as a replacement for MZM.

3. Further numerical investigation on AACC signal should be made with WDM channel to realise a very high-capacity optical fibre communication system.

4. As the data transmission rates of short-reach interconnects for high-speed data centres applications continue to increase incessantly, the development of new advanced modulation formats with IM/DD eases the lane data rate for reducing the bandwidth requirements of either electronic or optical components. Hybrid modulation formats are of considerable interest since it is able to greatly improve the spectral efficiency. Therefore it is worth to combining AACC signal with any phase signal e.g. DPSK and transmit simultaneously and detected by two receivers for different applications (a single PD receiver for AACC and a dual PD balanced receiver for DPSK).

Appendix

A – Minimizing the ISI Penalty in VCSEL-based MMF Systems

Transmission configuration, which was used for NRZ-AACC signal to verify its analytical BER performance is shown in Fig. A1. In fact, the electrical signal used to directly modulate the VCSEL device operating at the wavelength of 850 nm at room temperature. The VCSEL was biased using a drive current (I) of 6 mA. The signal used to directly modulate the VCSEL device operating at the wavelength of 850 nm at room temperature. The output power (P) of the VCSEL is about 0 dBm. It must be noted that the "P" and "I" relationship is the key in achieving the optimal system performance. The corresponding four-level signalling and the optical spectra at the output of the VCSEL are illustrated in Insets (b) and (c), respectively.

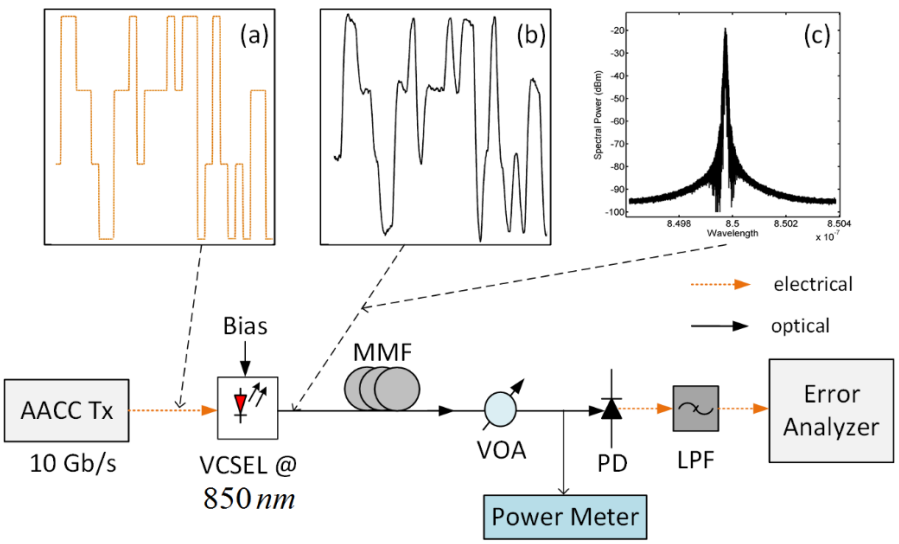


Figure A1: Overview of test setup; Insets (a)-(c) Electrical, optical AACC four-level signalling and optical spectra.

Fig. A2 (a) illustrates the static PI characteristics for the VCSEL used in our setup at temperatures ranging from 10 to 95 °C. The 10-Gb/s modulated signals were then launched over MMF with different lengths. Note that the type of the MMF link utilised in this work is OM3 with the attenuation of ~2.3 dB/km and a bandwidth-distance product of 2000 MHz.km to match the properties of the Corning ClearCurve fibre at 850 nm. At the receiver side, a variable optical attenuator was used to adjust the received optical power. The signal was then detected by using a PIN detector with responsivity equal to 0.8 A/W, followed by a low-pass Gaussian filter. Finally, the error analyser employed MATLAB®-based programing for data recovery and BER calculation. All system parameters were kept equivalent to the experimental setup. For a fair comparison, the setup of 4-PAM transmission was exactly the same as NRZ-AACC scenario.

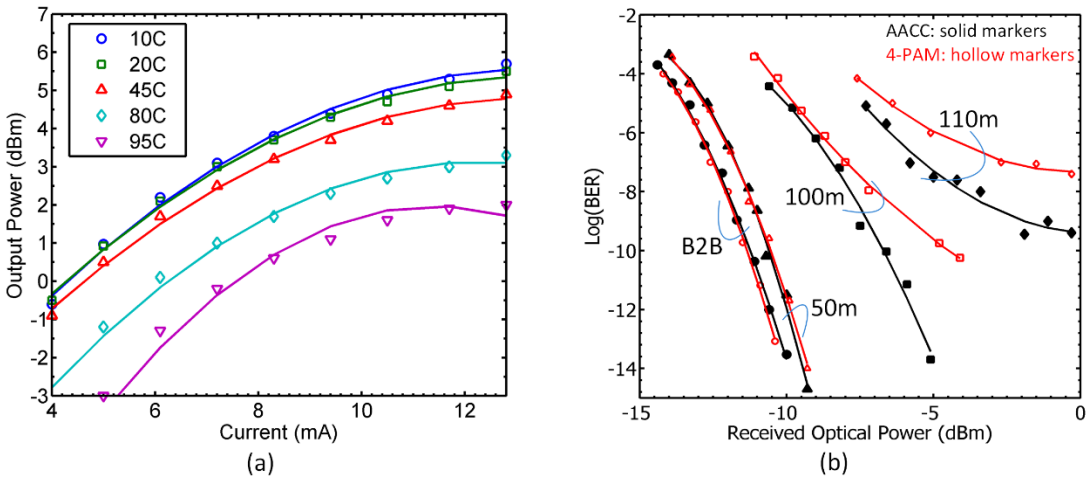


Figure A2: (a) Output power - current characteristics for a 10-Gb/s VCSEL at temperatures ranging from 10 to 95 C and (b) BER results of AACC (solid markers) and 4-PAM (hollow markers) after transmission over different MMF lengths.

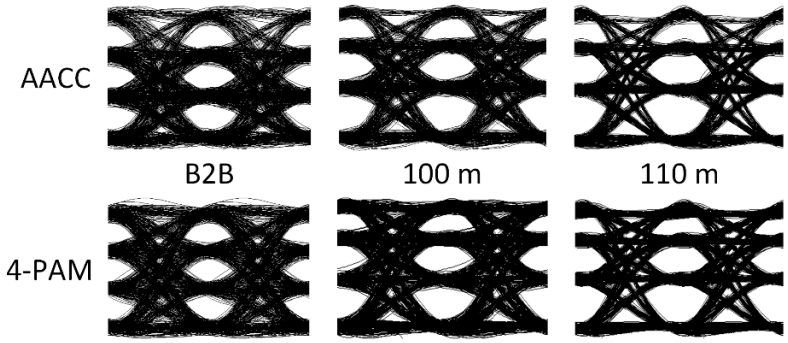


Figure A3: Received eye diagrams of NRZ-AACC and 4-PAM for B2B, after 100 m and 110 m of MMF.

The performance comparison between NRZ-AACC (solid markers) and 4-PAM (hollow markers) signals at 10-Gb/s over MMF links are shown in Fig. A2. The B2B sensitivity at BER = 10^{-9} of both modulation formats was about -12 dBm, which agrees well with the experimental results in [25]. No penalty was achieved after 50 m of MMF for both formats. Focusing on transmission over 100 m, the sensitivity of 4-PAM was about 1.5 dB worse than NRZ-AACC. At 110 m, 4-PAM performance was further degraded, and an error floor was observed at BER = $5x10^{-8}$ while NRZ-AACC sensitivity at BER = 10^{-9} could be acceptable in practical applications. The BER performance is degraded significantly due to modal dispersion-induced ISI in MMF. Corresponding eye diagrams are displayed in Fig. A3 for qualitative comparison. The closing of the 4-PAM eye diagram – especially the top eye, reflects degradation in receiver performance and corresponds to an increase in the BER.

B – Sensitivity enhancement by optimising the level spacing of AACC signal

It is shown in Section 4.2 that the enhanced AACC transmission system by optimizing the level spacing results in substantially better receiver sensitivity of ~8 dB in comparison to conventional AACC in B2B circumstance. It is verified by numerical simulations as a proof of concept by proposing a method based on DD-MZM to improve the amplitude distribution among eye diagrams; 8 dB power penalty has been realised which is in an agreement with theoretical results. The simulated system is displayed in Fig. B1.

Fig. B2 exhibits the calculated eye diagrams for AACC system using conventional MZM and DD-MZM. As illustrated in Fig. B2 (a), at the received optical power of -28.3 dBm, Q-factors located at first and second level are more than 7, which are much higher than that of third level. The performance of top eye is worse due to the higher standard deviation of the noise variation at its level in comparison to others. Therefore at the same received optical power, eyes with minimum variations of noise has the best performance (e.g. bottom) and vice versa.

In order to enhance AACC transmission system, similar Q-factors that link to top, middle and bottom eyes should be achieved. This can be done by suitably driving the bias voltages at both ports of DD-MZM to increase the height of top eye and decrease the eye height in lower levels (implementing the quadratic level spacing) and also maintaining the maximum power as displayed in Fig. B2 (b).

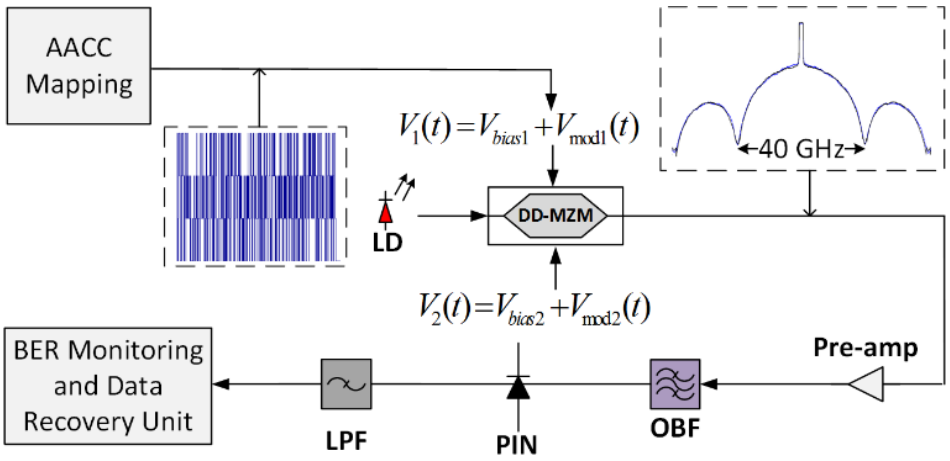


Figure B1: AACC transmission setup using DD-MZM.

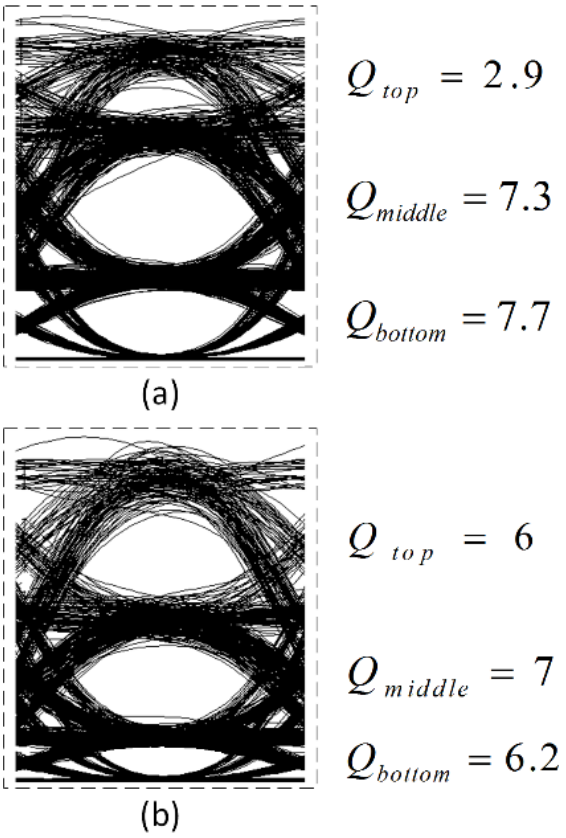


Figure B2: Received eye diagram of the AACC signal measured at the sensitivity of -28.3 dBm. (a) Conventional AACC using conventional MZM and (b) Optimised AACC using dual-drive MZM.

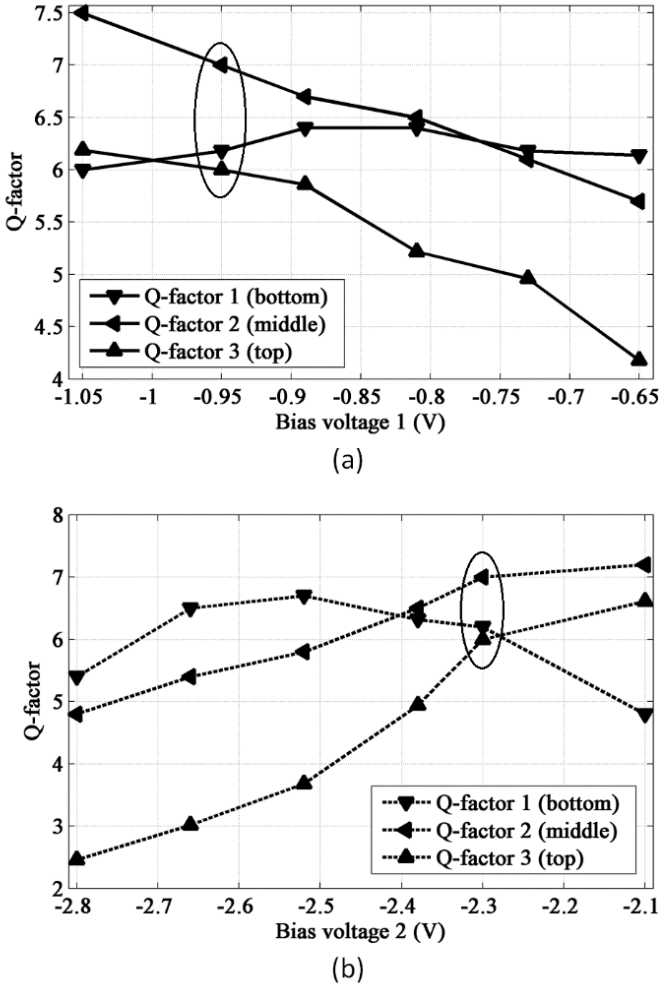


Figure B3: Dependence of Q-factors on the applied bias voltages (a) V_{b1} and (b) V_{b2}.

The optimum bias voltages are considered for two different conditions as shown in Fig. B3. The dependence of Q-factors for all three eyes with various bias voltage 1 (V_{b1}) at fixed received power of -28.3 dBm (receiver sensitivity of conventional AACC system at BER of 10^{-9}) is depicted in Fig. B3 (a). As can be clearly seen, the optimum V_{b1} is around -0.95 V. In a similar manner of optimizing V_{b1}, the optimum V_{b2} of -2.3 V are found (Fig. B3 (b)).

At fixed received power of -28.3 dBm, Fig. B2 (b) shows an enhanced AACC eye diagram utilising DD-MZM with optimised bias voltages. In comparison to conventional AACC eye diagram, Q-factor corresponds to top eye is greatly improved (from 2.9 to 6) and Q-factor that related to bottom eye

is reduced (from 7.7 to 6.2). As a result of improving the quality of third level eye, the performance of AACC system is remarkably improved.

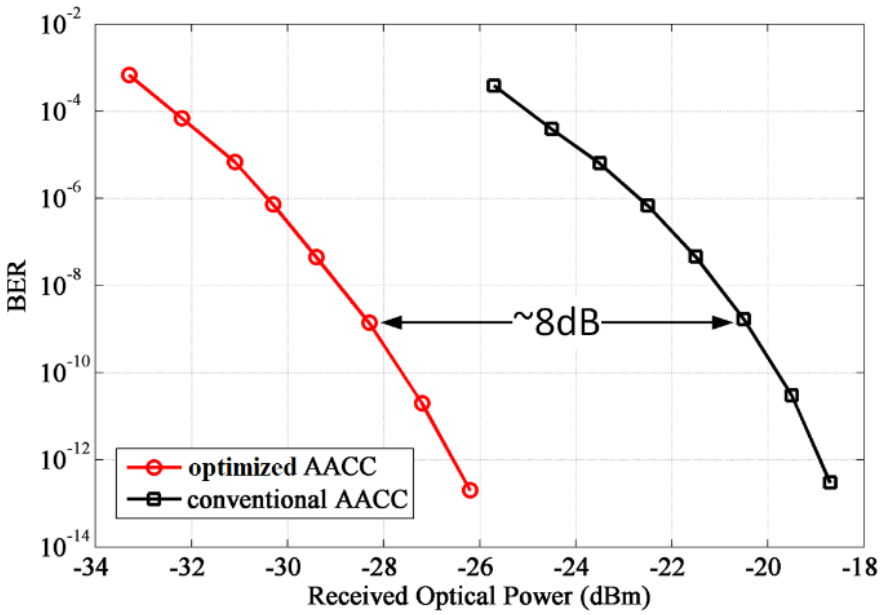


Figure B4: Calculated receiver sensitivity of optimised AACC in comparison to conventional AACC at 40-Gb/s.

Fig. B4 shows the receiver sensitivity of AACC signal using conventional MZM, compared to optimised AACC using DD-MZM. It can be seen that the latter technique improves the receiver sensitivity of around 8 dB. The reasons for this sensitivity enhancement can be realised by optimising the level spacing in eye diagrams.

C – AACC-Based DSP (MATLAB code)

```
clear all; close all; clc;

%%%%%%%%%%%%%% LANE 1
prbs7=importdata('PRBS7.txt');
b = prbs7;
b(b==0) = -1;       % convert all 0 to -1 (PRECODER)//////// bit
sequence in polar form
N = length(prbs7);
% Tb = 0.01;
% T = Tb*N;
Rb = 3e9;
fs = 4*Rb;
Ts = 1/fs;
rho = 4;
L = round(N*rho);

% Duobinary pulse
s = zeros(1,L);         % initialization
figure(3)
for i=1:N
    t = (-(i-1)*rho:L-1-(i-1)*rho)/fs;
    tt1 = sinc(Rb*t);
    tt2 = 1 - Rb*t;
    index = find(tt2 ~= 0);
    ind0 = find(tt2 == 0);
    p3(index) = b(i)*tt1(index)./tt2(index);
    p3(ind0) = b(i);
    s = s + p3;
    subplot(2,1,1), plot(p3,'k')
    hold on
end
xlabel('Time')
ylabel('Pulse amplitude')
title('Sequence of individual duobinary encoder')
xlabel('Time')
ylabel('Signal amplitude')
title('Generated signal using duobinary encoder)
```

References

[1] Chi H. Lee, *Microwave photonics*, 2nd ed. CRC Press, 2013.

[2] A. Seeds, "Microwave photonics," *J. Lightw. Technol.*, vol. 24, no. 12, pp. 4628–4641, 2002.

[3] J. Capmany and D. Novak, "Microwave photonics combines two worlds," *Nat. Photonics*, vol. 1, no. 6, pp. 319–330, 2007.

[4] A. Samani, M. Chagnon, E. Elfiky, D. Patel, M. Jacques, V. Veerasubramanian, and D. Plant, "Silicon photonics modulator architectures for multi-level signal generation and transmission," in *Optical Fiber Communication Conference*, 2017, p. Tu2H.4.

[5] http://www.marketsandmarkets.com, "Photonics market by application (display, photovoltaic, lighting, manufacturing technology), end-use industry (building, construction, media, broadcasting & telecommunication, consumer & business automation, medical, industrial) - global forecasts to 2021," 2016.

[6] H. Mardoyan, M. A. Mestre, J. M. Estar, F. Jorge, F. Blache, P. Angelini, A. Konczykowska, M. Riet, V. Nodjiadjim, J. Dupuy, and S. Bigo, "84-, 100-, and 107-GBd PAM-4 intensity-modulation direct-detection transceiver for datacenter interconnects," *J. Lightw. Technol.*, vol. 35, no. 6, pp. 1253–1259, 2017.

[7] T. Kishi, M. Nagatani, S. Kanazawa, W. Kobayashi, H. Yamazaki, M. Ida, K. Kurishima, M. Nogawa, S. Kimura, and H. Nosaka, "56-Gb/s optical transmission performance of an InP HBT PAM4 driver compensating for nonlinearity of extinction curve of EAM," *J. Lightw. Technol.*, vol. 35, no. 1, pp. 75–81, 2017.

[8] J. Xu, J. Du, R. Ren, Z. Ruan, and Z. He, "Optical interferometric synthesis of PAM4 signals based on dual-drive Mach–Zehnder modulation," *Opt. Commun.*, vol. 402, pp. 73–79, 2017.

[9] C. Sun, S. H. Bae, and H. Kim, "Transmission of 28-Gb/s duobinary and PAM-4 signals using DML for optical access network," *IEEE Photonics Technol. Lett.*, vol. 29, no. 1, pp. 130–133, 2017.

[10] G. Agrawal, *Fiber-optic communication systems*, 4th ed. John Wiley & Sons, 2010.

[11] A. Neophytos, G. Ellinas, and R. Ioannis, *WDM systems and networks*. New

York: Springer, 2012.

[12] "IEEE 802.3 ethernet working group." [Online]. Available: http://www.ieee802.org/3/.

[13] J. Zhou, C. Yu, G. Mohan, and H. Kim, "25-Gb/s OOK transmission using 1.5-μm 10G-class VCSEL for optical access network," *J. Lightw. Technol.*, vol. 34, no. 16, pp. 3790–3795, 2016.

[14] Y. Guo, Y. Yin, Y. Song, H. Mengyuan, Y. Li, G. Kuang, Z. Fu, X. Huang, P. Cai, Z. Ma, M. Li, and D. Pan, "Demonstration of 25Gbit/s per channel NRZ transmission with 35 dB power budget using 25G Ge/Si APD for next generation 100G-PON," in *Optical Fiber Communication Conference*, 2017, p. M3H.6.

[15] H. Ji, L. Yi, Z. Li, L. Xue, X. Li, Q. Yang, S. Wang, Y. Yang, S. Yu, and W. Hu, "Field demonstration of a real-time 100-Gb/s PON based on 10G-class optical devices," *J. Lightw. Technol.*, vol. 35, no. 10, pp. 1914–1921, 2017.

[16] E. Lach and W. Idler, "Modulation formats for 100G and beyond," *Opt. Fiber Technol.*, vol. 17, no. 5, pp. 377–386, 2011.

[17] P. J. Winzer, "High-spectral-efficiency optical modulation formats," *J. Lightw. Technol.*, vol. 30, no. 24, pp. 3824–3835, 2012.

[18] J. Li, E. Tipsuwannakul, T. Eriksson, M. Karlsson, and P. A. Andrekson, "Approaching nyquist limit in WDM systems by low-complexity receiver-side duobinary shaping," *J. Lightw. Technol.*, vol. 30, no. 11, pp. 1664–1676, 2012.

[19] T. N. Huynh, L. Nguyen, and L. P. Barry, "Phase noise characterization of SGDBR lasers using phase modulation detection method with delayed self-heterodyne measurements," *J. Lightw. Technol.*, vol. 31, no. 8, pp. 1300–1308, 2013.

[20] L. Tao, Y. Wang, Y. Gao, and N. Chi, "High order CAP system using DML for short reach optical communications," *IEEE Photonics Technol. Lett.*, vol. 26, no. 13, pp. 1348–1351, 2014.

[21] H. Sanjoh, T. Fujisawa, S. Kanazawa, and W. Kobayashi, "25 Gbaud/s 4-PAM (50 Gbit/s) modulation and 10 km SMF transmission with 1.3 μm InGaAlAs-based DML," *Electron. Lett.*, vol. 50, no. 4, pp. 299–300, 2014.

[22] A. S. Karar, J. C. Cartledge, J. Harley, and K. Roberts, "Electronic pre-compensation for a 10.7-Gb/s system employing a directly modulated laser," *J. Lightw. Technol.*, vol. 29, no. 13, pp. 2069–2076, 2011.

[23] M. Bi, S. Xiao, L. Yi, H. He, J. Li, X. Yang, and W. Hu, "Power budget improvement of symmetric 40-Gb/s DML-based TWDM-PON system," *Opt. Express*, vol. 22, no. 6, p. 6925, 2014.

[24] X. Pang, O. Ozolins, S. Gaiarin, A. Kakkar, J. R. Navarro, M. I. Olmedo, R. Schatz, A. Udalcovs, U. Westergren, D. Zibar, S. Popov, and G. Jacobsen, "Experimental study of 1.55- μm EML-based optical IM/DD PAM-4/8 short reach systems," *Photonics Technol. Lett.*, vol. 29, no. 6, pp. 523–526, 2017.

[25] J. A. Tatum, D. Gazula, L. A. Graham, J. K. Guenter, R. H. Johnson, J. King, C. Kocot, G. D. Landry, I. Lyubomirsky, A. N. MacInnes, E. M. Shaw, K. Balemarthy, R. Shubochkin, D. Vaidya, M. Yan, and F. Tang, "VCSEL-based interconnects for current and future data centers," *J. Lightw. Technol.*, vol. 33, no. 4, pp. 727–732, 2015.

[26] D. Mahgerefteh, Y. Matsui, X. Zheng, and K. McCallion, "Chirp managed laser and applications," *IEEE J. Sel. Top. Quantum Electron.*, vol. 16, no. 5, pp. 1126–1139, 2010.

[27] Y. Matsui, D. Mahgerefteh, X. Zheng, C. Liao, Z. F. Fan, K. McCallion, and P. Tayebati, "Chirp-managed directly modulated laser (CML)," *IEEE Photonics Technol. Lett.*, vol. 18, no. 2, pp. 385–387, 2006.

[28] Q. Chang, Y. Tian, J. Gao, T. Ye, Q. Li, and Y. Su, "Generation and transmission of optical carrier suppressed-optical differential (Quadrature) phase-shift keying (OCS-OD(Q)PSK) signals in radio over fiber systems," *J. Lightw. Technol.*, vol. 26, no. 15, pp. 2611–2618, 2008.

[29] P. J. Winzer and J. Essiambre, "Advanced Optical Modulation Formats," *Proc. IEEE*, vol. 94, no. 5, pp. 952–985, 2006.

[30] D. Penninckx, M. Chbat, L. Pierre, and J. P. Thiery, "The Phase-Shaped Binary Transmission (PSBT): A new technique to transmit far beyond the chromatic dispersion limit," *IEEE Photonics Technol. Lett.*, vol. 9, no. 2, pp. 259–261, 1997.

[31] J. C. Cartledge, "Performance of 10 Gb/s lightwave systems based on lithium niobate Mach-Zehnder modulators with asymmetric Y-branch waveguides," *IEEE Photonics Technol. Lett.*, vol. 7, no. 9, pp. 1090–1092, 1995.

[32] J. C. Cartledge, C. Rolland, S. Lemerle, and A. Solheim, "Theoretical performance of 10 Gb/s lightwave systems using a III-V semiconductor Mach-Zehnder modulator," *J. Lightw. Technol.*, vol. 6, no. 2, pp. 282–284, 1994.

[33] A. Samani, M. Chagnon, D. Patel, V. Veerasubramanian, S. Ghosh, M. Osman, Q. Zhong, and D. V. Plant, "A low-voltage 35-GHz silicon photonic modulator-enabled 112-Gb/s transmission system," *IEEE Photonics J.*, vol. 7, no. 3, pp. 1–13, Jun. 2015.

[34] B. G. Lee, N. Dupuis, R. Rimolo-Donadío, T. Huynh, C. W. Baks, D. M. Gill, and W. M. Green, "Driver-integrated 56-Gb/s segmented electrode silicon mach zehnder modulator using optical-domain equalization," in *Optical Fiber*

Communication Conference, 2017, p. Th1B.1.

[35] A. Samani, V. Veerasubramanian, E. El-Fiky, D. Patel, and D. V. Plant, "A Silicon Photonic PAM-4 Modulator Based on Dual-Parallel Mach–Zehnder Interferometers," *IEEE Photonics J.*, vol. 8, no. 1, pp. 1–10, Feb. 2016.

[36] K. P. Ho and H. W. Cuei, "Generation of arbitrary quadrature signals using one dual-drive modulator," *J. Lightw. Technol.*, vol. 23, no. 2, pp. 764–770, 2005.

[37] N. Dong-Nhat and A. Malekmohammadi, "Transmission of duobinary signal in optical 40 GHz millimeter-wave radio-over-fiber systems utilizing dual-arm LiNbO3 Mach–Zehnder modulator for downstream," *J. Opt. Commun.*, vol. 37, no. 2, pp. 155–161, 2016.

[38] S. K. Ibrahim, S. Bhandare, and R. Noé, "Performance of 20 Gb/s quaternary intensity modulation based on binary or duobinary modulation in two quadratures with unequal amplitudes," *IEEE J. Sel. Top. Quantum Electron.*, vol. 12, no. 4, pp. 596–602, 2006.

[39] X. Chen, P. R. Horche, and A. M. Minguez, "A low-cost alternative scheme to detect a 100 Gbps PM-DQPSK signal," *Photonic Netw. Commun.*, vol. 28, no. 3, pp. 203–213, 2014.

[40] W. Jia, Y. Matsui, D. Mahgerefteh, I. Lyubomirsky, and C. K. Chan, "Generation and transmission of 10-gbaud optical 3/4-RZ-DQPSK signals using a chirp-managed DBR laser," *J. Lightw. Technol.*, vol. 30, no. 21, pp. 3299–3305, 2012.

[41] W. Freude, R. Schmogrow, B. Nebendahl, M. Winter, A. Josten, D. Hillerkuss, S. Koenig, J. Meyer, M. Dreschmann, M. Huebner, C. Koos, J. Becker, and J. Leuthold, "Quality metrics for optical signals: Eye diagram, Q-factor, OSNR, EVM and BER," in *International Conference on Transparent Optical Networks*, 2012, p. Mo.B1.5.

[42] C. J. Anderson and J. A. Lyle, "Technique for evaluating system performance using Q in numerical simulations exhibiting intersymbol interference," *Electron. Lett.*, vol. 30, no. 1, pp. 71–72, 1994.

[43] A. Malekmohammadi, M. H. Al-Mansoori, G. A. Mahdiraji, A. F. Abas, and M. K. Abdullah, "Performance enhancement of Absolute Polar Duty Cycle Division Multiplexing with Dual-Drive Mach–Zehnder-Modulator in 40Gbit/s optical fiber communication systems," *Opt. Commun.*, vol. 283, no. 16, pp. 3145–3148, 2010.

[44] A. Malekmohammadi, G. A. Mahdiraji, A. F. Abas, M. K. Abdullah, M. Mokhtar, and M. F. A. Rasid, "Realization of high capacity transmission in fiber optic communication systems using Absolute Polar Duty Cycle Division

Multiplexing (AP-DCDM) technique," *Opt. Fiber Technol.*, vol. 15, no. 4, pp. 337–343, 2009.

[45] T. Tokle, C. Peucheret, and P. Jeppesen, "Advanced modulation formats in 40 Gbit/s optical communication systems with 80 km fibre spans," *Opt. Commun.*, vol. 225, no. 1–3, pp. 79–87, 2003.

[46] A. F. Elrefaie, R. E. Wagner, D. A. Atlas, and D. G. Daut, "Chromatic dispersion limitations in coherent lightwave transmission systems," *J. Lightw. Technol.*, vol. 6, no. 5, pp. 704–709, 1988.

[47] A. Mendez and T. F. Morse, *Speciality optical fibers handbook*. USA: Elsevier, 2007.

[48] T. Mizuochi, K. Ishida, T. Kobayashi, J. Abe, K. Kinjo, K. Motoshima, and K. Kasahara, "A comparative study of DPSK and OOK WDM transmission over transoceanic distances and their performance degradations due to nonlinear phase noise," *J. Lightw. Technol.*, vol. 21, no. 9, pp. 1933–1943, 2003.

[49] B. Shin, J. Jeong, and J. Lee, "25-Gb/s optical NRZ transmission over 40km of single-mode fiber at 1550nm without dispersion compensation," *Opt. Fiber Technol.*, vol. 20, no. 5, pp. 461–466, 2014.

[50] V. Cristofori, F. Da Ros, O. Ozolins, M. E. Chaibi, L. Bramerie, Y. Ding, X. Pang, A. Shen, A. Gallet, G. Duan, K. Hassan, S. Olivier, S. Popov, G. Jacobsen, L. K. Oxenløwe, and C. Peucheret, "25-Gb/s transmission over 2.5-km SSMF by silicon MRR enhanced 1.55-μm III-V/SOI DML," *IEEE Photonics Technol. Lett.*, vol. 29, no. 12, pp. 960–963, 2017.

[51] Z. Li, J. Xia, Y. Guo, Y. Yin, Y. Li, Y. Song, J. Chen, and M. Wang, "Investigation on the equalization techniques for 10G-class optics enabled 25G-EPON," *Opt. Express*, vol. 25, no. 14, pp. 16228–16234, 2017.

[52] E. Forestieri, M. Secondini, F. Fresi, G. Meloni, L. Poti, and F. Cavaliere, "Extending the reach of short-reach optical interconnects with DSP-free direct detection," *J. Lightw. Technol.*, vol. 35, no. 15, pp. 3174–3181, 2017.

[53] F. Tian, X. Zhang, L. Xi, A. Stark, S. E. Ralph, and G. Chang, "Investigation of interchannel nonlinear tolerance of 256-Gb/s polarization-division multiplexing return-to-zero 16-ary quadrature amplitude modulation in a hybrid wavelength-division multiplexing transmission system using optical comb," *Opt. Eng.*, vol. 53, no. 1, p. 16111, 2014.

[54] V. Mikhailov, C. R. Doerr, S. Appathurai, R. I. Killey, and P. Bayvel, "Fiber nonlinearity and dispersion mitigation in 40-Gb/s NRZ WDM transmission using a multichannel optical equalizer," *IEEE Photonics Technol. Lett.*, vol. 18, no. 2, pp. 376–378, 2006.

[55] P. J. Winzer and R.-J. Essiambre, "Advanced modulation formats for ultra-high-speed transport networks," *J. Lightw. Technol.*, vol. 24, no. 12, pp. 4711–4728, 2006.

[56] N. Dong-Nhat, M. A. Elsherif, H. Le Minh, and A. Malekmohammadi, "NRZ versus RZ over absolute added correlative coding in optical metro-access networks," *Opt. Commun.*, vol. 387, pp. 30–36, 2017.

[57] J. M. Kahn and K. P. Ho, "Spectral efficiency limits and modulation/detection techniques for DWDM systems," *IEEE J. Sel. Top. Quantum Electron.*, vol. 10, no. 2, pp. 259–272, 2004.

[58] J. C. Cartledge, "Combining self-phase modulation and optimum modulation conditions to improve the performance of 10-Gb/s transmission systems using MQW Mach–Zehnder Modulators," *J. Lightw. Technol.*, vol. 18, no. 5, pp. 647–655, 2000.

[59] U. Troppenz, M. Narodovitch, C. Kottke, G. Przyrembel, W. D. Molzow, A. Sigmund, H. G. Bach, and M. Moehrle, "1.3 μm electroabsorption modulated lasers for PAM4/PAM8 single channel 100 Gb/s," in *26th International Conference on Indium Phosphide and Related Materials*, 2014, p. Th-B2-5.

[60] K. Sekine, N. Kikuchi, S. Sasaki, S. Hayase, C. Hasegawa, and T. Sugawara, "40 Gbit⁄s, 16-ary (4 bit⁄symbol) optical modulation⁄demodulation scheme," *Electron. Lett.*, vol. 41, no. 7, p. 430, 2005.

[61] K. Zhong, X. Zhou, T. Gui, L. Tao, Y. Gao, W. Chen, J. Man, L. Zeng, A. P. T. Lau, and C. Lu, "Experimental study of PAM-4, CAP-16, and DMT for 100 Gb/s short reach optical transmission systems," *Opt. Express*, vol. 23, no. 2, pp. 1176–1189, 2015.

[62] L. Tao, Y. Ji, J. Liu, A. Tao Lau, N. Chi, and C. Lu, "Advanced modulation formats for short reach optical communication systems," *IEEE Netw.*, vol. 27, no. 6, pp. 6–13, 2013.

[63] N. Sotiropoulos, T. Koonen, and H. De Waardt, "Advanced differential modulation formats for optical access networks," *J. Lightw. Technol.*, vol. 31, no. 17, pp. 2829–2843, 2013.

[64] S. Randel, F. Breyer, S. C. J. Lee, and J. W. Walewski, "Advanced modulation schemes for short-range optical communications," *IEEE J. Sel. Top. Quantum Electron.*, vol. 16, no. 5, pp. 1280–1289, 2010.

[65] C. Cole, I. Lyubomirsky, A. Ghiasi, and V. Telang, "Higher-order modulation for client optics," *IEEE Commun. Mag.*, vol. 51, no. 3, pp. 50–57, 2013.

[66] D. T. Van Veen and V. E. Houtsma, "Proposals for cost-effectively upgrading

passive optical networks to a 25G line rate," *J. Lightw. Technol.*, vol. 35, no. 6, pp. 1180–1187, 2017.

[67] X. Xu, E. Zhou, G. N. Liu, T. Zuo, Q. Zhong, L. Zhang, Y. Bao, X. Zhang, J. Li, and Z. Li, "Advanced modulation formats for 400-Gbps short-reach optical inter-connection," *Opt. Express*, vol. 23, no. 1, p. 492, 2015.

[68] Y. Wang, J. Yu, N. Chi, and G.-K. Chang, "Experimental demonstration of 120-Gb/s nyquist PAM8-SCFDE for short-reach optical communication," *IEEE Photonics J.*, vol. 7, no. 4, pp. 1–5, 2015.

[69] R. Safaisini, K. Szczerba, P. Westbergh, E. Haglund, B. Kögel, J. S. Gustavsson, M. Karlsson, P. Andrekson, and A. Larsson, "High-Speed 850 nm Quasi-Single-Mode VCSELs for Extended-Reach Optical Interconnects," *J. Opt. Commun. Netw.*, vol. 5, no. 7, pp. 686–695, Jul. 2013.

[70] A. Tatarczak, S. M. R. Motaghiannezam, C. Kocot, S. Hallstein, I. Lyubomirsky, D. Askarov, H. M. Daghighian, S. Nelson, I. Tafur Monroy, and J. A. Tatum, "Reach extension and capacity enhancement of VCSEL-based transmission over single-lane MMF links," *J. Lightw. Technol.*, vol. 35, no. 4, pp. 565–571, 2017.

[71] J. D. Ingham, J. L. Wei, R. V Penty, and I. H. White, "Hybrid Modulation Formats for Advanced Datacommunications," in *2014 16th International Conference on Transparent Optical Networks (ICTON)*, 2014, p. Mo.D1.1.

[72] M. A. Elsherif and A. Malekmohammadi, "Performance enhancement of mapping multiplexing technique utilising dual-drive Mach–Zehnder modulator for metropolitan area networks," *IET Optoelectron.*, vol. 9, no. 2, pp. 108–115, 2014.

[73] N. Alic, E. Myslivets, and S. Radic, "Non-coherent high spectral efficiency long haul waveband transmission," *IEEE Photonics Technol. Lett.*, vol. 24, no. 2, pp. 113–115, 2012.

[74] I. Lyubomirsky, "Quadrature duobinary for high-spectral efficiency 100G transmission," *J. Lightw. Technol.*, vol. 28, no. 1, pp. 91–96, 2010.

[75] J. L. Wei, J. D. Ingham, D. G. Cunningham, R. V. Penty, and I. H. White, "Comparison of 100 Gb/s Ethernet links using PAM-8, multipulse, and hybrid CAP-16/QAM-16 modulation schemes," in *Optical Fiber Communication Conference*, 2013, p. Th.1.F.2.

[76] C. Xu, X. Liu, L. F. Mollenauer, and X. Wei, "Comparison of return-to-zero differential phase-shift keying and on-off keying in long-haul dispersion managed transmission," *IEEE Photonics Technol. Lett.*, vol. 15, no. 4, pp. 617–619, 2003.

[77] E. Forestieri, "Evaluating the error probability in lightwave systems with chromatic dispersion, arbitrary pulse shape and pre- and postdetection filtering,"

J. Lightw. Technol., vol. 18, no. 11, pp. 1493–1503, 2000.

[78] J. L. Rebola and A. V. T. Cartaxo, "New Gaussian approximation for performance assessment of optically preamplified receivers with arbitrary optical and electrical filters," *IET Optoelectron.*, vol. 148, no. 3, pp. 135–142, 2001.

[79] J. Ma, J. Yu, C. Yu, X. Xin, J. Zeng, and L. Chen, "Fiber dispersion influence on transmission of the optical millimeter-waves generated using LN-MZM intensity modulation," *J. Lightw. Technol.*, vol. 25, no. 11, pp. 3244–3256, 2007.

[80] M. I. Hayee and A. E. Willner, "NRZ versus RZ in 10 – 40-Gb/s dispersion-managed WDM transmission systems," *IEEE Photonics Technol. Lett.*, vol. 11, no. 8, pp. 991–993, 1999.

[81] M. Pfennigbauer, M. M. Strasser, M. Pauer, and P. J. Winzer, "Dependence of optically preamplified receiver sensitivity on optical and electrical filter bandwidths - measurement and simulation," *IEEE Photonics Technol. Lett.*, vol. 14, no. 6, pp. 831–833, 2002.

[82] K. Schuh, E. Lach, B. Junginger, and B. Franz, "53.5 Gbit/s NRZ-VSB modulation applying a single Mach-Zehnder modulator and transmission over 21 km SSMF with electronic dispersion compensation," in *Optical Fiber Communication Conference*, 2009, p. OThC7.

[83] E. Pincemin, C. Gosset, N. Boudrioua, A. Tan, D. Grot, and T. Guillossou, "Experimental performance comparison of duobinary and PSBT modulation formats for long-haul 40 Gb/s transmission on G 0.652 fibre.," *Opt. Express*, vol. 20, no. 27, pp. 28171–28190, 2012.

[84] S. Walklin and J. Conradi, "Multilevel signaling for increasing the reach of 10 Gb/s lightwave systems," *J. Lightw. Technol.*, vol. 17, no. 11, pp. 2235–2248, 1999.

[85] J. Lee, M. S. Chen, and H. D. Wang, "Design and comparison of three 20-Gb/s backplane transceivers for duobinary, PAM4, and NRZ data," *IEEE J. Solid-State Circuits*, vol. 43, no. 9, pp. 2120–2133, 2008.

[86] E. Ip and J. M. Kahn, "Power spectra of return-to-zero optical signals," *J. Lightw. Technol.*, vol. 24, no. 3, pp. 1610–1618, 2006.

[87] W. Kaiser, T. Wuth, M. Wichers, and W. Rosenkranz, "Reduced complexity optical duobinary 10-Gb/s transmitter setup resulting in an increased transmission distance," *IEEE Photonics Technol. Lett.*, vol. 13, no. 8, pp. 884–886, 2001.

[88] C. Xie, L. Möller, and R. Ryf, "Improvement of optical NRZ- and RZ-duobinary transmission systems with narrow bandwidth optical filters," *IEEE Photonics*

Technol. Lett., vol. 16, no. 9, pp. 2162–2164, 2004.

[89] C. C. Chien and I. Lyubomirsky, "Comparison of RZ versus NRZ pulse shapes for optical duobinary transmission," *J. Lightw. Technol.*, vol. 25, no. 10, pp. 2953–2958, 2007.

[90] H. Rastegarfar, L. Yan, K. Szczerba, and E. Agrell, "PAM performance analysis in multicast-enabled wavelength-routing data centers," *J. Lightw. Technol.*, vol. 35, no. 13, pp. 2569–2579, 2017.

[91] B. Xu, L. Zhang, and K. Qiu, "Memory-based pulse amplitude modulation for short-reach fiber communications with intensity modulation and direct detection," *Opt. Express*, vol. 24, no. 11, pp. 11876–11884, 2016.

[92] K. Fang, J. Yu, H. Wang, and X. Li, "56 Gbps signal generation from one 10-G class laser diode for 400G intra-data center interconnection," *Opt. Fiber Technol.*, vol. 36, pp. 210–214, 2017.

[93] A. H. M. R. Islam, M. Bakaul, and A. Nirmalathas, "Multilevel intensity modulations for simplified full-duplex millimeter-wave radio-over-fiber system for gigabit access," *IEEE Photonics J.*, vol. 4, no. 5, pp. 1956–1972, 2012.

[94] N. A. Kaliteevskiy, W. A. Wood, J. D. Downie, J. Hurley, and P. Sterlingov, "Power penalties for multi-level PAM modulation formats at arbitrary bit error rates," in *Proc. SPIE*, 2016, vol. 9775, p. 977508.

[95] M. N. Sakib and O. Liboiron-Ladouceur, "A study of error correction codes for PAM signals in data center applications," *IEEE Photonics Technol. Lett.*, vol. 25, no. 23, pp. 2274–2277, 2013.

[96] S. Dris, P. Bakopoulos, N. Argyris, C. Spatharakis, and H. Avramopoulos, "Scaling single-wavelength optical interconnects to 180 Gb/s with PAM-M and pulse shaping," in *Proc. SPIE*, 2016, vol. 9775, p. 977506.

[97] K. Szczerba, P. Westbergh, M. Karlsson, P. A. Andrekson, and A. Larsson, "70 Gbps 4-PAM and 56 Gbps 8-PAM using an 850 nm VCSEL," *J. Lightw. Technol.*, vol. 33, no. 7, pp. 1395–1401, 2015.

[98] J.-Y. Dupuy, M. Riet, A. Konczykowska, V. Nodjiadjim, F. Jorge, H. Aubry, and A. Adamiecki, "84 GBd (168 Gbit/s) PAM-4 3.7 Vpp power DAC in InP DHBT for short reach and long haul optical networks," *Electron. Lett.*, vol. 51, no. 20, pp. 1591–1593, 2015.

[99] R. Van Der Linden, N.-C. Tran, E. Tangdiongga, and T. Koonen, "Increasing Flexibility and Capacity in Real PON Deployments by Using 2/4/8-PAM Formats," *J. Opt. Commun. Netw.*, vol. 9, no. 1, pp. 10–12, 2016.

[100] S. H. Bae, H. K. Shim, U. H. Hong, H. Kim, A. Agata, K. Tanaka, M. Suzuki,

and Y. C. Chung, "25-Gb/s TDM optical link using EMLs for mobile fronthaul network of LTE-A system," *IEEE Photonics Technol. Lett.*, vol. 27, no. 17, pp. 1825–1828, 2015.

[101] N. Dong-Nhat, M. A. Elsherif, and A. Malekmohammadi, "Investigations of high-speed optical transmission systems employing Absolute Added Correlative Coding (AACC)," *Opt. Fiber Technol.*, vol. 30, pp. 23–31, 2016.

[102] C. R. Doerr, S. Chandrasekhar, P. J. Winzer, A. R. Chraplyvy, A. H. Gnauck, L. W. Stulz, R. Pafchek, and E. Burrows, "Simple multichannel optical equalizer for mitigating intersymbol interference for 40-Gb/s nonreturn-to-zero signals," *J. Lightw. Technol.*, vol. 22, no. 1, pp. 249–256, 2004.

[103] Z. Li, L. Yi, H. Ji, and W. Hu, "100-Gb/s TWDM-PON based on 10G optical devices," *Opt. Express*, vol. 24, no. 12, pp. 12941–12948, 2016.

[104] H. K. Shim, H. Kim, and Y. C. Chung, "Effects of electrical and optical equalizations in 28-Gb/s RSOA-based WDM PON," *IEEE Photonics Technol. Lett.*, vol. 28, no. 22, pp. 2537–2540, 2016.

[105] C. R. Doerr, A. H. Gnauck, L. W. Stulz, and D. M. Gill, "Using an optical equalizer to transmit a 43-Gb/s signal with an 8-GHz bandwidth modulator," *IEEE Photonics Technol. Lett.*, vol. 15, no. 11, pp. 1624–1626, 2003.

[106] P. J. Winzer, G. Raybon, C. R. Doerr, M. Duelk, and C. Dorrer, "107-Gb/s optical signal generation using electronic time-division multiplexing," *J. Lightw. Technol.*, vol. 24, no. 8, pp. 3107–3113, 2006.

[107] H. K. Shim, H. Kim, and Y. C. Chung, "20-Gb/s polar RZ 4-PAM transmission over 20-km SSMF using RSOA and direct detection," *IEEE Photonics Technol. Lett.*, vol. 27, no. 10, pp. 1116–1119, 2015.

[108] H. Kim, "10-Gb/s operation of RSOA using a delay interferometer," *IEEE Photonics Technol. Lett.*, vol. 22, no. 18, pp. 1379–1381, 2010.

[109] T. Su, M. Zhang, X. Chen, Z. Zhang, M. Liu, L. Liu, and S. Huang, "Improved 10-Gbps uplink transmission in WDM-PON with RSOA-based colorless ONUs and MZI-based equalizers," *Opt. Laser Technol.*, vol. 51, pp. 90–97, 2013.

[110] Z. Li, L. Yi, X. Wang, and W. Hu, "28 Gb/s duobinary signal transmission over 40 km based on 10 GHz DML and PIN for 100 Gb/s PON," *Opt. Express*, vol. 23, no. 16, pp. 20249–20256, 2015.

[111] V. Mikhailov, R. I. Killey, and P. Bayvel, "Optical equalization of nonlinear signal distortion in 42.7-Gb/s RZ transmission," *IEEE Photonics Technol. Lett.*, vol. 20, no. 5, pp. 381–383, 2008.

[112] A. Bhardwaj, C. R. Doerr, S. Chandrasekhar, and L. W. Stulz, "Reduction of

nonlinear distortion from a semiconductor optical amplifier using an optical equalizer," *IEEE Photonics Technol. Lett.*, vol. 16, no. 3, pp. 921–923, 2004.

[113] P. Dong, C. Xie, L. L. Buhl, Y.-K. Chen, J. H. Sinsky, and G. Raybon, "Silicon in-phase/quadrature modulator with on-chip optical equalizer," *J. Lightw. Technol.*, vol. 33, no. 6, pp. 1191–1196, 2015.

[114] N. Dong-Nhat, L. Nguyen, and A. Malekmohammadi, "Combining filtered antipodal signaling and optical equalization for extended-reach access networks," in *Advanced Photonics - Signal Processing in Photonic Communications*, 2017, p. SpM2F.1.

[115] Z. Li, L. Yi, W. Wei, M. Bi, H. He, S. Xiao, and W. Hu, "Symmetric 40-Gb/s, 100-km passive reach TWDM-PON with 53-dB loss budget," *J. Lightw. Technol.*, vol. 32, no. 21, pp. 3991–3998, 2014.

[116] J. Lavrencik, V. A. Thomas, S. Varughese, and S. Ralph, "DSP enabled 100Gbps PAM-4 VCSEL MMF links," *J. Lightw. Technol.*, vol. 35, no. 15, pp. 3189–3196, 2017.

[117] M. S. Khaliq, M. Cantono, S. Straullu, and V. Curri, "Performance assessment of short-reach multi-level pulse-amplitude modulation transmission exploiting least-mean-square equalisation," *IET Optoelectron.*, vol. 11, no. 4, pp. 134–140, 2017.

[118] F. Karinou, N. Stojanovic, C. Prodaniuc, and Q. Zhang, "Experimental demonstration of an electro-absorption modulated laser for high-speed transmissions at 1.55-μm window using digital signal processing," *Photonics*, vol. 4, no. 1, pp. 1–11, 2017.

[119] S. Y. Kao and S. I. Liu, "A 10-Gb/s adaptive parallel receiver with joint XTC and DFE using power detection," *IEEE J. Solid-State Circuits*, vol. 48, no. 11, pp. 2815–2826, 2013.

[120] Y. Lu and E. Alon, "Design techniques for a 66 Gb/s 46 mW 3-tap decision feedback equalizer in 65 nm CMOS," *IEEE J. Solid-State Circuits*, vol. 48, no. 12, pp. 3243–3257, 2013.

[121] J. F. Bulzacchelli, C. Menol, T. J. Beukema, D. W. Storaska, J. J. Hertle, D. R. Hanson, P. Hsieh, S. V Rylov, D. Furrer, D. Gardellini, A. Prati, T. Morf, V. Sharma, R. Kelkar, H. A. Ainspan, W. R. Kelly, L. R. Chieco, G. A. Ritter, J. A. Sorice, J. D. Garlett, R. Callan, M. Brändli, P. Buchmann, M. Kossel, T. Toifl, and D. J. Friedman, "A 28-Gb/s 4-Tap FFE/15-Tap DFE serial link transceiver in 32-nm SOI CMOS technology," *J. Solid-State Circuits*, vol. 47, no. 12, pp. 1–17, 2012.

[122] A. Agrawal, J. F. Bulzacchelli, T. O. Dickson, Y. Liu, J. A. Tierno, and D. J.

Friedman, "A 19-Gb/s serial link receiver with both 4-Tap FFE and 5-Tap DFE functions in 45-nm SOI CMOS," *IEEE J. Solid-State Circuits*, vol. 47, no. 12, pp. 3220–3231, 2012.

[123] H. Wang, C. Lee, A. Lee, and J. Lee, "A 21-Gb/s 87-mW transceiver with FFE/DFE/analog linear equalizer in 65-nm CMOS technology," *IEEE J. Solid-State Circuits*, vol. 45, no. 4, pp. 909–920, 2010.

[124] J. F. Bulzacchelli, M. Meghelli, S. V. Rylov, W. Rhee, A. V. Rylyakov, H. A. Ainspan, B. D. Parker, M. P. Beakes, A. Chung, T. J. Beukema, P. K. Pepeljugoski, L. Shan, Y. H. Kwark, S. Gowda, and D. J. Friedman, "A 10-Gb/s 5-tap DFE/4-tap FFE transceiver in 90-nm CMOS technology," *IEEE J. Solid-State Circuits*, vol. 41, no. 12, pp. 2885–2898, 2006.

[125] F. Loi, E. Mammei, S. Erba, M. Bassi, and A. Mazzanti, "A 25mW highly linear continuous-time FIR equalizer for 25Gb/s serial links in 28-nm CMOS," *IEEE Trans. Circuits Syst. I Regul. Pap.*, vol. 64, no. 7, pp. 1903–1913, 2017.

[126] Y. H. Kim, T. Lee, H. K. Jeon, D. Lee, and L. S. Kim, "An input data and power noise inducing clock jitter tolerant reference-less digital CDR for LCD intra-panel interface," *IEEE Trans. Circuits Syst. I Regul. Pap.*, vol. 64, no. 4, pp. 823–835, 2017.

[127] J. Proakis and M. Salehi, *Digital Communications*, 5th ed. New York: McGraw-Hill, 2008.

[128] J. H. Winters and R. D. Gitlin, "Electrical signal processing techniques in long-haul fiber-optic systems," *IEEE Trans. Commun.*, vol. 38, no. 9, pp. 397–403, 1990.

[129] V. Houtsma, D. T. Van Veen, and H. Chow, "Demonstration of symmetrical 25 Gb/s TDM-PON with multilevel interleaving of users," *J. Lightw. Technol.*, vol. 34, no. 8, pp. 2005–2010, Apr. 2016.

[130] L. Tao, Y. Wang, Y. Gao, A. P. T. Lau, N. Chi, and C. Lu, "Experimental demonstration of 10 Gb/s multi-level carrier-less amplitude and phase modulation for short range optical communication systems.," *Opt. Express*, vol. 21, no. 5, pp. 6459–65, 2013.

[131] A. Moscoso-Mártir, J. Müller, J. Hauck, N. Chimot, R. Setter, A. Badihi, D. E. Rasmussen, A. Garreau, M. Nielsen, E. Islamova, S. Romero-García, B. Shen, A. Sandomirsky, S. Rockman, C. Li, S. S. Azadeh, G.-Q. Lo, E. Mentovich, F. Merget, F. Lelarge, and J. Witzens, "Silicon photonics WDM transceiver with SOA and semiconductor mode-locked laser," *Opt. Express*, vol. 25, no. 1, pp. 1395–1401, 2016.

[132] F. Karinou, C. Prodaniuc, N. Stojanovic, M. Ortsiefer, A. Daly, R. Hohenleitner,

B. Kogel, and C. Neumeyr, "Directly PAM-4 modulated 1530-nm VCSEL enabling 56 Gb/s/ lamda data-center interconnects," *IEEE Photonics Technol. Lett.*, vol. 27, no. 17, pp. 1872–1875, 2015.

[133] C. Yang, R. Hu, M. Luo, Q. Yang, C. Li, H. Li, and S. Yu, "IM/DD-Based 112-Gb/s/lambda PAM-4 Transmission Using 18-Gbps DML," *IEEE Photonics J.*, vol. 8, no. 3, pp. 1–7, Jun. 2016.

[134] J. Zhou, C. Yu, and H. Kim, "Transmission performance of OOK and 4-PAM signals using directly modulated 1.5-μm VCSEL for optical access network," *J. Lightw. Technol.*, vol. 33, no. 15, pp. 3243–3249, 2015.

[135] B. Moeneclaey, F. Blache, J. Van Kerrebrouck, R. Brenot, G. Coudyzer, M. Achouche, X. Z. Qiu, J. Bauwelinck, and X. Yin, "40-Gb/s TDM-PON downstream link with low-cost EML transmitter and APD-based electrical duobinary receiver," *J. Lightw. Technol.*, vol. 35, no. 4, pp. 1083–1089, 2017.

[136] N. Cheng, X. Yan, N. Chand, and F. Effenberger, "10 Gb/s upstream transmission in TWDM PON using duobinary and PAM-4 modulations with directly modulated tunable DBR laser," in *Asia Communications and Photonics Conference*, 2013, p. ATh3E.4.

[137] K. Szczerba, P. Westbergh, E. Agrell, M. Karlsson, P. A. Andrekson, and A. Larsson, "Comparison of intersymbol interference power penalties for OOK and 4-PAM in short-range optical links," *J. Lightw. Technol.*, vol. 31, no. 22, pp. 3525–3534, 2013.

[138] F. Karinou, L. Deng, R. R. Lopez, K. Prince, J. B. Jensen, and I. T. Monroy, "Performance comparison of 850-nm and 1550-nm VCSELs exploiting OOK, OFDM, and 4-PAM over SMF/MMF links for low-cost optical interconnects," *Opt. Fiber Technol.*, vol. 19, no. 3, pp. 206–212, 2013.

[139] S. Zhou, X. Li, L. Yi, Q. Yang, and S. Fu, "Transmission of 2 × 56 Gb/s PAM-4 signal over 100 km SSMF using 18 GHz DMLs," *Opt. Lett.*, vol. 41, no. 8, pp. 1805–1808, 2016.

[140] M. Chagnon, S. Lessard, and D. V. Plant, "336 Gb/s in direct detection below KP4 FEC threshold for intra data center applications," *IEEE Photonics Technol. Lett.*, vol. 28, no. 20, pp. 2233–2236, 2016.

[141] E. El-Fiky, M. Chagnon, M. Sowailem, A. Samani, M. Morsy-Osman, and D. V. Plant, "168-Gb/s single carrier PAM4 transmission for intra-data center optical interconnects," *IEEE Photonics Technol. Lett.*, vol. 29, no. 3, pp. 314–317, 2017.

[142] S. Kanazawa, H. Yamazaki, Y. Nakanishi, Y. Ueda, W. Kobayashi, Y. Muramoto, H. Ishii, and H. Sanjoh, "214-Gb/s 4-PAM operation of flip-chip interconnection EADFB laser module," *J. Lightw. Technol.*, vol. 35, no. 3, pp.

418–422, 2017.

[143] T. Ye, J. Zhang, J. Dang, Y. Song, X. Yi, C. Yu, and K. Qiu, "Experimental demonstration of 50 Gb/s PAM-4 transmission over 50-km SSMF using 10-GHz DML," in *Asia Communications and Photonics Conference*, 2016, p. ATh3C.4.

[144] K. Zhong, X. Zhou, Y. Gao, W. Chen, J. Man, L. Zeng, A. P. T. Lau, and C. Lu, "140-Gb/s 20-km transmission of PAM-4 Signal at 1.3 μm for short reach communications," *IEEE Photonics Technol. Lett.*, vol. 27, no. 16, pp. 1757–1760, 2015.

[145] J. D. Ingham, R. V. Penty, and I. H. White, "Transmitter-based equalisation for extended-reach multimode-fibre datacommunication links," *Electron. Lett.*, vol. 43, no. 4, p. 240, 2007.

[146] J. E. Proesel, B. G. Lee, A. V Rylyakov, C. W. Baks, and C. L. Schow, "Ultra-low-power 10 to 28.5 Gb/s CMOS-driven VCSEL-based optical links [Invited]," *J. Opt. Commun. Netw.*, vol. 4, no. 11, pp. 114–123, 2012.

[147] C. Stamatiadis, R. Matsumoto, Y. Yoshida, A. Agata, A. Maruta, and K. I. Kitayama, "Full-duplex RSOA-based PONs using 4-PAM with pre-equalization," *IEEE Photonics Technol. Lett.*, vol. 27, no. 1, pp. 73–76, 2015.

[148] N. Eiselt, H. Griesser, J. Wei, R. Hohenleitner, A. Dochhan, M. Ortsiefer, M. H. Eiselt, C. Neumeyr, J. J. V. Olmos, and I. T. Monroy, "Experimental demonstration of 84 Gb/s PAM-4 over up to 1.6 km SSMF using a 20-GHz VCSEL at 1525 nm," *J. Lightw. Technol.*, vol. 35, no. 8, pp. 1342–1349, 2017.

[149] M. Bohn and C. Xia, "Electrical and optical equalization strategies in direct detected high-speed transmission systems," *AEU - Int. J. Electron. Commun.*, vol. 63, no. 7, pp. 526–532, 2009.

[150] S. Andrew, S. Nareshi, and B. Hyeon-Min, "Electronic dispersion compensation," *IEEE Signal Process. Mag.*, pp. 110–130, 2008.

[151] M. A. Elsherif and A. Malekmohammadi, "Power efficiency evaluation of mapping multiplexing technique and pulse amplitude modulation for noncoherent systems," *IEEE Photonics J.*, vol. 7, no. 4, pp. 1–11, 2015.

[152] J. Karout, E. Agrell, K. Szczerba, and M. Karlsson, "Optimizing constellations for single-subcarrier intensity-modulated optical systems," *IEEE Trans. Inf. Theory*, vol. 58, no. 7, pp. 4645–4659, 2012.

[153] S. Hranilovic and F. R. Kschischang, "Optical intensity-modulated direct detection channels: Signal space and lattice codes," *IEEE Trans. Inf. Theory*, vol. 49, no. 6, pp. 1385–1399, 2003.

[154] K. Szczerba, J. Karout, P. Westbergh, E. Agrell, M. Karlsson, P. Andrekson,

and A. Larsson, "Experimental comparison of modulation formats in IM/DD links.," *Opt. Express*, vol. 19, no. 10, pp. 9881–9889, 2011.

[155] A. Malekmohammadi, M. K. Abdullah, G. A. Mahdiraji, A. F. Abas, M. Mokhtar, M. F. A. Rasid, and S. M. Basir, "Analysis of return-to-zero-on-off-keying over absolute polar duty cycle division multiplexing in dispersive transmission medium," *IET Optoelectron.*, vol. 3, no. 4, pp. 197–206, 2009.

[156] K. Szczerba, P. Westbergh, J. Karout, J. S. Gustavsson, Å. Haglund, M. Karlsson, P. A. Andrekson, E. Agrell, and A. Larsson, "4-PAM for high-speed short-range optical communications," *J. Opt. Commun. Netw.*, vol. 4, no. 11, pp. 885–894, 2012.

[157] N. Dong-Nhat, M. A. Elsherif, and A. Malekmohammadi, "Assessment of absolute added correlative coding in optical intensity modulation and direct detection channels," *Opt. Eng.*, vol. 55, no. 6, p. 66115, 2016.

[158] M. Verplaetse, R. Lin, J. Van Kerrebrouck, O. Ozolins, T. De Keulenaer, X. Pang, R. Pierco, R. Vaernewyck, A. Vyncke, R. Schatz, U. Westergren, G. Jacobsen, S. Popov, J. Chen, G. Torfs, J. Bauwelinck, and X. Yin, "Real-time 100 Gb/s transmission using three-level electrical duobinary modulation for short-reach optical interconnects," *J. Lightw. Technol.*, vol. 35, no. 7, pp. 1313–1319, 2017.

[159] J. C. Cartledge and A. F. Elrefaie, "Effect of chirping-induced waveform distortion on the performance of direct detection receivers using traveling-wave semiconductor optical preamplifiers," *J. Lightw. Technol.*, vol. 9, no. 2, pp. 209–219, 1991.

[160] R. Motaghiannezam, T. Pham, A. Chen, T. Du, C. Kocot, J. Xu, and B. Huebner, "52 Gbps PAM4 receiver sensitivity study for 400GBase-LR8 system using directly modulated laser," *Opt. Express*, vol. 24, no. 7, p. 7374, 2016.

[161] S. D. Personick, "Receiver design for optical fiber systems," *Proc. IEEE*, vol. 65, no. 12, pp. 1670–1678, 1977.

[162] A. H. N. Avlonitis, E. M. Yeatman, M. Jones, "Multilevel amplitude shift keying in dispersion uncompensated optical systems," *IET Optoelectron.*, vol. 153, no. 3, pp. 101–108, 2006.

[163] O. K. Tonguz and L. G. Kazovsky, "Theory of direct-detection lightwave receivers using optical amplifiers," *J. Lightw. Technol.*, vol. 9, no. 2, pp. 174–181, 1991.

[164] G. Nicholl and C. Fludger, "Update on technical feasibility for PAM modulation," in *IEEE 802.3 NG100GE PMD Study Group*, 2012.

[165] N. Dong-Nhat, L. Nguyen, and A. Malekmohammadi, "75 Gbit/s transmission over single mode fibre links using 8-PAM and 8-AACC modulations," *Electron. Lett.*, vol. 53, no. 5, pp. 326–328, 2017.

[166] N. Dong-Nhat and A. Malekmohammadi, "Absolute added correlative coding: an enhanced M-PAM modulation format," *Electron. Lett.*, vol. 51, no. 20, pp. 1593–1595, 2015.

[167] K. Yu, H. Lee, N. Park, D. Lee, and O. Solgaard, "Optical bandpass filter with tunable chromatic dispersion and optical bandwidth using a variable MEMS reflector," in *OFC/NFOEC 2007 - Optical Fiber Communication and the National Fiber Optic Engineers Conference*, 2007, p. OWO3.

[168] L. Tao, Y. Wang, J. Xiao, and N. Chi, "Enhanced performance of 400 Gb/s DML-based CAP systems using optical filtering technique for short reach communication," *Opt. Express*, vol. 22, no. 24, pp. 29331–29339, 2014.

[169] H. Sunnerud, M. Sköld, M. Westlund, and P. A. Andrekson, "Characterization of complex optical modulation formats at 100 Gb/s and beyond by coherent optical sampling," *J. Lightw. Technol.*, vol. 30, no. 24, pp. 3747–3759, 2012.

[170] J. D. Ingham, R. V Penty, and I. H. White, "100 Gb/s PAM4-CAP2 real-time modulation of a single optical source for next-generation datacommunication links," in *Optical Fiber Communication Conference*, 2014, p. W1F.1.

[171] S. Kanazawa, Y. Nakanishi, S. Tsunashima, H. Yamazaki, Y. Ueda, W. Kobayashi, Y. Muramoto, H. Ishii, and H. Sanjoh, "Equalizer-free transmission of 100-Gbit/s 4-PAM signal generated by flip-chip interconnection EADFB laser module," *J. Lightw. Technol.*, vol. PP, no. 99, pp. 775–780, 2016.

[172] M. Morsy-Osman, M. Chagnon, M. Poulin, S. Lessard, and D. V. Plant, "224-Gb/s 10-km transmission of PDM PAM-4 at 1.3 μm using a single intensity-modulated laser and a direct-detection MIMO DSP-based receiver," *J. Lightw. Technol.*, vol. 33, no. 7, pp. 1417–1424, 2015.

[173] S. Yin, T. Chan, and W. I. Way, "100-km DWDM transmission of 56-Gb/s PAM4 per lambda via tunable laser and 10-Gb/s InP MZM," *IEEE Photonics Technol. Lett.*, vol. 27, no. 24, pp. 2531–2534, 2015.

[174] F. Karinou, N. Stojanovic, A. Daly, C. Neumeyr, and M. Ortsiefer, "1.55-μm long-wavelength VCSEL-based optical interconnects for short-reach networks," *J. Lightw. Technol.*, vol. 34, no. 12, pp. 2897–2904, 2016.

[175] P. Bakopoulos, S. Dris, N. Argyris, K. Tokas, and H. Avramopoulos, "120 Gb/s PAM-8 and 80 Gb/s PAM-4 optical interconnect with a sub-volt driven EAM," in *Asia Communications and Photonics Conference (ACP)*, 2015, p. AS4D.4.

[176] L. Wang, M. Forzati, and J. Mårtensson, "Analysis of NRZ- and RZ-DQPSK for 112 Gb/s DWDM transmission," in *ICTON 2009: 11th International Conference on Transparent Optical Networks*, 2009, p. Mo.C2.4.

[177] C. Rottondi, M. Tornatore, A. Pattavina, and G. Gavioli, "Routing, Modulation Level, and Spectrum Assignment in Optical Metro Ring Networks Using Elastic Transceivers," *J. Opt. Commun. Netw.*, vol. 5, no. 4, pp. 305–315, Apr. 2013.

[178] C. R. da Silveira, D. M. Pataca, M. A. Romero, and M. de Lacerda Rocha, "A cost-benefit analysis on modulation formats for 40-Gb/s optical communication systems," *Fiber Integr. Opt.*, vol. 30, no. 2, pp. 87–101, 2011.

[179] T. Otsuji, Y. Imai, E. Sano, S. Kimura, S. Yamaguchi, M. Yoneyama, T. Enoki, and Y. Umeda, "40-Gb/s IC' s for future lightwave," *IEEE J. Solid-State Circuits*, vol. 32, no. 9, pp. 1363–1370, 1997.

[180] Y. Miyamoto, M. Yoneyama, T. Otsuji, K. Yonenaga, and N. Shimizu, "40-Gbit/s TDM transmission technologies based on ultra-high-speed IC's," *IEEE J. Solid-State Circuits*, vol. 34, no. 9, pp. 1246–1253, 1999.

[181] M. Yoneyama, K. Yonenaga, Y. Kisaka, and Y. Miyamoto, "Differential precoder IC modules for 20- and 40-Gbit/s optical duobinary," *IEEE Trans. Microw. Theory Tech.*, vol. 47, no. 12, pp. 2263–2270, 1999.

[182] Q. Zhang, N. Stojanovic, C. Prodaniuc, F. Karinou, and C. Xie, "Cost-effective single-lane 112 Gb/s solution for mobile fronthaul and access applications," *Opt. Lett.*, vol. 41, no. 24, pp. 5720–5723, Dec. 2016.

[183] V. Curri, R. Gaudino, A. Napoli, and P. Poggiolini, "Electronic equalization for advanced modulation formats in dispersion-limited systems," *IEEE Photonics Technol. Lett.*, vol. 16, no. 11, pp. 2556–2558, 2004.

[184] M. Secondini, E. Forestieri, and G. Prati, "Performance of MSE configured PLC optical equalizers for chromatic dispersion compensation," *Photonics Technol. Lett.*, vol. 15, no. 2, pp. 248–250, 2003.

[185] J. Ma and J. Zhang, "Full duplex fiber link for alternative wired and wireless access based on SSB optical millimeter-wave with 4-PAM signal," *Opt. Commun.*, vol. 338, pp. 578–584, 2015.

[186] A. Wiberg, P. Pérez-Millán, M. V. Andrés, P. A. Andrekson, and P. O. Hedekvist, "Fiber-optic 40-GHz mm-wave link with 2.5-Gb/s data transmission," *IEEE Photonics Technol. Lett.*, vol. 17, no. 9, pp. 1938–1940, 2005.

[187] V. Houtsma and D. Van Veen, "A study of options for high speed TDM-PON beyond 10G," *J. Lightw. Technol.*, vol. 35, no. 4, pp. 1059–1066, 2017.

[188] J. Krause Perin, M. Sharif, and J. M. Kahn, "Sensitivity improvement in 100

Gbit/s-per-wavelength links using semiconductor optical amplifiers or avalanche photodiodes," *J. Lightw. Technol.*, vol. 34, no. 33, pp. 5542–5553, 2016.

[189] D. Van Veen and V. Houtsma, "Bi-directional 25G/50G TDM-PON with extended power budget using 25G APD and coherent amplification," in *Optical Fiber Communication Conference*, 2017, p. Th5A.4.

[190] J. Chen, Z. S. He, T. Lengyel, K. Szczerba, P. Westbergh, J. S. Gustavsson, H. Zirath, and A. Larsson, "An energy efficient 56 Gbps PAM-4 VCSEL transmitter enabled by a 100 Gbps driver in 0.25 µm InP DHBT technology," *J. Lightw. Technol.*, vol. 34, no. 21, pp. 4954–4964, 2016.

[191] M. Theurer, H. Zhang, Y. Wang, W. Chen, L. Zeng, U. Troppenz, G. Przyrembel, A. Sigmund, M. Moehrle, and M. Schell, "2 x 56 GB/s from a double side electroabsorption modulated DFB laser and application in novel optical PAM4 generation," *J. Lightw. Technol.*, vol. 35, no. 4, pp. 706–710, 2016.

[192] J. Verbrugghe, R. Vaernewyck, B. Moeneclaey, X. Yin, G. Maxwell, R. Cronin, G. Torfs, X. Qiu, C. P. Lai, P. Townsend, and J. Bauwelinck, "Multichannel 25 Gb/s low-power driver and transimpedance amplifier integrated circuits for 100 Gb/s optical links," *J. Lightw. Technol.*, vol. 32, no. 16, pp. 2877–2885, 2014.

[193] C. Shen, Y. Guo, H. M. Oubei, T. K. Ng, G. Liu, K.-H. Park, K.-T. Ho, M.-S. Alouini, and B. S. Ooi, "20-meter underwater wireless optical communication link with 15 Gbps data rate," *Opt. Express*, vol. 24, no. 22, p. 25502, 2016.

List of Publications and Awards

Peer Reviewed Publications

Journal Publications:

P1. N. Dong-Nhat and A. Malekmohammadi, "Absolute added correlative coding: an enhanced M-PAM modulation format," *Electron. Lett.*, vol. 51, no. 20, pp. 1593–1595, 2015.

P2. N. Dong-Nhat, M. A. Elsherif, and A. Malekmohammadi, "Investigations of high-speed optical transmission systems employing Absolute Added Correlative Coding (AACC)," *Opt. Fiber Technol.*, vol. 30, pp. 23–31, 2016.

P3. N. Dong-Nhat and A. Malekmohammadi, "Transmission of duobinary signal in optical 40 GHz millimeter-wave radio-over-fiber systems utilizing dual-arm $LiNbO_3$ Mach–Zehnder modulator for downstream," *J. Opt. Commun.*, vol. 37, no. 2, pp. 155–161, 2016.

P4. N. Dong-Nhat and A. Malekmohammadi, "RZ-absolute added correlative coding (AACC) transmission system featuring improved receiver sensitivity for high-speed optical transport," *Electron. Lett.*, vol. 52, no. 8, pp. 639–641, 2016.

P5. N. Dong-Nhat, M. A. Elsherif, and A. Malekmohammadi, "Assessment of Absolute Added Correlative Coding in optical intensity modulation and direct detection channels," *Opt. Eng.*, vol. 55, no. 6, p. 66115, 2016.

P6. N. Dong-Nhat, M. A. Elsherif, H. Le Minh, and A. Malekmohammadi, "NRZ versus RZ over Absolute Added Correlative Coding in optical metro-access networks," *Opt. Commun.*, vol. 387, pp. 30–36, 2017.

P7. N. Dong-Nhat, L. Nguyen, and A. Malekmohammadi, "75 Gbit/s transmission over single mode fibre links using 8-PAM and 8-AACC modulations," *Electron. Lett.*, vol. 53, no. 5, pp. 326–328, 2017.

P8. N. Dong-Nhat, L. Nguyen, and A. Malekmohammadi, "Using duobinary with first- and second-order optical equalizers for extending transmission distance of optical access networks," *IET Opto.*, (accepted).

Conference Publications:

P9. N. Dong-Nhat and A. Malekmohammadi, "100 Gb/s hybrid data transmission using 1.3-μm DML for optical interconnect applications," in *CLEO: QELS_Fundamental Science*, USA, 2016, p. JTh2A.130.

P10. N. Dong-Nhat, L. Nguyen, and A. Malekmohammadi, "Combining filtered antipodal signaling and optical equalization for extended-reach access networks," in *Advanced Photonics - Signal Processing in Photonic Communications*, USA, 2017, p. SpM2F.1.

P11. N. Dong-Nhat and A. Malekmohammadi, "28-Gb/s PAM-4 transmission over 50-km of SSMF using a Mach-Zehnder modulator and linear equalizers," in *IONS – Okinawa*, Japan, 2017.

Conference Meetings

- *Topical Meeting on Photonics,* organised by IEEE Malaysia Chapter and IEEE Photonics Society, August 2015.

- *Conference on Lasers and Electro-Optics (CLEO),* organised by Optical Society – USA, San Jose, June 2016.

- *Conference on Optoelectronics and Optical Communications (COOC),* organised by Optical Society – Korea, Busan, June 2017.

- International Optical Society of America Network of Students (IONS) – Okinawa, October 2017.

Awards

- Best Project Award, International Engineering and Technology Exhibition (IETE), Malaysia, 2015.

- UNMC Graduate Student Conference Funding, 2016.

- UNMC Academically Excellent Postgraduate Student, 2016.

- Student Travel Fellowship, International Optical Society of America Network of Students (IONS) – Okinawa, Japan, 2017.